

PEM FUEL CELL DEGRADATION: NUMERICAL INVESTIGATION AND
EFFECTS ON THE PERFORMANCE OF SOLAR-HYDROGEN BASED
RENEWABLE ENERGY SYSTEMS

A THESIS SUBMITTED TO
THE GRADUATE SCHOOL OF NATURAL AND APPLIED SCIENCES
OF
MIDDLE EAST TECHNICAL UNIVERSITY

BY

ENDER ÖZDEN

IN PARTIAL FULFILLMENT OF THE REQUIREMENTS
FOR
THE DEGREE OF DOCTOR OF PHILOSOPHY
IN
MECHANICAL ENGINEERING

MARCH 2015

Approval of the thesis:

**PEM FUEL CELL DEGRADATION: NUMERICAL INVESTIGATION AND
EFFECTS ON THE PERFORMANCE OF SOLAR-HYDROGEN BASED
RENEWABLE ENERGY SYSTEMS**

submitted by **ENDER ÖZDEN** in partial fulfillment of the requirements for the degree of **Doctor of Philosophy in Mechanical Engineering Department, Middle East Technical University** by,

Prof. Dr. M. Gülbin Dural Ünver
Dean, Graduate School of **Natural and Applied Sciences**

Prof. Dr. Tuna Balkan
Head of Department, **Mechanical Engineering**

Assoc. Prof. Dr. İlker Tari
Supervisor, **Mechanical Engineering Dept., METU**

Examining Committee Members:

Assoc. Prof. Dr. Cemil Yamalı
Mechanical Engineering Dept., METU

Assoc. Prof. Dr. İlker Tari
Mechanical Engineering Dept., METU

Assoc. Prof. Dr. Derek K. Baker
Mechanical Engineering Dept., METU

Assist. Prof. Dr. Cüneyt Sert
Mechanical Engineering Dept., METU

Prof. Dr. Mecit Sivrioğlu
Mechanical Engineering Dept., Gazi University

Date: 03.03.2015

I hereby declare that all information in this document has been obtained and presented in accordance with academic rules and ethical conduct. I also declare that, as required by these rules and conduct, I have fully cited and referenced all material and results that are not original to this work.

Name, Last name: Ender Özden

Signature :

ABSTRACT

PEM FUEL CELL DEGRADATION: NUMERICAL INVESTIGATION AND EFFECTS ON THE PERFORMANCE OF SOLAR-HYDROGEN BASED RENEWABLE ENERGY SYSTEMS

Özden, Ender

Ph.D, Department of Mechanical Engineering

Supervisor: Assoc. Prof. Dr. İlker Tarı

March 2015, 188 pages

A hybrid (Solar-Hydrogen) renewable energy system consisting of Photovoltaic (PV) panels, Proton Exchange Membrane (PEM) fuel cells, PEM based electrolyzers and hydrogen storage has been investigated for a stand-alone application. A complete model of the hybrid renewable energy system has been developed using TRNSYS against a reference system, which was established for the emergency room of Keçiören Research and Training Hospital in Ankara. The main goal of the study is to verify that the system meets the electrical power demand of the emergency room without any shortage for a complete year. The emergency room has a peak electrical load of 5 kW and a yearly load of 37.23 MWh. The PV panels with a total area of 300 m² are mounted on a tiltable platform to improve the performance of the system. The PEM fuel cells have a total capacity of 5 kW. The hydrogen storage pressure is 55 bars with the capacity of 30 m³. Energy and exergy analyses of the system are performed together with a detailed economic analysis.

The PEM fuel cells are numerically modeled in ANSYS Fluent in order to obtain data for the TRNSYS model. The obtained simulation data is used both for the PEM fuel cells and the PEM based electrolyzers. The developed numerical model later modified to include cell degradation. Again, using the data from the degraded model, the TRNSYS model is updated and the performance of the system after two years of operation is predicted.

After the performed analyses, it is concluded that solar-hydrogen based renewable energy systems can be a possible alternative to fossil fuel based energy systems especially in long-term emergency blackout conditions. Furthermore, it is determined that the system is capable of continuously working throughout a whole year when the hydrogen storage capacity is increased to 45 m³ and the overall efficiency of the system is improved by using variable angle of incidence for the PV panels. Additionally, it is concluded that the degradation of PEM based system components is an important phenomenon, which has detrimental effects on the overall system performance.

Keywords: PEM fuel cell degradation; Hybrid renewable energy systems; ANSYS Fluent; TRNSYS; Energy analysis; Exergy analysis; Economical analysis

ÖZ

PEM YAKIT HÜCRESİ BOZUNMASI: SAYISAL İNCELEME VE GÜNEŞ- HİDROJEN TEMELLİ YENİLENEBİLİR ENERJİ SİSTEMLERİ PERFORMANSI ÜZERİNDEKİ ETKİLERİ

Özden, Ender

Doktora, Makina Mühendisliği Bölümü

Tez Yöneticisi: Doç. Dr. İlker Tarı

Mart 2015, 188 Sayfa

Fotovoltaik (PV) paneller, Proton Değişim Membranlı (PEM) yakıt hücreleri, PEM temelli elektrolizörler ve hidrojen depolamadan oluşan bir hibrit (Güneş-Hidrojen) yenilenebilir enerji sistemi şebekeden bağımsız bir uygulama için incelenmiştir. Hibrit yenilenebilir enerji sisteminin sistem modeli TRNSYS yazılımı kullanılarak referans bir sistem olarak Ankara'da bulunan Keçiören Eğitim ve Araştırma Hastanesi acil servisi için geliştirilmiştir. Çalışmanın ana amacı acil servisin elektriksel güç talebini kesintisiz olarak bir yıl boyunca karşılandığını göstermektir. Acil servisin pik elektrik yükü 5 kW ve yıllık olarak 37.23 MWh'tir. Sistemin performansını artırmak için, 300 m² alana sahip PV panelleri eğimlendirilebilir bir platform üzerine yerleştirilmiştir. PEM yakıt hücrelerinin toplam kapasitesi 5kW'tır. 30 m³ kapasiteye sahip olan hidrojen tanklarının depolama basıncı 55 bar'dır. Sistemin enerji ve ekserji analizleri ayrıntılı bir ekonomik analizle birlikte yapılmıştır. PEM yakıt hücresi, TRNSYS modeli için veri elde edebilmek amacı ile ANSYS Fluent kullanılarak sayısal olarak modellenmiştir. Elde edilen benzetim verileri, hem PEM yakıt hücreleri hem de PEM temelli elektrolizörler için

kullanılmıştır. Geliştirilen sayısal model daha sonra hücre bozunmasını da içerecek şekilde değiştirilmiştir. Ayrıca, bozunma modeli verileri kullanılarak TRNSYS modeli güncellenmiş ve sistem performansı iki yıllık çalışma sonrasında tahmin edilmiştir.

Gerçekleştirilen analizlerden sonra, özellikle uzun süreli acil durum kesinti durumlarında güneş-hidrojen temelli yenilenebilir enerji sistemlerinin fosil yakıt temelli enerji sistemlerine makul bir alternatif olabileceği sonucuna varılmıştır. Ayrıca, hidrojen depolama kapasitesi 45 m³'e çıkarıldığında, sistemin bir yıl boyunca sürekli olarak çalışabilme kabiliyeti kazandığı ve değişken geliş açılı PV panelleri kullanılarak genel sistem veriminin iyileştirildiği saptanmıştır. Dahası, PEM temelli sistem bileşenlerinin bozunmasının genel sistem performansı üzerinde zararlı etkileri olan önemli bir olgu olduğu sonucuna varılmıştır.

Anahtar Sözcükler: PEM yakıt hücresi bozunması; Hibrit yenilenebilir enerji sistemleri; ANSYS Fluent; TRNSYS; Enerji analizi; Ekserji analizi; Ekonomik analiz

To My Family

ACKNOWLEDGEMENTS

The author wishes to express his deepest gratitude to his supervisor Dr. İlker Tari for his close guidance, invaluable supervision, encouragement, support, criticism and insight throughout the study. The author also thankful to Dr. Tari for sharing his experiences and advices about real life. It was an honor for the author to study with Dr. Tari throughout this study.

The author would like to thank Dr. Frano Barbir for his cooperation in PEM Fuel Cell Laboratory in University of Split, Croatia. The author would also like to thank his colleagues Ali Karakuş, Ivan Tolj and Dario Bezmalinovic, for their practical help and support throughout the study.

The author would gratefully appreciate the support of all his colleagues in TAI but especially Hilmi Cavlı.

The author gratefully thanks to his family for their continuous encouragement, understanding and support.

This study was supported by TÜBİTAK (project no: TÜBİTAK 106G130).

TABLE OF CONTENTS

ABSTRACT	v
ÖZ	vii
ACKNOWLEDGEMENTS	x
TABLE OF CONTENTS	xi
LIST OF TABLES	xv
LIST OF FIGURES	xvii
LIST OF SYMBOLS	xxi
LIST OF ABBREVIATIONS	xxviii
CHAPTERS	
1. INTRODUCTION	1
1.1 Motivation.....	1
1.2 Objective.....	2
1.3 Literature Survey	3
1.3.1 Hybrid Renewable Energy Systems	3
1.3.2 System Modeling.....	6
1.3.3 Proton Exchange Membrane (PEM) Fuel Cells	9
1.3.3.1 Membrane Electrode Assembly (MEA)	11
1.3.3.2 Porous Electrode - Gas Diffusion Layer.....	11
1.3.3.3 Bipolar Plates.....	12
1.3.4 CFD Modeling.....	14
1.3.5 PEM Fuel Cell Degradation.....	19
1.3.5.1 Membrane Degradation	21
1.3.5.2 Catalyst Layer Degradation	22
1.3.5.3 GDL Degradation	23
1.3.5.4 Bipolar Plate Degradation.....	23
1.3.5.5 Sealing Gasket Degradation	24
1.4 Contribution	24

1.5 Thesis Layout	25
2. SYSTEM MODELING	27
2.1 System Description	27
2.1.1 Load Profile	29
2.1.2 PV Panels	30
2.1.3 Inverters	32
2.1.4 PEM Fuel Cell.....	34
2.1.5 PEM Electrolyzer.....	37
2.1.6 Gas Storage Tanks	38
2.2 System Simulations	38
2.2.1 Energy Analysis of the System	52
2.2.2 Exergy Analysis of the System	56
2.2.2.1 Exergy Analysis of the PV Panels	57
2.2.2.2 Exergy Analysis of the PEM Electrolyzer	62
2.2.2.3 Exergy Analysis of the PEM Fuel Cell.....	65
2.2.2.4 Exergy Analysis of the Inverters.....	68
2.2.2.5 Overall Exergy Analysis of the System.....	69
2.3 Economic Analysis of the System.....	72
2.4 Discussions.....	73
3. CFD MODELING	77
3.1 PEM Fuel Cell Model	77
3.1.1 Boundary and Operating Conditions.....	78
3.1.2 Model Domain	82
3.1.3 ANSYS Fluent Solver.....	85
3.2 Simulation Results	86
3.2.1 Velocity Distribution	86
3.2.2 Species Distribution	88
3.2.3 Current Density Distribution.....	90
3.2.4 Temperature Distribution.....	91
3.2.5 Pressure Distribution.....	95
3.2.6 Fuel Cell Performance	97

3.3 Stack Modeling	102
3.3.1 Sizing of a Fuel Cell Stack	106
3.3.2 Stack Performance	107
3.4 Discussions	111
4. FUEL CELL DEGRADATION	113
4.1 Degradation Modes	113
4.1.1 Membrane Degradation	114
4.1.2 Catalyst Layer Degradation	115
4.1.3 GDL Degradation	116
4.1.4 Bipolar Plate Degradation.....	117
4.2 Degraded Single Cell	118
4.3 Parametric Analysis	121
4.4 Degraded Stack Simulations	127
4.5 System Simulations with Degraded PEM Fuel Cells	130
4.6 Economic Analysis for Degraded System	133
4.7 Discussions	134
5. CONCLUSIONS	135
REFERENCES	139

APPENDICES

A. LEVELIZED COST OF ELECTRICITY (LCE) ANALYSIS OF THE HYBRID RENEWABLE ENERGY SYSTEM.....	159
A.1 LCE Analysis Method.....	159
A.2 LCE Analysis Assumptions.....	161
A.3 LCE Analysis for a PV/battery system.....	162
A.4 LCE Analysis for a Diesel Generator System.....	164
B. PEM FUEL CELL GOVERNING EQUATIONS.....	167
B.1 Continuity.....	168
B.2 Momentum.....	168
B.3 Species.....	168
B.4 Energy.....	169

B.5 Liquid Water Transport Equation.....	170
B.6 Potential Equations.....	171
C. DESIGNING HEAT EXCHANGER WITH VARIABLE SURFACE AREA FOR PASSIVE COOLING OF PEM FUEL CELL	173
C.1 Introduction.....	173
C.2 Methodology.....	176
C.3 Boundary Conditions.....	179
C.4 Results and Discussion.....	180
C.5 Conclusions.....	185
VITA	187

LIST OF TABLES

TABLES

Table 1 Summary of major failure modes in PEM fuel cells [81] [86].	25
Table 2 Electrical and thermal properties of the PV panels (adapted from internet source [107]).	31
Table 3 Monthly optimum PV panel slope for Ankara (adapted from TÜBİTAK Project Report [108]).	32
Table 4 Technical data of the PEM fuel cell system.	35
Table 5 Technical data of the PEM electrolyzer.	38
Table 6 Energy flow values of the system.	53
Table 7 Average energy and exergy efficiencies of the system components.	70
Table 8 Geometrical parameters and material details of the CFD model.	79
Table 9 Boundary and operating conditions of the CFD model.	81
Table 10 Inlet velocities.	81
Table 11 Mesh details.	85
Table 12 Comparison of performance of single cell fuel cell with multi-cell fuel cells.	108
Table 13 Average outlet temperatures of the anode and the cathode sides.	109
Table 14 Summary of the degraded parameters used in the degraded PEM fuel cell model.	118
Table 15 Details of the parametric analysis.	123
Table 16 Results of the parametric analysis (details are tabulated in Table 15).	126
Table 17 Energy flow values of the degraded system (after 2 years).	133
Table 18 The assumptions used in the LCE analysis.	162
Table 19 Comparison of assumptions of the batteries with other equipment.	163
Table 20 Details of the LCE analysis of the pure diesel generator system.	165

Table 21 Values for parameters used in CFD model experimental set-up [204].
..... 177

LIST OF FIGURES

FIGURES

Figure 1 Illustration of the investigated hybrid renewable energy system.	2
Figure 2 Basic operating principles and schematic representation of a PEM fuel cell.....	10
Figure 3 Flow field patterns used in bipolar plates of PEM fuel cells (adapted from Larminie and Dicks [33])......	13
Figure 4 Photograph of the solar-hydrogen based hybrid renewable energy system.	28
Figure 5 Simplified TRNSYS model of the system.....	29
Figure 6 Load profile of the system.	30
Figure 7 Tilttable platform of the PV panels.	33
Figure 8 Schematic representation of the system.....	33
Figure 9 Typical I-V curve of the fuel-cell module.....	36
Figure 10 TRNSYS model of the system.....	40
Figure 11 Monthly electricity production of the PV panels.....	42
Figure 12 Daily power output of the PV panels.	43
Figure 13 Power profiles of the components for a typical sunny summer day [time (hr)]......	44
Figure 14 Power profiles of the components for a typical cloudy winter day [time (hr)]......	45
Figure 15 Pressure level of the hydrogen tanks.	48
Figure 16 Power consumed by the PEM electrolyzer.....	49
Figure 17 Yearly operating time of the PEM fuel cell and the PEM electrolyzer.	50
Figure 18 Power profiles of the components and operating time of the PEM based components for a typical period of simulation time (23th and 24th of April).....	51

Figure 19 Energy flow-chart of the system.....	55
Figure 20 Comparison of the monthly electricity production of the PEM fuel cells and the PV Panels.	56
Figure 21 Grassmann diagram for the PV panels.	60
Figure 22 Energy end exergy efficiencies of the PV panels.	61
Figure 23 Grassmann diagram for the PEM electrolyzer.....	65
Figure 24 Grassmann diagram for the PEM fuel cell.....	68
Figure 25 Grassmann diagram for the exergy losses of the system.	71
Figure 26 PEM fuel cell model.	78
Figure 27 Simplified representation of the solution domain (not to scale).	80
Figure 28 Model domain.	83
Figure 29 Cross-section of the single channel of the domain.	84
Figure 30 Velocity distribution in the anode channel (high inlet humidity BC).	87
Figure 31 Velocity distribution in the cathode channel (high inlet humidity BC).	88
Figure 32 Mass fraction of H ₂ (high inlet humidity BC).	89
Figure 33 Mass fraction of H ₂ O (high inlet humidity BC).	90
Figure 34 Current density distribution on the MEA surface for high inlet humidity BC (for 0.35 A/cm ² current density).....	91
Figure 35 Temperature distribution of the membrane (high inlet humidity BC).	92
Figure 36 Temperature distribution at the mid-plane of the membrane (for $le/2$).	93
Figure 37 Temperature distributions inside 1 st , 5 th , 15 th and 20 th flow channels (high inlet humidity BC).	94
Figure 38 Section view of temperature distributions inside the 9 th , 10 th and 11 th flow channels (high inlet humidity BC).....	95
Figure 39 Pressure distribution inside the cathode flow channel (high inlet humidity BC).....	96

Figure 40 Pressure distribution inside the anode flow channel (high inlet humidity BC).	97
Figure 41 Voltage losses in the fuel cell and resulting polarization curve (adapted from Barbir [32]).....	99
Figure 42 Comparison of the theoretical and numerical polarization curves (high inlet humidity BC).....	101
Figure 43 Comparison of polarization curves for high inlet humidity and low inlet humidity boundary conditions.	102
Figure 44 Typical fuel cell stack configuration (adapted from Spiegel [156]).	103
Figure 45 Arrangement of the major cell components in a fuel cell stack (adapted from internet source [157]).	104
Figure 46 2-cell stack PEM fuel cell model.....	106
Figure 47 Comparison of stack performances with the single cell case.	110
Figure 48 Schematic diagram of a bulk electrical interface (adapted from Timsit [176]).	117
Figure 49 Comparison of performances of the fresh cell and the degraded cell (after 2 years).	119
Figure 50 Comparison of temperature contours of; (a) degraded cell (after 2 years), (b) fresh cell.	120
Figure 51 Comparison of temperature distribution of the membrane for: (a) degraded cell (after 2 years), (b) fresh cell.	121
Figure 52 Performances of the fresh stack and the degraded stack (2-cells, after 2 years).....	128
Figure 53 Performances of the fresh stack and the degraded stack (3-cells, after 2 years).....	129
Figure 54 Performances of the fresh stack and the degraded stack (4-cells, after 2 years).....	130
Figure 55 Comparison of pressure levels in the hydrogen tanks (after 2 years).	132

Figure 56 Half-cell cross-section of the PEM fuel cell (adapted from Kumar and Reddy [57]).....	167
Figure 57 Temperature and relative humidity profiles along the fuel cell cathode channel for two cases a) isothermal and b) non-isothermal so that relative humidity is kept close to 100% (adapted from Tolj et al. [204]).	175
Figure 58 PEM fuel cell segment (left); 3D PEM fuel cell model (right).	178
Figure 59 Heat transfer paths of the model.	179
Figure 60 Required heat exchanger area along the cathode channel.	181
Figure 61 Resulting heat exchanger with variable length fins.	183
Figure 62 Heat exchanger coupled with cathode side of the PEM fuel cell segment.	183
Figure 63 Temperature distribution of the heat exchanger.	184
Figure 64 Relative humidity of air along the cathode channel (air entrance is on the right side).....	185

LIST OF SYMBOLS

a	Water activity
A_{PEM}	PEM active surface area (cm ²)
A_{PV}	PV panel area (m ²)
A_r	Reaction area (cm ²)
A_w	Wall area (m ²)
c_i	Concentration of species i (mol/cm ³)
c_p	Heat capacity (kJ/kg K)
CP_i	Price of each equipment (\$)
C_t	Capacitance of a fuel cell stack (J/kg)
d	Annual interest rate (%)
d_c	Distance between channels (mm)
D_i	Diffusivity of species i (cm ² /s)
D_l	Membrane water diffusivity (cm ² /s)
E	Thermodynamic potential (V)
E_Dump	Dumped energy by the controller (MWh)
E_Elz	Energy directed to the electrolyzer by the controller (MWh)
E_FC	Energy generated by the PEM fuel cell (MWh)
E_H_2in	Energy capacity of the generated hydrogen by the electrolyzer (MWh)
E_H_2out	Energy capacity of consumed the hydrogen by the PEM fuel cell (MWh)
$E_Inverter$	Energy directed to the inverter by the controller (MWh)
E_PV	Energy produced by the PV panels (MWh)
E_Solar	Solar irradiation on the PV panels (MWh)

E_{User}	Energy supplied to the emergency room (MWh)
$\dot{E}\chi_{Elz,dest}$	Exergy destruction rate of the electrolyzer (W)
$\dot{E}\chi_{Elz,in,el}$	Electrical exergy input to the electrolyzer (W)
$\dot{E}\chi_{Elz,out,H_2}$	Hydrogen exergy output from the electrolyzer (W)
$\dot{E}\chi_{FC,dest}$	Exergy destruction rate of the fuel cell (W)
$\dot{E}\chi_{FC,in,H_2}$	Exergy input rate of the fuel cell (W)
$\dot{E}\chi_{FC,out,usf}$	Useful exergy output rate of the fuel cell (W)
$\dot{E}\chi_{S,dest}$	Exergy destruction rate of PV panels (W)
$\dot{E}\chi_{S,in}$	Exergy input of the PV panels (W)
$\dot{E}\chi_{S,loss}$	Exergy loss of the PV panels (W)
$\dot{E}\chi_{S,out,usf}$	Net useful exergy output of the PV panels (W)
ex_{ch}	Specific chemical exergy (kJ/kg)
ex_{ph}	Specific physical exergy (kJ/kg)
F	Faraday's constant (96485 C/mol)
g	Gravitational acceleration (9.81 m/s ²)
h_c	Channel height (mm)
h_{conv}	Convective heat transfer coefficient (W/m ² K)
\hat{h}	Specific enthalpy (kJ/kg)
\widehat{h}_0	Specific enthalpy calculated with respect to the reference state (kJ/kg)
I	Current (A)
$I_{H_2}^{xover}$	Hydrogen crossover current density (A/cm ²)
i_a	Anode current density (A/cm ²)
i_c	Cathode current density (A/cm ²)
I_{Elz}	Current of the electrolyzer (A)
i_L	Limiting current density (A/cm ²)

i_{loss}	Current loss (A/cm ²)
I_m	Maximum current of the PV panels (A)
i_0	Reference exchange current density (A/cm ²)
I_{FC}	Current of the fuel cell (A)
I_{sc}	Current temperature coefficient (A)
j_a	Transfer current density for anode side (A/m ³)
j_c	Transfer current density for cathode side (A/m ³)
J_w^{diff}	Back diffusion coefficient (cm ² /s)
k^{eff}	Effective thermal conductivity (W/m K)
k_{bp}	Bipolar plate thermal conductivity (W/m K)
k_{GDL}	GDL thermal conductivity (W/m K)
k_{MEA}	MEA thermal conductivity (W/m K)
k_w	Thermal conductivity of water (W/m K)
K	Absolute permeability (m ²)
K_{GDL}	GDL permeability (m ²)
l_e	Electrode length (cm)
M_m	Equivalent weight of membrane (g)
M_{h_2o}	Equivalent weight of H ₂ O (g)
\bar{M}_i	Molecular weight of species i (kg/mole)
\dot{m}_{Elz,H_2}	Hydrogen production rate of electrolyzer (kg/s)
\dot{m}_{FC,H_2}	Hydrogen consumption rate of fuel cell (kg/s)
n	Number of electrons involved
\hat{n}	Number of agglomerates per unit volume (m ⁻³)
ny	Number of years (in LCE analysis)
NC_p	Net present cost (\$)

N_{cell}	Number of cells in the fuel cell stack
OMC_P	Present operating and maintenance cost (\$)
P_{ele}	Electrolyzer power (W)
P_{fc}	Fuel cell power (W)
P_{pv}	PV panels power (W)
P_{mpp}	Power temperature coefficient (W)
p_{PEM}	PEM fuel cell operating pressure (N/m ²)
p_i	Partial pressure of component i (N/m ²)
p_c	Capillary pressure (N/m ²)
p_{H_2}	Partial pressure of hydrogen (N/m ²)
p_0	Reference state pressure (N/m ²)
PT_i	Projected lifetime of each equipment (years)
P_{sat}	Saturation pressure (N/m ²)
P_{wv}	Water vapor pressure (N/m ²)
$\dot{Q}_{S,loss}$	Heat loss rate (W)
Q_w	Heat transfer rate (W)
R	Gas constant (8.314 J/mol K)
R_f	Internal resistance (ohm-cm ²)
R_t	Overall thermal resistance of a fuel cell stack (K/W)
RT_i	Remaining lifetime of each equipment (years)
r_w	Condensation rate
s	Water saturation ratio
\hat{s}	Specific entropy (kJ/kg K)
\hat{s}_0	Specific entropy calculated with respect to reference state (kJ/kg K)
SC_{an}	Annualized cost of the system (\$/y)

SC_p	Present system cost (\$)
SS_p	Present system salvage (\$)
S_i	Source term for species ($\text{kg}/\text{m}^3 \text{ s}$)
S_{mass}	Source term for continuity equation ($\text{kg}/\text{m}^3 \text{ s}$)
S_{mom}	Source term for momentum equation (N/m^3)
S_S	Solar irradiation on the PV panels (W/m^2)
S_T	Heat source term for energy equation (W/m^3)
S_ϕ	Source term for potential equations (A/m^3)
t_{CL}	Catalyst layer thickness (micron)
t_{GDL}	GDL thickness (micron)
t_{MEA}	MEA thickness (micron)
T	Temperature (K)
T_{amb}	Ambient temperature (K)
T_{PEM}	Fuel cell operating temperature (K)
T_{PV}	PV panel surface temperature (K)
T_0	Reference state temperature (K)
T_{stack}	Stack operating temperature (K)
T_{sun}	Temperature of sun (K)
T_w	Wall temperature (K)
UE_{an}	Annual useful electricity (kWh/y)
U_0	Thermodynamic equilibrium potential (V)
V_{oc}	Voltage temperature coefficient (V)
V_{cell}	Cell potential (V)
V_{st}	Stack voltage (V)
V_{ctg}	Volume of polymer coating around agglomerate nucleus (m^3)

V_{ELZ}	Voltage of the electrolyzer (V)
V_{FC}	Voltage of the fuel cell (V)
V_m	Maximum voltage of PV panels (V)
V_{nuc}	Volume of agglomerate nucleus (m ³)
V_w	Wind velocity (m/s)
\vec{V}	Velocity vector
w_c	Channel width (mm)
w_e	Electrode width (cm)
W_{FC}	Stack power output (W)
X_i	Mass fraction of species i

GREEK SYMBOLS

α	Transfer coefficient
γ	Ratio of partial pressures of reactants
ε	Wet porosity
ε_{agg}	Volume fraction of polymer in agglomerate nucleus
ε_{cat}	Porosity of cathode catalyst layer
ε_{GDL}	GDL porosity
ε_N	Volume fraction of polymer electrolyte in cathode
ε_s	Volume fraction of platinum and carbon in cathode
η	Overvoltage (V)
η_{act}	Activation overvoltage (V)
η_{ohmic}	Ohmic overvoltage (V)
η_{stack}	Fuel cell stack efficiency
κ, δ	Coefficients of mass source term equation

λ	Water content of the membrane
μ_l	Liquid viscosity (Pa s)
ξ_{H_2}	Concentration of hydrogen in solution domain
ρ	Density (kg/m ³)
ρ_m	Density of the membrane (kg/m ³)
ρ_l	Liquid density (kg/m ³)
σ_{mem}	Membrane phase conductivity (1/(ohm m))
σ_{sol}	Solid phase conductivity (1/(ohm m))
φ	Adiabatic exponent
Φ_{mem}	Membrane phase potential (V)
Φ_{sol}	Solid phase potential (V)
ψ_{Elz}	Exergy efficiency of the electrolyzer
ψ_{FC}	Exergy efficiency of the PEM fuel cell
ψ_{IN}	Exergy efficiency of the inverters
ψ_s	Exergy efficiency of the PV panels
ψ_{Sys}	Overall exergy efficiency of the system
ω, β	Phase conductivity model constants

LIST OF ABBREVIATIONS

AC	Alternating Current
ARC	Annualized Replacement Cost
BC	Boundary Condition
BCGSTAB	Bi-Conjugate Gradient Stabilized Method
CFD	Computational Fluid Dynamics
CRF	Capital Recovery Factor
DC	Direct Current
GDL	Gas Diffusion Layer
HOMER	Hybrid Optimization Model for Electric Renewable
HVAC	Heating Ventilation and Air Conditioning
ICC	Initial Capital Cost
IEC	Ion-Exchange Capacities
LCE	Levelized Cost of Electricity
MEA	Membrane Electrode Assembly
PEM	Proton Exchange Membrane
PTFE	Poly Tetra-Fluoro-Ethylene
PV	Photovoltaic
RC	Replacement Cost
SAPS	Stand Alone Power System
SIMPLE	Semi-Implicit Method for Pressure Linked Equations
SOC	State of Charge
TMY	Typical Meteorological Year
TRNSYS	Transient Systems Simulation
VDC	Volts of Direct Current

CHAPTER 1

INTRODUCTION

1.1 Motivation

This thesis is an integrated part of the TÜBİTAK project 106G130. In this project, completely environmentally friendly and solar powered system that supplies continuous electricity to the emergency room of a hospital was developed and installed.

Among all of the public services, health services and hospitals providing that service should be able to run continuously especially after disasters. Power failure is intolerable in a hospital environment; thus, utilizing a backup power system is an important requirement. It is hard to meet the energy demand of the user (hospital emergency room) especially in emergency blackout conditions. The easiest solution would be the use of diesel power generators. However, as commonly accepted, fossil fuels have various undesirable impacts on environment, and they may be hard to continuously obtain during a long lasting emergency. The motivation of this study is to demonstrate that a solar-hydrogen based renewable energy system can be a viable alternative to fossil fuel energy systems. The long-term performance of a hydrogen based systems is not clear in minds. This motivates us to fully investigate feasibility of utilizing environmentally friendly solar-hydrogen based energy system and reliability of such systems that can be affected by the degradation of the hydrogen based components.

1.2 Objective

In this study, solar-hydrogen based hybrid renewable energy system that was built for the emergency room of Keçiören Research and Training Hospital is simulated. The system provides continuous, off-grid electricity during the period of a whole year without any external electrical power supply. The system consists of Photovoltaic (PV) panels, Proton Exchange Membrane (PEM) based electrolyzers and fuel cells, hydrogen and oxygen tanks, controllers and inverters. In Figure 1, illustration of the investigated solar-hydrogen based hybrid renewable energy system is shown. A complete model of the system is developed using Transient Systems Simulation (TRNSYS). The objective of this work is to investigate the overall performance of the established hybrid renewable energy system and PEM fuel cell degradation. Then, the results of the degraded PEM fuel cell are implemented within the system model and the overall performance of the system with the degraded PEM fuel cells is studied.

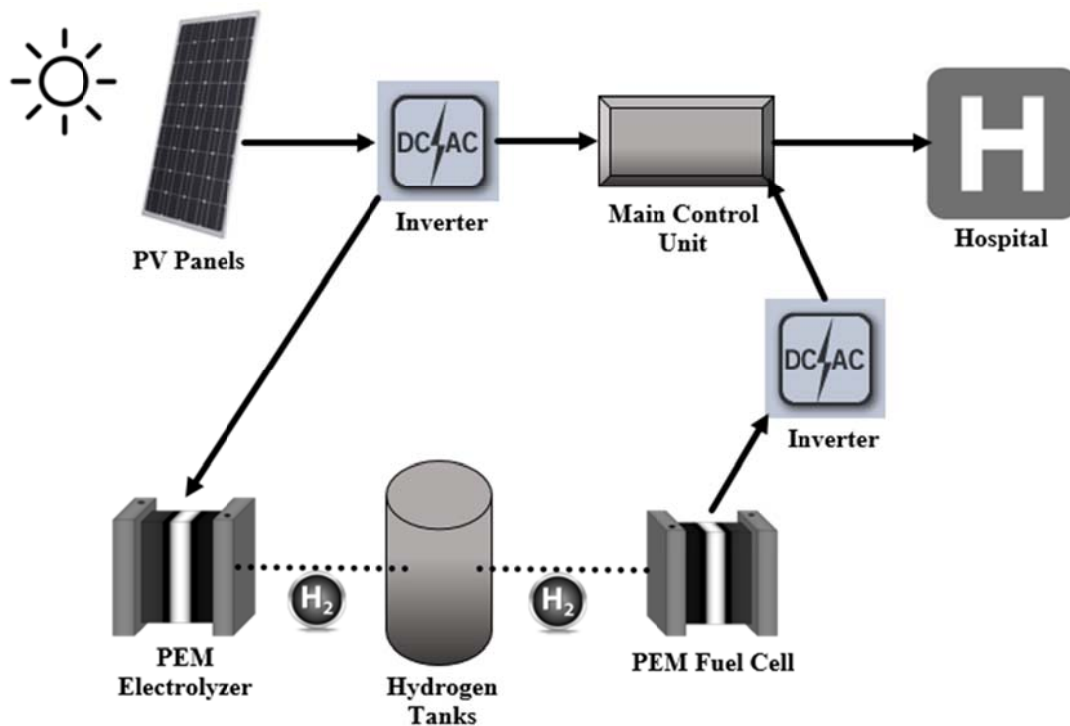


Figure 1 Illustration of the investigated hybrid renewable energy system.

1.3 Literature Survey

Hydrogen technologies and hydrogen energy are not commonly used in Turkey. But, hydrogen energy is a fast developing area which needs to be considered and investigated globally and for Turkey. Çelikleş and Koçar [1] claimed that hydrogen technologies are forecasted to have great socioeconomic impacts in the future. Also, more integration and cooperation of different research areas needed to encourage hydrogen research and development studies. Yolcular [2] studied hydrogen production for energy use in Turkey and highlighted the importance of hydrogen production from primary renewable energy sources. Yazıcı [3] mentioned the social and the economic benefits of hydrogen technologies for Turkey.

Literature survey starts with a brief overview of hybrid renewable energy systems. Then, a review of system modeling literature is presented. Next, PEM fuel cells are introduced and Computational Fluid Dynamics (CFD) modeling of PEM fuel cells is discussed. Last, PEM fuel cell degradation phenomenon is discussed in detail.

1.3.1 Hybrid Renewable Energy Systems

Ever increasing energy demand and the fossil fuel use for satisfying this demand causes global warming and rapid depletion of conventional fuel sources. Emission problems and increasing cost of the fossil fuels are the main problems that make people to consider alternative resources for energy production. Renewable energy is a rational option that continues to gain acceptance of people. It is possible to generate renewable energy from natural sources like wind, sun, geothermal, biofuels or hydro-electric power.

For low energy demand off-grid systems, single technology based renewable energy systems (solar, wind, small hydro) seems to be a feasible option. However, it is not possible to meet the demand throughout the year by using only a single technology based system, because renewable energy resources are extremely site-specific and

intermittent. Some of the energy sources are available in abundance in certain seasons and others in other seasons.

According to Chauhan and Saini [4] high system costs and low reliability are usually associated with single technology based renewable energy systems. Therefore, energy systems should be coupled to form an off-grid and independent energy supply system. This type of systems is called hybrid renewable energy systems.

The investigated system is capable of working in stand-alone mode. From this point of view, the investigated system can also be called as Stand Alone Power System (SAPS). In the stand-alone mode, transportation of conventional energy sources is rather difficult and renewable energy sources are usually preferred to feed the system. Utilization of locally accessible resources seems to be the best possible choice to meet the energy requirements. SAPS are commonly used in off-grid locations, such as base stations. Also, a SAPS is needed in an emergency situation, in which it may not be possible to obtain energy from the grid.

In hybrid renewable energy systems, integrated use of different energy resources reduces energy storage requirement. Also it is possible to improve the reliability of the system and the quality of the power by using hybrid systems. Renewable energy systems should be coupled with storage systems, in order to cope with intermittency of renewable resources like solar energy. Barton and Infield [5] stated that it is possible to smooth out load variations, control and reduce the peak power demand, and have uninterrupted energy sources, when energy storage systems are used with hybrid renewable energy systems. According to Abbey et al. [6] energy storage technologies, which are applicable to power systems, are grouped based on storage duration: short term storage (capacitors, super-capacitors and flywheels), medium term storage (batteries, fuel cells and compressed air) and long term storage (pumped storage).

In the investigated renewable energy system, hydrogen is used as an energy carrier forming an idealized “energy cycle”, which is discussed by Marshall [7] in detail. In the ideal energy cycle, water is split into hydrogen and oxygen using renewable energy sources. Then, the hydrogen is stored to be used in a fuel cell to generate electricity with water as a byproduct. Thus, so called “hydrogen cycle” is utilized in the system. The only output of this cycle is the electrical energy generated by the fuel cell, and the only input is the renewable energy from environmentally friendly sources. The investigated energy system has the advantage that, unlike other hybrid systems, power demand from the system is taken as constant (there is no seasonal or monthly variations). Therefore, utilizing hydrogen cycle for the investigated system is a rational option.

Hydrogen fueled PEM fuel cell based energy systems have some important advantages over other types of energy systems [8]:

- very quiet operation
- high energy conversion efficiency
- high flexibility (high working efficiency at low powers)
- zero emissions
- operating at lower temperatures
- easy and inexpensive maintenance (very few moving parts, no lubrication need)

In the investigated hybrid renewable energy system PEM electrolyzers are used with PEM fuel cells, because PEM electrolyzers have various advantages compared to other types of electrolyzers, such as alkaline electrolyzers. The advantages of using PEM electrolyzers are as follows [9]:

- high efficiency
- high operating current
- high operating pressure
- ease of operation
- compactness

PEM electrolyzers mainly operate at low DC voltages; so, they have also the advantage of direct coupling to PV Panels.

High performance PV panels are used in the system. Inverters and main control unit are used in the system to meet the demand of the emergency room effectively. DC/AC inverters are used between the PV panels and the main control unit and between the PEM fuel cell stack and the main control unit. Produced hydrogen is stored in the hydrogen tanks. Produced oxygen will be used in the hospital, thus an oxygen tank is also included in the system.

1.3.2 System Modeling

Sinha and Chandel [10] stated that because of the multiple energy generation systems, hybrid renewable energy system modeling is complex and requires to be analyzed deeply. Software tools and models are required for the design, analysis, optimization and economical planning of hybrid renewable energy system modeling. Software tools are extensively used for optimal sizing of hybrid renewable energy systems. Turcotte et al. [11] classified software tools related with hybrid energy system modeling in four categories; pre-feasibility, sizing, simulation and open architecture research tools. Pre-feasibility tools are commonly used for coarse sizing and extensive cost analysis. Sizing tools are usually used for dimensioning of the system providing detailed information about energy flows through the system. In simulation tools, each component of the system is specified in detail in order to see the overall performance of the system. In open architecture research tools, user can modify the algorithms and interactions between components of the system. This type of research tools can be programmed and compiled in a computer language, such as FORTRAN, C or Pascal. Main advantages of using a computer language with a software tool are that new components can be added and the existing components can be improved.

In the literature, among various software tools, TRNSYS, HOMER, MATLAB Simulink and BCVTB are used for system modeling of hybrid renewable energy systems. Among other simulation tools, here, TRNSYS is selected for system simulations. TRNSYS has some advantages over other simulation tools. Shahrestani et al. [12] stated that full integration capability of the user defined components within TRNSYS is an important advantage. Duffy et al. [13] mentioned that flexibility, computing time, and the user friendly interface, which requires less input effort, are the main advantages of TRNSYS over other simulation tools.

In this study, TRNSYS (version 16) is used for system modeling. In literature, TRNSYS is classified as an open architecture research tool [11]. TRNSYS was developed by The Solar Energy Laboratory at the University of Wisconsin, Madison. TRNSYS is a transient simulation program mainly used in the fields of renewable energy systems, building simulation, HVAC systems, solar systems, cogeneration systems and fuel cell systems [14]. TRNSYS simulates the overall performance of the complete energy system by dividing it into separate components. Many of the components commonly used in thermal and electrical energy systems are available in TRNSYS library. Also, it is possible to define new components or modify existing components by using a FORTRAN compiler.

TRNSYS is widely used in several renewable energy system simulation studies in literature. Ulleberg and Morner [15] used TRNSYS to simulate yearly performance of a renewable hydrogen generation and utilization system. Rockendorf et al. [16] used TRNSYS for modeling photovoltaic–solar thermal collector hybrid systems. Schucan [17] used TRNSYS for PV array sizing. Samaniego et al. [18] performed economic and technical investigation of a hybrid wind-fuel cell energy system by using TRNSYS. Almeida et al. [19] used TRNSYS to simulate and optimize solar-thermal energy system. Chargui and Sammouda [20] mathematically modeled a typical house in Tunisia and investigated energy consumption and air-conditioning load of the house by using TRNSYS. Kalogirou [21] used TRNSYS for analyzing a hybrid PV-thermal system and stated that by using a hybrid energy system, it is

possible to increase the efficiency of an existing solar energy system from 2.8% to 7.7%. Ulleberg [22] conducted system simulations for a stand-alone photovoltaic-hydrogen energy plant in Jülich, Germany by using TRNSYS. In [22], mathematical and dynamic thermal models for an alkaline electrolyzer were developed and implemented in TRNSYS. System simulations are conducted for a period of a whole year. It was concluded that it is possible to improve the electrolyzer operating strategies by performing system modeling study. Ulleberg [23] also studied control strategies of a PV-hydrogen system including electrolyzer, hydrogen storage and fuel cell. TRNSYS was used to test the same reference system in Jülich, Germany. Ghosh et al. [24] also analyzed the same system by using TRNSYS. It was stated that there was an energy deficit of 10-14% observed in the system. The main reason of the deficit was reported as the inclination angle of the PV panels.

Rohani and Nour [25] modeled and simulated a stand-alone hybrid renewable energy system in United Arab Emirates by using HOMER (Hybrid Optimization Model for Electric Renewable). Also, techno-economic analysis of the energy system was performed and found that hybrid renewable energy systems are feasible than fossil fuel based systems because of the increasing fossil fuel prices. Zoulias and Lymberopoulos [26] also used HOMER for modeling a hybrid renewable energy system, in which hydrogen based energy systems were compared with diesel generator-battery systems. It was concluded that hydrogen based energy systems decrease emissions, noise and fossil fuel necessity. Khan and Iqbal [27] used HOMER for modeling a stand-alone hybrid energy system in which hydrogen was used as an energy carrier. Sizing, performance and economic aspects of the system were analyzed by using HOMER.

El-Shatter et al. [28] designed and simulated a hybrid PV-fuel cell-electrolyzer system by using MATLAB Simulink, in which solar radiation incident on the surface of the PV panels and the surface temperature of the PV panels were coupled to obtain maximum solar power from the PV panels under variable solar radiation conditions.

Jiang [29] worked on control strategies of a hybrid renewable energy system by using Building Controls Virtual Test Bed (BCVTB). It was concentrated on maximum power tracking of PV panels. It was shown that the developed power strategy effectively controls the power of each component accurately.

In Subsection 1.3.3 literature survey of PEM fuel cells and modeling of PEM fuel cells are presented. The PEM fuel cells are modeled in ANSYS Fluent in order to obtain data for the system model. The obtained simulation data is used both for the PEM fuel cells and the PEM based electrolyzers in the system simulations.

1.3.3 Proton Exchange Membrane (PEM) Fuel Cells

A fuel cell is an electrochemical energy converting device, which transforms the chemical energy stored in a fuel into electrical energy. PEM is the abbreviation of Proton Exchange Membrane or Proton Electrolyte Membrane in literature. In PEM fuel cells, proton conductive polymer membrane is used as the electrolyte. PEM fuel cells present a promising alternative energy source over fossil fuels. Barbir [30] stated that the advantages, such as zero emission capability, fast response to varying loads, low operating temperatures, comparatively quick start-up, high power density (in kW/kg and kW/l) and high efficiency make PEM fuel cells a reasonable technological option.

Basic operating principles and a schematic representation of cell configuration of a PEM fuel cell are presented in Figure 2. Membrane is the most important component of a PEM fuel cell. Membrane has unique characteristics. It is impermeable to gases but it has high protonic conductivity. Membrane is sandwiched between two porous electrodes which are generally made out of carbon cloth or carbon-fiber paper. Between the electrode and the membrane a catalyst layer exists. The polymer electrolyte membrane is bonded to the catalyst layer. In literature, membrane-catalyst layer assembly is usually referred as Membrane Electrode Assembly (MEA).

Electrochemical reactions take place at the surface of the catalyst layer. Hydrogen is supplied on one side of the membrane as fuel. Hydrogen splits into protons and electrons at the catalyst layer. Protons travel over the membrane and the electrons travel through the electrodes, collector plate, outside circuit and returns to the other side of the membrane. At the other side of the membrane, electrons encounter with protons that travel over the membrane and oxygen that is supplied on that side. In the electrochemical reactions water is formed. The hydrogen side is negative; thus, this side is called the anode. On the other hand, the oxygen side is positive; thus, this side is called the cathode.

In this thesis, low temperature fuel cells are studied. In low temperature fuel cells a solid polymer membrane is used as the electrolyte. This type of fuel cells operates at temperatures below 100°C. Low temperature operation results in better durability and rapid start-up.

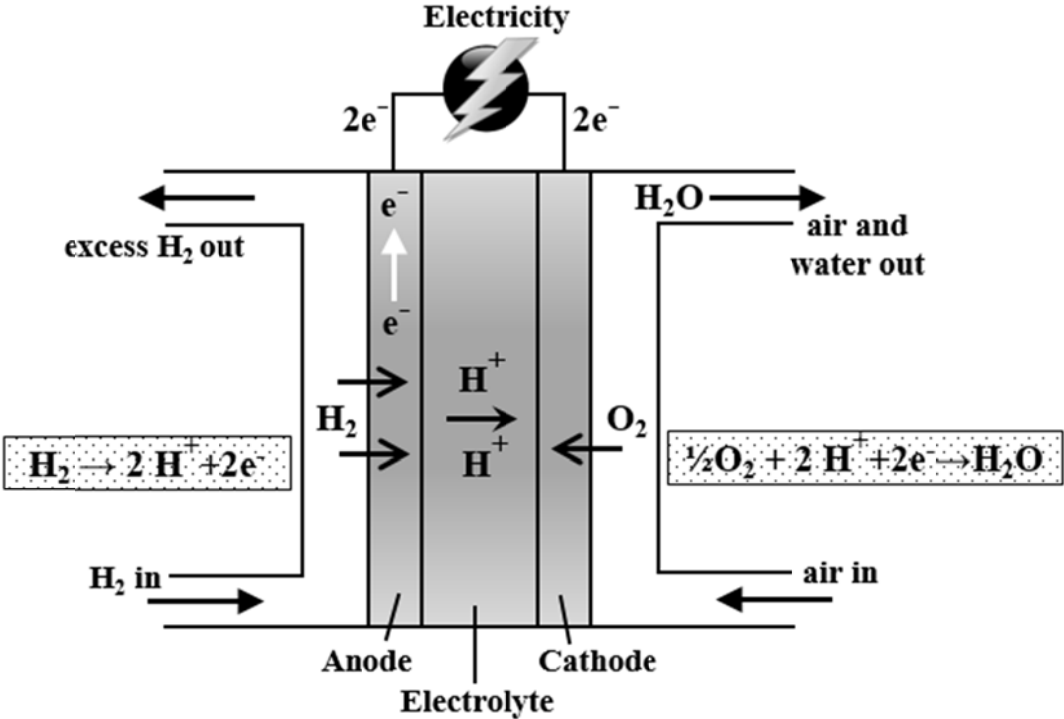


Figure 2 Basic operating principles and schematic representation of a PEM fuel cell.

The key components of a basic PEM fuel cell including MEA, porous electrode and bipolar plates are explained in Subsections 1.3.3.1, 1.3.3.2 and 1.3.3.3.

1.3.3.1 Membrane Electrode Assembly (MEA)

Membrane of a fuel cell is squeezed between two electrodes. Catalyst layers of the fuel cell are usually embedded at the sides of the membrane forming MEA of the cell. The function of the membrane of a fuel cell is to be a good barrier to mixing of fuel and reactant gases. Also, the membrane must be a good distributor and conductor of protons, and insulator for electrons by directing them to go through the external circuit. Moreover, Gottesfeld and Zawodzinski [31] stated that the membrane shall be chemically and mechanically stable in the fuel cell operating medium.

Catalyst layer, which is embedded at the sides of the membrane, is the layer where the electrochemical reactions take place. Gases, electrons and protons, are the three kinds of species that take place in the electrochemical reactions, are available on the catalyst surface. The most frequently used catalyst material in PEM fuel cells is platinum. According to Barbir [32], successful utilization of Platinum leads to significant improvement on the PEM fuel cell performance.

1.3.3.2 Porous Electrode - Gas Diffusion Layer

The layer between the catalyst layer and the bipolar plates is called porous electrode or Gas Diffusion Layer (GDL) of the PEM fuel cell. The GDL does not have a direct role in the electrochemical reactions, but GDL has various important functions in PEM fuel cells. The main functions of the GDL are listed below [32] [33]:

- It provides a structural support between the bipolar plates and the catalyst layer.
- It distributes the reactant gases through the flow field to the catalyst layer.
- It provides a passageway for water from the MEA to the gas flow channels.

- It allows the electrons to complete the electrical circuit by electrically connecting the MEA with the bipolar plate.
- It controls the MEA temperature by removing heat from the reaction sites.

Generally carbon-fiber paper and carbon cloth materials are used in the GDL. These materials are very soft and vulnerable to deformation. Therefore, the GDL must be carefully compressed to minimize the contact resistance losses without deforming the material.

1.3.3.3 Bipolar Plates

PEM fuel cells are constructed by putting together multiple cells connected in series with bipolar plates. Two plates on each side of the MEA can be regarded as two halves of a bipolar plate. Bipolar plates perform various functions simultaneously in PEM fuel cells [34] [35]:

- They distribute the reactants through the flow-field channels that are machined on them.
- They separate the reactants between adjacent cells.
- They provide structural support for the thin MEA and the entire PEM fuel cell.
- They remove excess heat from the PEM fuel cell.
- They provide electrically conductive part between adjacent cells.
- They facilitate water management within the cell.

There are several configurations of flow-field channels that have been used in PEM fuel cells. In Figure 3, samples of different flow field pattern designs are presented. These flow field patterns are commonly used in PEM fuel cells. The main purpose of the flow-field is to ensure uniform distribution of the reactant gases through the flow channels. Each flow-field design has advantages and disadvantages.

In Figure 3-a, the parallel flow-field design is shown. The problem of this design is that it is possible for liquid water or some reactants to build up in one of the

channels. This results in a region of the electrode without supplied with reactants. To avoid a blockage in the channel, serpentine type flow fields are designed (see Figure 3-b). The problem with this type of flow-field design is the path length and the large number of U-turns causing high pressure drop through the cell. Parallel serpentine flow-field design is used for taking advantages of both the parallel and the serpentine flow-fields (see Figure 3-c).

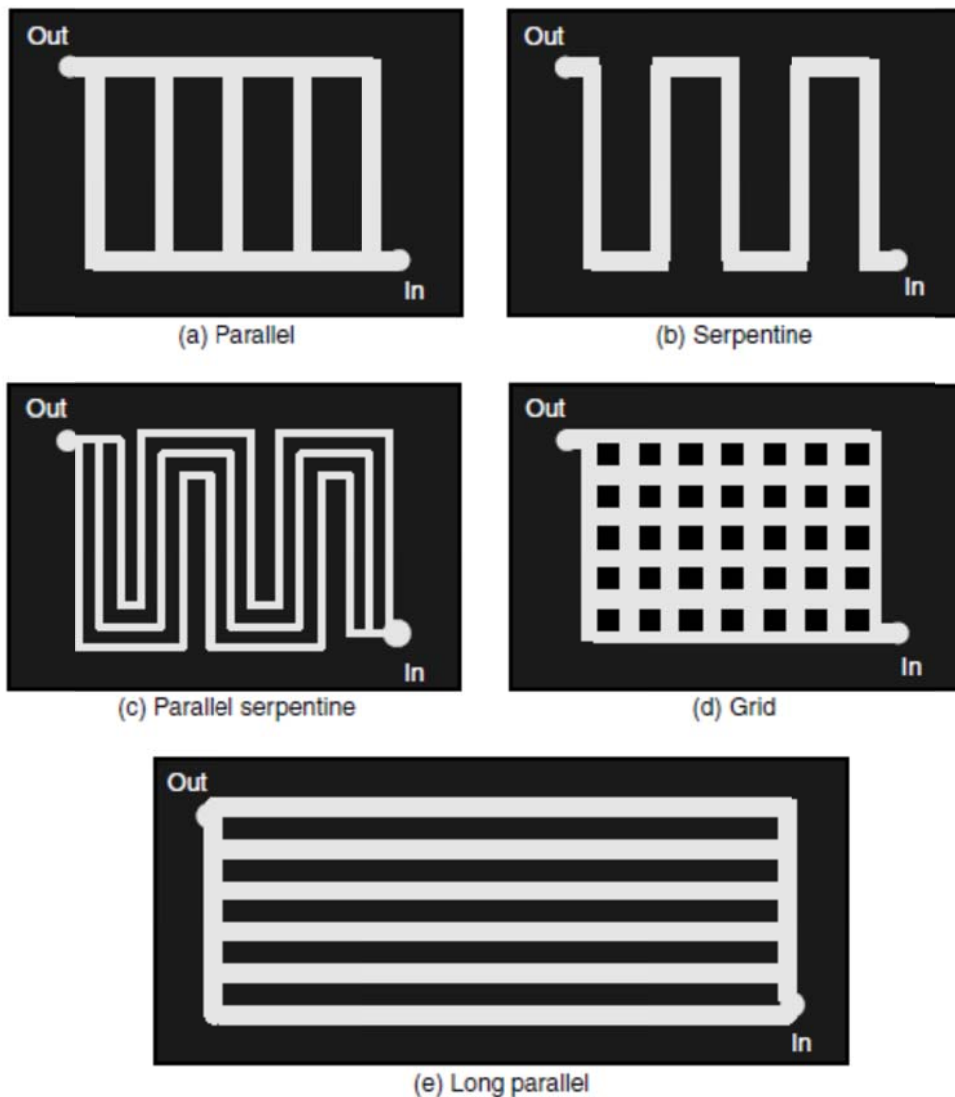


Figure 3 Flow field patterns used in bipolar plates of PEM fuel cells (adapted from Larminie and Dicks [33]).

The pattern of Figure 3-d is described as “intensely parallel”. The reactants can swirl over the face of the GDL. Nonetheless, it could still be possible to form water droplets, which could block some part of the flow-field.

Using rectangular bipolar plates is another option (see Figure 3-e). This type of flow-field consists of long straight parts, which has the advantage of being long enough to have reasonable pressure drop with no ineffective bends and turns. However, the main disadvantage of this design can be explained as the difficulty of having same amount of flow rate in each channel.

Li and Sabir [34] claimed that serpentine type flow field design can improve reactant flow distribution across the MEA surface of the PEM fuel cells. Consequently, in this study, it is decided to investigate PEM fuel cells with serpentine type flow channels. It is accepted that uniformity of the flow across the cell is more important than the pressure drop throughout the cell.

The MEA, the GDL and the bipolar plates are the important components of a PEM fuel cell and these components must be successfully modeled in a complete PEM fuel cell model. In Subsection 1.3.4 the literature survey about CFD modeling of PEM fuel cells is presented.

1.3.4 CFD Modeling

In this thesis, CFD modeling is performed by using ANSYS Fluent version 14.5. Fuel Cell and Electrolysis add-on module is used for modeling the PEM fuel cell in the present solar-hydrogen hybrid renewable energy system. By using Fuel Cell and Electrolysis module, it is possible to model all of the components of PEM fuel cells. In this add-on module, two electric potential fields are solved simultaneously. One of the potentials is solved in the membrane and the catalyst layer. The other is solved in the catalyst layer, GDL and the bipolar plates. The rate of electro-chemical reactions are calculated in catalyst layers of the anode and the cathode [36].

CFD is a very effective tool for analyze of internal phenomena throughout each component of a PEM fuel cell. Siegel stated that [37] because of the spatial dimensions of PEM fuel cells, it is very difficult to measure internal quantities, such as species concentrations, temperature gradients or pressure distributions. According to Bıyıkođlu [38], when CFD modeling is used for PEM fuel cell modeling, it is possible to investigate detailed geometries and it is easier to handle complex situations by expending less time and effort than experimental studies. In literature, CFD modeling is extensively used for simulating multi-physics phenomena of fuel cells [39]. Moreover, CFD modeling is mentioned as a practical tool for optimizing fuel cell designs [30].

Djilali [40] stated that one of the most inspiring aspects of CFD modeling of PEM fuel cells is the multi-physics nature of the transport processes, and the coupling between these processes. Computational fuel cell modeling has been started with 1D models. Using specified boundary conditions general transport equations are solved for desired parameters. These 1D models provide valuable information to researchers, especially while developing 2D and 3D models. More realistic models have been developed by using 2D models. 2D models are mostly used for the investigation of heat and mass transfer and fluxes in the 2D domain. If the boundary and initial conditions are selected carefully, 1D and 2D models provide necessary information to the 3D models. It is better to develop a 3D model, when the overall performance of the PEM fuel cell is going to be analyzed.

In the literature, 2D models using CFD techniques presented mainly for representing heat and mass transfer and fluxes inside the fuel cells. Gurau et al. [41] developed a 2D mathematical model for the complete domain of PEM fuel cell. Porous medium model was used for the solving equations characterizing transport phenomena observed in the membrane, catalyst layers, and gas diffusing layers. Um et al. [42] set a transient, multidimensional model to analyze PEM fuel cells. Using a finite volume based CFD technique, conservation equations for flow channels, gas

diffusion layers and MEA were numerically analyzed. The numerical model was validated using published experimental data. Wang et al. [43] studied two-phase flow inside the cathode flow channels of the PEM fuel cells. Finite volume based CFD technique was used with multi component mixture model for modeling the flow two-phase flow phenomenon inside cathode channels.

2D models cannot capture the complexity of a single cell; thus, 3D models are required to represent all the physical and chemical phenomena inside the fuel cell. Berning et al. [44] developed a complete, non-isothermal, 3D model of a PEM fuel cell. The developed model resolves all main transport phenomena inside the PEM fuel cell excluding phase change phenomenon. The model was implemented in a CFD code. 3D distributions of reactant concentrations, current densities, and temperature and water fluxes were included in the developed model. Sivertsen and Djilali [45] performed a similar study by developing a 3D model of PEM fuel cells, in which parallel computing was used. The developed model simulated the heat transfer and fluid transport phenomena inside the channels and the GDL of PEM fuel cells. Berning and Djilali [46] developed a similar model including phase change and heat transfer. Berning and Djilali [47] also performed a parametric study on analysis of transport phenomena in PEM fuel cells including the effect of operational parameters such as the temperature and pressure on the fuel cell performance. Al-Baghdadi and Al-Janabi [48] [49] conducted an optimization study using a complete 3D, multi-phase, non-isothermal model of PEM fuel cells. The developed model includes the important processes and parameters affecting the performance of fuel cells. Detailed analyses of the performance of the fuel cell under several operating conditions were examined by using CFD.

In literature, by using CFD serpentine type flow field designs are investigated in detail. Dutta et al. [50] established a numerical model for PEM fuel cells. The 3D Navier-Stokes equations for serpentine type geometry are solved with multispecies mixture model. Nguyen [51] also developed a 3D computational model of PEM fuel cell with serpentine type flow channels, in which a voltage to current algorithm,

which solves for the potential fields, is implemented for the calculation of the activation potential. Same model was used by Nguyen et al. [52] [53] for modeling the transport phenomena in PEM fuel cells including electrode kinetics, convective and diffusive heat and mass transfer, and potential fields.

ANSYS Fluent is extensively used for PEM fuel cell modeling in the literature. Shimpalee et al. [54] [55] developed multi-dimensional PEM fuel cell models using ANSYS Fluent. Current density and temperature distribution inside the fuel was computationally investigated. Kumar and Reddy [56] [57] [58] developed a three-dimensional half-cell model using ANSYS Fluent for investigating the effects of bipolar plate design on fuel cells performance. Reddy and Javanti [59] investigated different heat removal strategies for a fuel cell stack using ANSYS Fluent. Iranzo et al. [60] [61] developed CFD model for a fuel cell with serpentine and parallel flow fields with ANSYS Fluent. CFD model was validated using local water distributions, which were measured with neutron imaging [62]. Quan et al. [63] simulated various PEM fuel cell operating conditions using ANSYS Fluent, in which water management phenomenon inside the flow channels was investigated. Hontanon et al. [64] performed 3D numerical simulations of gas flow phenomenon in PEM fuel cells by using ANSYS Fluent, in which two types of flow distributions were investigated: a porous material and a conventional bipolar plate with parallel flow channels. The main goal of the authors was to optimize the design of the gas flow distribution system for PEM fuel cells.

In the present study, Fuel Cell and Electrolysis add-on module of the ANSYS Fluent is used for modeling the PEM fuel cells in detail. In the literature, instead of the add-on module, user defined functions are commonly used. Zhang and Pitchumani [65] presented a 2D, non-isothermal steady-state computational model to simulate the performance of an air-breathing PEM fuel cell, in which there are no flow channels at the cathode side; thus, air is supplied by natural convection, in which, the effects of various operating parameters on the cell performance were analyzed. ANSYS Fluent with user defined functions was used to solve the

developed model. Rajani and Kolar [66] studied 2D, steady state, single phase, non-isothermal, comprehensive model of an air-breathing PEM fuel cell, in which ANSYS Fluent with user defined functions was also used. Meng [67] presented a transient, two-phase, non-isothermal PEM fuel cell model. The investigated fuel cell model was developed in ANSYS Fluent, through user defined functions. Pasaogullari and Wang [68] developed an isothermal, two-phase model of a PEM fuel cell by using ANSYS Fluent. User defined functions was implemented into the CFD model, in which SIMPLE algorithm was used to solve discretized equations. A model fully coupling the flow, species transport, and electrochemical kinetics in PEM fuel cells was presented by Wang and Wang [69]. SIMPLE algorithm with user defined functions was also used to implement the developed model into ANSYS Fluent. De Giorgi and Ficarella [70] implemented a 3D, non-isothermal computational model of PEM fuel cell in ANSYS Fluent using user defined functions.

Besides ANSYS Fluent, CFX, CFD-ACE, STAR-CD and COMSOL Multi-physics (FEMLAB) are some of the other powerful CFD software tools, which are also used for PEM fuel cell modeling in the literature. Berning et al. [44] [46] conducted comprehensive thermal and water management study for PEM fuel cells by using CFX. Mazumder and Cole [71] [72] used CFD-ACE for modeling PEM fuel cells. Shimpalee et al. [73] [74] [75] studied the transient response of serpentine flow field PEM fuel cells, in which STAR-CD with an add-on PEM fuel cell module was used. Ju and Wang [76] also used STAR-CD for modeling PEM fuel cells. Karnoven et al. [77] developed isothermal 2D and 3D PEM fuel cell flow field models by using FEMLAB, in which the models were analyzed with governing equations simplified based on some approximations. Yalcinoz and Alam [78] developed a dynamic model of an air-breathing PEM fuel cell for mobile applications by using MATLAB, in which the PEM fuel cell model was compared with different air-breathing PEM fuel cell designs.

In this study, PEM fuel cells are numerically modeled in ANSYS Fluent. The developed numerical model later modified to include cell degradation in order to obtain data for the degraded system model in TRNSYS. In Subsection 1.3.5, the literature survey related with PEM fuel cell degradation is presented.

1.3.5 PEM Fuel Cell Degradation

Robustness of PEM fuel cells can be defined as the capability of a PEM fuel cell to resist against permanent transformation in terms of performance over time. Because of the voltage potential difference, which can result in undesired reactions, and corrosive working environment, PEM fuel cells are vulnerable to degradation. In general, degradation is accelerated by the following factors [79]:

- Operation at low-humidity or high-temperature conditions
- Destructive load cycling from low to high cell voltages
- Substantial temperature or humidity fluctuations in the operating environment including freezing

PEM fuel cell robustness is an important phenomenon, which has been delaying commercialization of the PEM fuel cells. In the literature, much attention is currently given to investigating the factors that affect PEM fuel cell durability, in order to extend lifetime of fuel cells without sacrificing cost or performance [80].

Wu et al. [81] reviewed and categorized various degradation mechanisms of PEM fuel cells; in that work, investigation of the durability of the individual components of PEM fuel cells was presented. Borup et al. [82] studied durability targets, durability testing methods and the effect of operating conditions on durability. Membrane, electro-catalysts and gas-diffusion media degradation issues were also studied by the authors.

Experimental studies and theoretical models about the degradation of PEM fuel cells are available in the literature. Madden et al. [83] and Gummala et al. [84] conducted experimental and theoretical studies on degradation of PEM fuel cells.

Effects of oxygen concentration, relative humidity, temperature, and membrane thickness were discussed under open-circuit decay conditions.

There has been an interest in the study of degradation phenomenon in PEM fuel cells. This has been driven by the need to ensure stability, durability and reliability of performance of the fuel cells, as in [85]. Following terms are defined in the literature to figure out MEA integrity and performance decay in PEM fuel cells [81] [86] [87] [88]:

- **Reliability:** MEA failure is normally defined as the inability of the MEA to operate at start-up, or after a period of time. Reliability study of the MEA includes failure modes, which can result in catastrophic failure or very low performance. MEA reliability problems are generally related with the quality of the MEA manufacturing process.
- **Durability:** This subject is directly related with degradation and can be defined as the capability of the MEA to withstand irreversible changes over time. Durability decay rate is increased by permanent material changes occurring in the cell.
- **Stability:** The capability of recovering from a possible performance drop during continuous operation is the stability of a PEM fuel cell. MEA performance loss can be observed due to stability decay. This performance loss is related with operating conditions (i.e. water management, temperature) and reversible changes of the materials.

Recently, different aspects of PEM fuel cell degradation are investigated by considering recoverable degradation and natural degradation phenomena resulting from certain non-operative period. Zhan et al. [89] investigated natural degradation and stimulated recovery of PEM fuel cells by analyzing performance degradation of a PEM fuel cell stack over a storage duration of 40,000 hours. It was concluded that natural degradation of the fuel cells primarily caused by dehydration of the membrane. Wang et al. [90] studied recoverable degradation of PEM fuel cells under various operating conditions. Mainly, the authors concentrated on the effects

of relative humidity under drive cycle. It was reported that after 5 hours of operation time, the cell performance was decreased for the both anode side and the cathode side. It was observed that the performance loss was mostly recovered after one night rest at most of the humidity conditions except the low humidity condition. In other words, unrecoverable degradation was directly related with dehydration of the membrane. Zhang et al. [91] conducted a study on the degradation mechanisms of catalyst layers of the PEM fuel cells considering recoverable and unrecoverable losses. It was emphasized that recoverable losses are associated with the reduction of Pt oxide inside the catalyst layer.

PEM electrolyzers share similar degradation problems with PEM fuel cells, since PEM electrolyzers have the same operating fluids and similar operating conditions with PEM fuel cells. Therefore, findings of and experiences gained from PEM fuel cell degradation studies can be implemented to PEM electrolyzers, as suggested by Liu et al. [92].

In the following subsections, major failure modes of different components of PEM fuel cells are discussed in detail.

1.3.5.1 Membrane Degradation

Membrane degradation mainly depends on operating conditions of the PEM fuel cell including temperature, humidity, freeze-thaw cycle, transient operation, and start-up/shut-down cycle [93]. Mechanical degradation, thermal degradation and chemical degradation are the three main degradation mechanisms of membrane of a fuel cell.

- **Mechanical Degradation:** This type of degradation causes early failure of the membrane, which may be resulted from poor production or improper installation of the MEA [81]. Improper installation causes mechanical stresses or insufficient humidification due to non-uniform pressure distribution.

- **Thermal Degradation:** Thermal stress mainly results in thermal degradation. Knights et al. [94] stated that degradation of the membrane speeds up with increasing temperature. According to Collier et al. [95] the foremost effect of temperature increase on the membrane is the decrease in water content, which may result in permanent deformation.
- **Chemical – Electrochemical Degradation:** Wu et al. [81] stated that radical attack and contamination caused by carboxylate end groups, which are formed during manufacturing process, causes chemical – electrochemical degradation of the membrane. When a PEM fuel cell is worked continuously below open circuit voltage and at low humidity conditions, the possibility of chemical degradation of the membrane is sped up [96].

Tang et al. [97] stated that the main reason of the mechanical degradation and failure of the membrane is repeating dimensional changes and stress cycles. Dimensional changes are resulted from thermal changes and stress cycles are resulted from sequential start-up and shut-down processes. Likewise, on the cathode side, membrane is exposed to a severely oxidizing environment, whereas on the anode side, membrane is exposed to a chemically reducing environment. Furthermore, peroxy and hydroperoxy radicals, which are formed inside the fuel cell, attack to the membrane. Collier et al. [95] stated that these attacks mainly results in chemical degradation of the membrane. According to Liu et al. [92] it is possible to encounter with performance loss and serious failures due to membrane thinning and pinhole formation when chemical degradation is combined with mechanical and thermal degradation.

1.3.5.2 Catalyst Layer Degradation

Products supplied to the fuel cell may lead to contamination in the catalyst layer. Cheng et al. [98] stated that this type of contamination results in loss of activation in the cell, mainly caused by the impurities of the reactants. According to Taniguchi et al. [99] PEM fuel cell durability is affected by corrosion of the carbon support of

the catalyst layer which results in conductivity loss throughout the cell. Also, corrosion of the Pt catalyst leads to a change in the structure inside the cell, which translates into a decrease in electrochemical active surface area of the MEA [100].

1.3.5.3 GDL Degradation

GDL has an important role on the overall performance of a PEM fuel cell. Wood and Borup stated that [101] appropriate implementation of the GDL leads to operation at high current densities without sacrificing cell potential, or stimulating extreme cell potential. The PTFE (Poly Tetra-Fluoro-Ethylene) content in the composition of the MEA gives PEM fuel cells their stable characteristics. GDL physical characteristics are also seriously affected by the loss of PTFE and carbon content. The conductivity and the permeability of the GDL decrease with decreasing PTFE and carbon content. This phenomenon lowers the overall performance of the fuel cell [102]. Additionally, corrosion inside the MEA results in conductivity loss through the GDL. Furthermore, mechanical stress on the GDL can lead to decrease in water management capability [81] and in-plane permeability [103] of PEM fuel cells.

1.3.5.4 Bipolar Plate Degradation

Mitani and Mitsuda [104] stated that bipolar plate material should possess superb durability in hot and humid conditions, corrosion resistance and mechanical strength. Electrical and thermal conductivity of the bipolar plates should also be excellent. Though, contact resistance between the bipolar plate and the GDL is one of the foremost problems that decrease the performance of the fuel cells. Electrically resistant oxide films formed on the surfaces between the bipolar plate and the GDL. According to Wu et al. [81] these oxide films increase the internal electrical resistance of the fuel cell. Furthermore, Wind et al. [105] stated that durability of the membrane and the catalyst is seriously affected by the corrosion and oxidation of metallic materials of bipolar plates, which results in conductivity loss. Another common concern, which increases possibility of the bipolar plate

degradation, is the possible fracture or deformation of the bipolar plates under the compressive forces. Hinds [85] proposed that the compressive forces are applied to provide adequate sealing through the cell and good electrical contact between the components of the fuel cell.

1.3.5.5 Sealing Gasket Degradation

PEM fuel cell stack assemblies are sealed by using sealing gaskets. However, the degradation of these sealing gaskets can lead to compression loss and may result in loss of retention force. Corrosion and mechanical stresses cause sealing gasket degradation.

To sum up, the major failure modes observed in PEM fuel cell components and their possible causes are summarized in Table 1.

1.4 Contribution

In literature survey, all of the mentioned studies are concentrated on certain aspects of the phenomena investigated in this study. However, a complete study, in which investigation of the degradation in PEM fuel cells or the effects of degradation on the overall system performance including energy and exergy analysis, is not available in the literature. In this study, a complete analysis is performed on; (i) system modeling on solar-hydrogen based hybrid renewable energy systems including energy-exergy analysis and economical analysis (ii) CFD modeling of PEM fuel cells with covering degradation phenomenon and (iii) the effects of degradation on the overall system performance.

Table 1 Summary of major failure modes in PEM fuel cells [81] [86].

Component	Failure Modes	Causes
Membrane	Mechanical degradation	Mechanical stress due to non-uniform pressure difference or insufficient humidification.
	Thermal degradation	Thermal stress
	Chemical-electrochemical degradation	Contamination, radical attack
Catalyst Layer	Activation Loss	Contamination
	Loss of conductivity	Corrosion
	Decrease in water management capability	Phase transformation and volume changes of water
GDL	Loss of conductivity	Corrosion
	Permeability	Decreasing PTFE and carbon content
	Decrease in water management capability	Mechanical stress
Bipolar Plate	Fracture or deformation	Mechanical stress
	Loss of conductivity	Corrosion, oxidation
Sealing Gasket	Mechanical failure	Mechanical stress, corrosion

1.5 Thesis Layout

After this introduction chapter, in the following chapter, system modeling of the solar-hydrogen based hybrid renewable energy system is analyzed. Each component of the system is discussed in detail and system modeling results are presented. Also, energy-exergy analyses are performed together with economical analysis.

In Chapter 3, CFD modeling of PEM fuel cells are studied. All of the components of the PEM fuel cell are modeled in detail. Simulations are performed for the CFD model and the results are compared with literature. After successfully modeling single cell of the PEM fuel cell, simulations are performed for fuel cell stacks. Results of the CFD models are discussed and this chapter is finalized.

In Chapter 4, PEM fuel cell degradation study is presented. Simulations are performed for degraded single cell and fuel cell stack. Also, a parametric study is conducted on fuel cell degradation. This chapter is concluded with system simulations including degraded PEM based components.

The thesis is concluded with Chapter 5 discussing results of the simulations and evaluation of the general modeling method. A summary of the contributions made in this thesis and recommendations for the future work are also presented.

CHAPTER 2

SYSTEM MODELING

In this chapter, system modeling of the solar-hydrogen hybrid renewable energy system, which was built for the emergency room of Keçiören Training and Research Hospital in Ankara, is discussed. The overall performance of the system is investigated by using TRNSYS. Energy and exergy analyses for the hydrogen cycle of the system are performed for whole period of a year. The performed energy analysis is mainly based on the first law of thermodynamics. However, the first law of thermodynamics gives no information on the quality of the different types of energy that are involved in the process. Energy efficiency only provides quantitative information about the system, whereas exergy efficiency provides both qualitative and quantitative information about the system. Therefore, exergy analysis of the each component is needed to have a complete analysis of the system. The energy and exergy analyses are complemented by a detailed through the lifetime economic analysis. An analysis method called as Levelized Cost of Electricity (LCE) is used.

2.1 System Description

Photograph of the hybrid renewable energy system that was established at the hospital is shown in Figure 4. The PV panels were mounted on the top of a small hill in order to operate the system effectively. The control room and the storage tanks were established close to the PV panels.

The simplified TRNSYS model of the system is presented in Figure 5. Primary function of the PV panels is to supply electricity directly to the emergency room

(User), which is also called the user of the system. If the power generated by the PV panels is greater than the demand, the excess power is sent to the electrolyzer via power conditioner. The electrolyzer generates hydrogen and fills it into the hydrogen tank. When the generated power is greater than the sum of the demands of the emergency room and the electrolyzer, extra power is dumped out. On the other hand, if PV power generation is less than the demand of the emergency room, the difference is supplied by the fuel cells utilizing the stored hydrogen. DC/AC inverters are used between PV panels and the emergency room, and between the fuel cells and the emergency room. The system is controlled by the main control unit (controller). The operating arrangements of the system elements are controlled by evaluating the system parameters. In the following subsections components of the system is discussed in detail.



Figure 4 Photograph of the solar-hydrogen based hybrid renewable energy system.

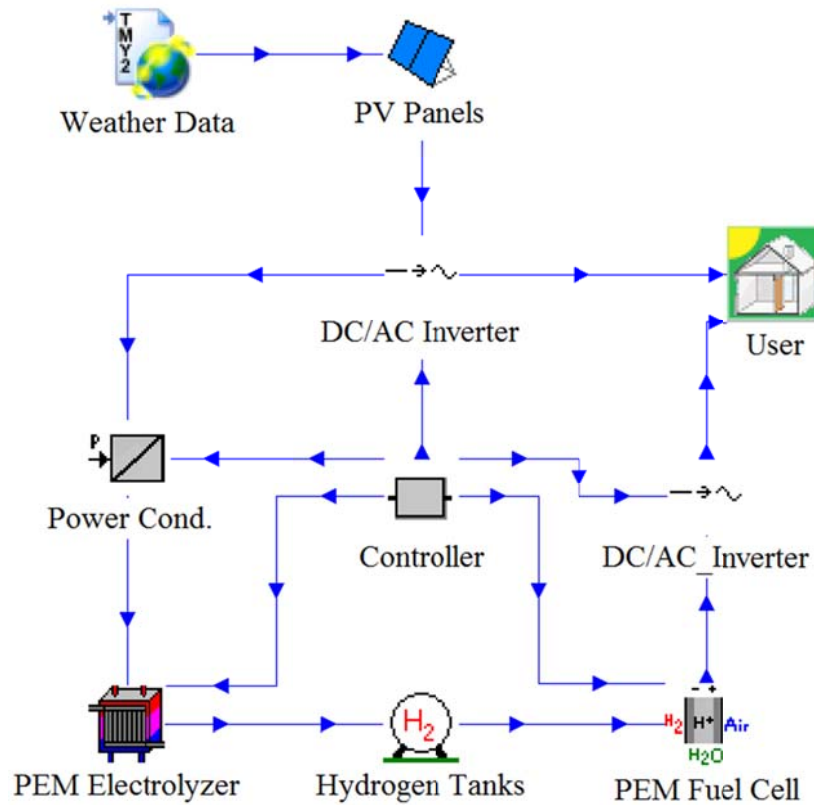


Figure 5 Simplified TRNSYS model of the system.

2.1.1 Load Profile

The maximum electricity demand of the emergency room is 5 kW. It is assumed that 5 kW is needed between 6 am and 24 pm, while 2 kW is sufficient for the rest of the day (Figure 6). Variations in the load are neglected for being able to interpret the results more easily. The emergency room has a daily load of 102 kWh and a yearly load of 37.23 MWh. Power demand of the other auxiliary equipment (hydrogen compressor, pumps, water deionizer and controller) are considered as a part of the load profile. Among the auxiliary equipment, only the controller of the system continuously operates, other equipment comes into action when the electrolyzer or the fuel cell is active. Since the demands of the auxiliary equipment are very small compared to the demand of the emergency room, these fluctuations are neglected in the load profile.

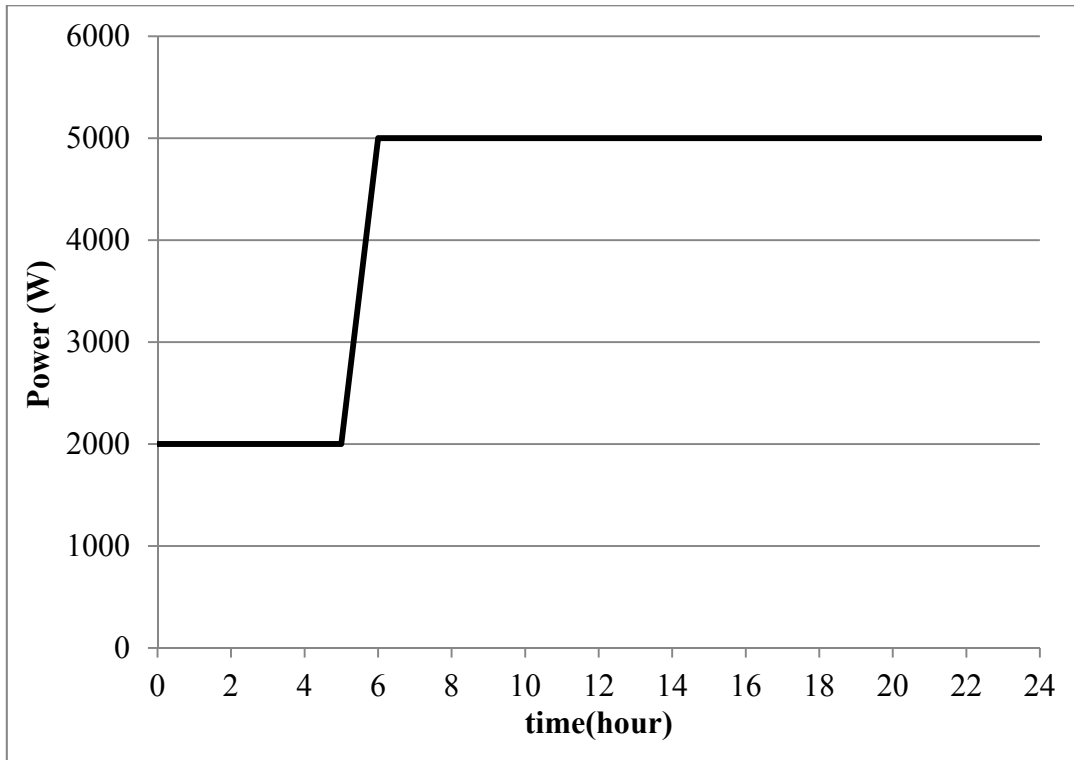


Figure 6 Load profile of the system.

2.1.2 PV Panels

High performance Bosch Solar Module c-Si P 60 type PV panels are used in the system. Technical specifications of the PV panels are tabulated in Table 2. These specifications are successfully implemented in the PV panel module of the TRNSYS. 180 PV panels were mounted in the parking lot of the hospital. The PV panels are directed to south direction. The total area covered by the PV panels is 330 m² (the net area is 300 m²). The total established power of the PV panels is 39.6 kW.

The power output of the PV panels is directly related to the slope of the panels. Consequently, the PV panels are mounted at the parking lot of the hospital on a tiltable platform to increase the power output of the system. By using the tiltable platform, it is possible to adjust the slope of PV panels according to the optimal

angle for each month. The motor power for the panel platform tilt angle adjustment is 1.1 kW. It takes approximately 10 seconds to change the angle of the platform. Thus, the energy consumption of the tiltable platform is negligible. The tiltable platform, which is actuated by hydraulic pistons and structured by HEA 300 I-beams, is presented in Figure 7. For a fixed tilt angle system in Ankara, the recommended (yearly optimum) PV panel slope angle is 39.4° [106]. However, the optimum angle is not constant throughout the year. In Table 3, the monthly optimum PV panel tilt angles are tabulated for Ankara. The differences between the monthly optimal slope angles and the yearly optimal slope angle are also shown in this table. Using each difference, monthly efficiency losses are calculated, and then the average efficiency loss is determined. It is observed that, by adjusting the slope of the PV panels monthly, it is possible to increase the power output of the panels by 16.4%.

Table 2 Electrical and thermal properties of the PV panels (adapted from internet source [107]).

Properties	Values
Maximum Power	220 W
Number of Panels	180
Maximum Power Voltage (V_m)	30.03 V
Maximum Power Current (I_m)	8.11 A
Open Circuit Voltage	37.50 V
Short Circuit Current	8.64 A
Reverse-current Load Capacity	15 A
Length	1660 mm
Width	990 mm
Frame Height	50 mm
Weight	21 kg
Nominal Operating Cell Temperature	46°C
Current Temperature Coefficient (I_{sc})	0.04%/K
Voltage Temperature Coefficient (V_{oc})	-0.31%/K
Power Temperature Coefficient (P_{mpp})	-0.44%/K

Table 3 Monthly optimum PV panel slope for Ankara (adapted from TÜBİTAK Project Report [108]).

Months	Optimum Angle (°)	Difference (°)	Efficiency Loss (%)
January	60.40	21.00	22.67
February	52.88	13.48	14.31
March	41.94	2.54	2.16
April	30.06	9.34	11.04
May	20.75	18.65	21.39
June	16.48	22.92	26.13
July	18.45	20.95	23.94
August	26.26	13.14	15.27
September	37.56	1.84	2.71
October	49.40	10.00	10.44
November	58.61	19.21	20.68
December	62.65	23.25	25.17
Average %			16.4

2.1.3 Inverters

An electrical sub-system sends the power generated by the PV panels and by the fuel cell to the user to meet the demand. At a given time, either the fuel cell or the electrolyzer operates depending on the power shortage or surplus of the PV panels, respectively. Inverters and a controller are used maintain these operations to meet the demand of the user effectively. The inverters and the main control unit (controller) are illustrated in the schematic representation of the system (see Figure 8). Controller of the system is developed and produced by Hidronerji A.Ş.. DC/AC inverters are used between the PV panels and the controller and between the PEM fuel cell and the controller. In total, seven inverters are used; six of them with nominal power capacities of 6000 VA are used with the PV panels and one of them with a nominal power capacity of 5000 VA is used with the fuel cell. The inverters have a maximum efficiency value of 95% and a maximum operating temperature value of 50°C.

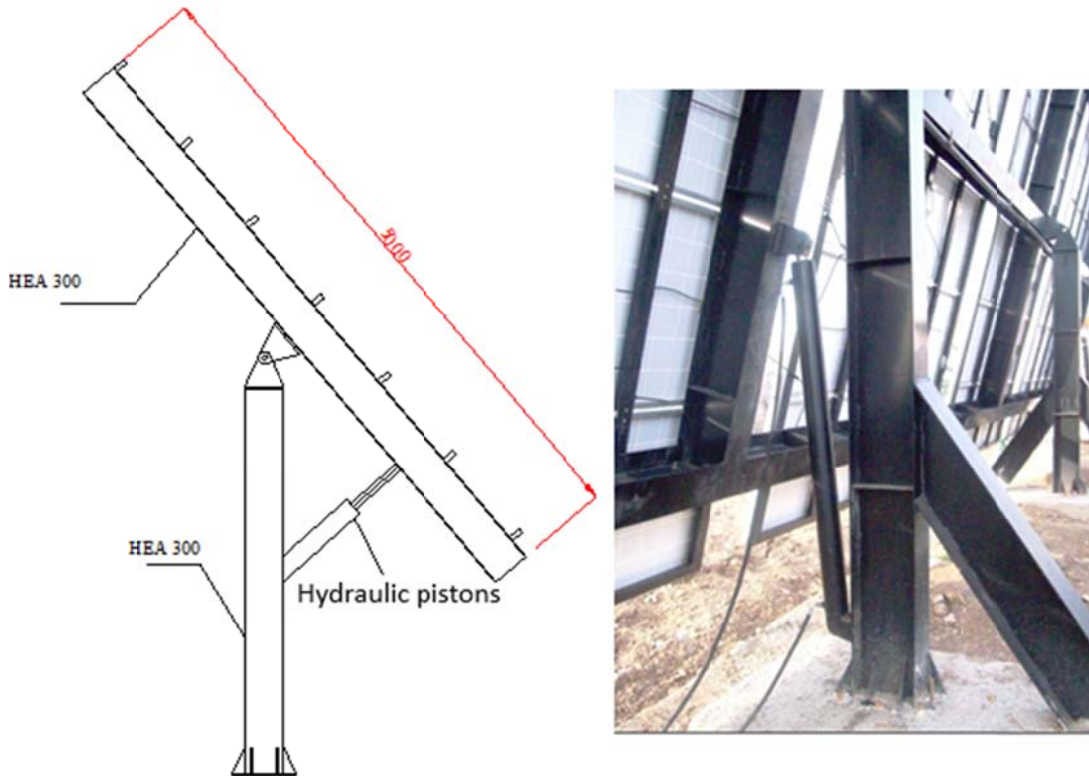


Figure 7 Tiltable platform of the PV panels.

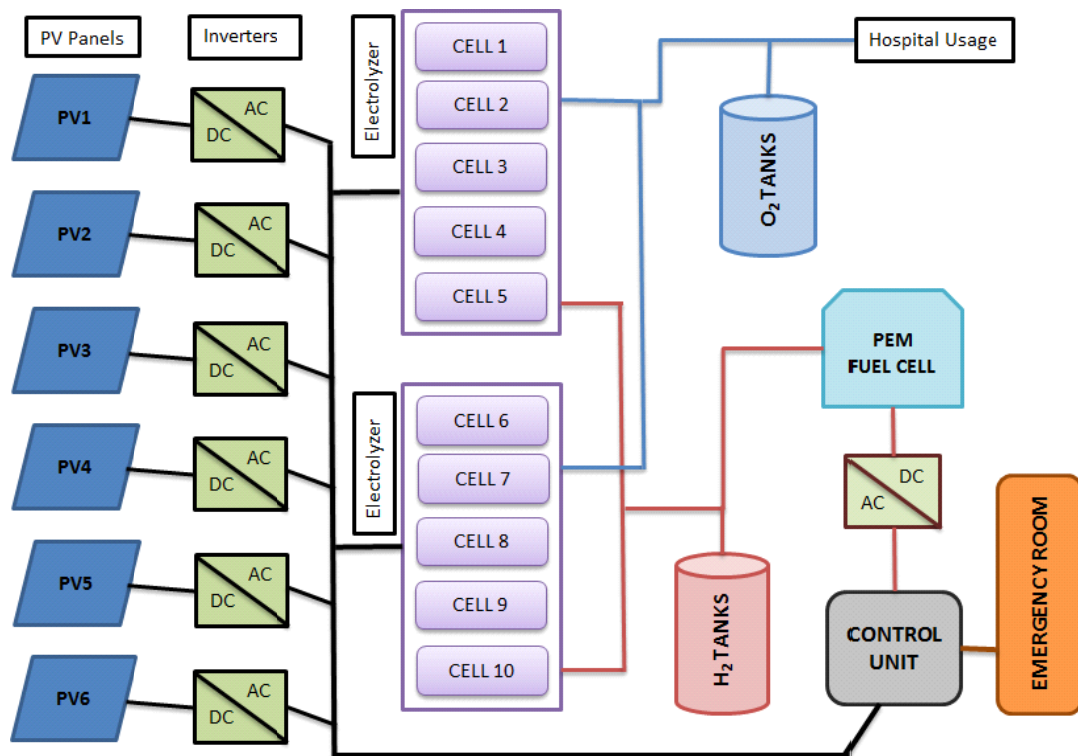


Figure 8 Schematic representation of the system.

2.1.4 PEM Fuel Cell

ElectraGen PEM fuel cell system with a capacity of 5 kW is used in the system. Technical specifications of PEM fuel cells are tabulated in Table 4. Assumptions of the PEM fuel cell module and the electrochemical model of the PEM fuel cell are discussed below.

Assumptions of the PEM fuel cell module:

- Type170f module of the TRNSYS is used for modeling PEM fuel cells. In this module, instead of pure oxygen, “air” is supplied to the cathode.
- The stack temperature is calculated internally (based on a set point temperature). It is assumed that the fuel cell reach its initial temperature during the initial time step. Final temperature for a time step is the average of the initial temperature and the set point temperature.
- The fuel cell is assumed in on-off operating condition with maximum available capacity.
- The membrane of the fuel cell is assumed well hydrated.
- Each cell in the stack is considered as one of identical cells connected in series.
- At the anode and the cathode inlets, stoichiometric coefficients of fluid flow are assumed constant.
- The fuel cell is working in steady state. Following parameters are assumed as constant throughout the fuel cell: open circuit voltage, heat capacities, molecular weights, densities and specific heat ratios of the reactants, and the lower heating value of hydrogen.
- Minimum allowable cell voltage is limited to 0.7 V.
- Maximum allowable current density is limited to 700 mA/cm².
- Experimental mode is selected for calculating the overall thermal resistance (R_t) and the capacitance (C_t) of the fuel cell stack. R_t is assumed as 0.05263 K/W and C_t is assumed as 35,000 J/kg [109].

Table 4 Technical data of the PEM fuel cell system.

Properties	Values
Maximum Power (kW)	5
Voltage Range (VDC)	24 to 28
Ambient Temperature (°C)	-5 to +46
Internal Fuel Tank Size (L)	22
Run Time (hrs)	40
Fuel Consumption (L/kWh)	1.1
Dimensions (cm)	135 x 115 x 176
Weight (kg)	295

Electrochemical Model:

In the fuel cell module, the performance of fuel cells is defined as a function of the thermodynamic potential, the activation overvoltage and the ohmic overvoltage, with mass transport losses combined with each term, as in [110]. Basic expression for the voltage of a single cell is given by the following equation:

$$V_{cell} = E + \eta_{act} + \eta_{ohmic} \quad (2.1)$$

where E is the thermodynamic potential, η_{act} is the activation overvoltage and η_{ohmic} is the ohmic overvoltage. These parameters can be calculated using the following equations [111] [112]:

$$E = 1.229 - 0.85 \cdot 10^{-3} \cdot (T_{stack} - 298.15) + 4.3085 \cdot 10^{-5} \cdot T_{stack} \ln(p_{H_2} \cdot p_{O_2}^{0.5}) \quad (2.2)$$

$$\eta_{act} = 0.9514 + 0.00312 \cdot T_{stack} - 0.000187 \cdot T_{stack} \cdot \ln(i) + 7.4 \cdot 10^{-5} \cdot T_{stack} \cdot \ln(c_{O_2}) \quad (2.3)$$

$$\eta_{ohmic} = \frac{-I_{FC} \cdot t_{PEM}}{A_{PEM}} \cdot \frac{8}{\exp\left[3.6 \cdot \left(\frac{T_{stack} - 353}{T_{stack}}\right)\right]} \cdot \left[1 + 1.64 \cdot \frac{I_{FC}}{A_{PEM}} + \gamma \cdot \left(\frac{I_{FC}}{A_{PEM}}\right)^3\right] \quad (2.4)$$

Voltage-current (I-V) curve is used to summarize the performance of PEM fuel cells. In a typical I-V curve, the current is normalized by the area of the fuel cell to make the outputs of the I-V curves comparable, since a smaller fuel cell can produce less energy than a larger fuel cell. In Figure 9, typical I-V curve of the fuel cell module is presented for two different operating temperatures (T_{stack}).

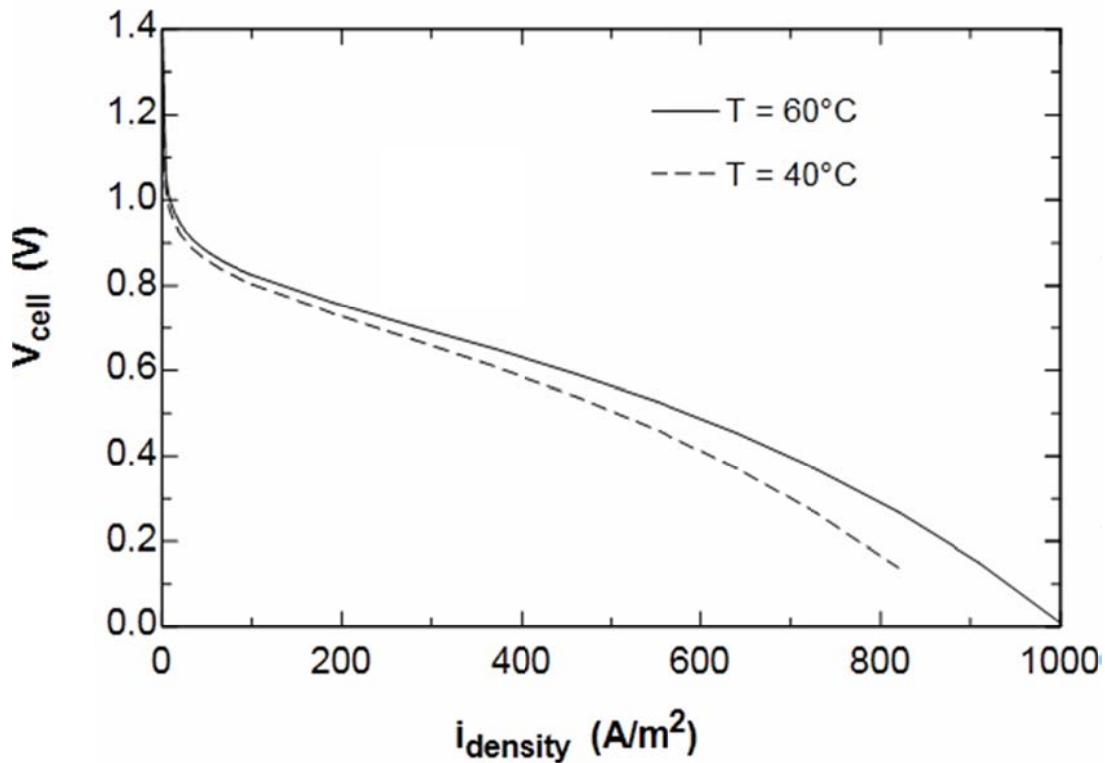


Figure 9 Typical I-V curve of the fuel-cell module.

In a fuel cell, the operating temperature is not uniform; it varies throughout the cell. The operating temperature of the cell can be assumed as equal to the cathode outlet temperature, because a great portion of the losses inside the fuel cell is observed at the cathode side. Even though, the cathode outlet temperature is slightly lower than the temperature of the cell, this approach is a reasonable approximation for determination of the operating temperature of the cell, as in [32].

2.1.5 PEM Electrolyzer

The PEM electrolyzer used in the system is developed in Niğde University. Technical parameters of the PEM electrolyzer are presented in Table 5. The electrolyzer system is divided into two groups, each group having 5 stacks. Connection diagram of the PEM electrolyzer stacks is presented in Figure 8. The electrolyzer system is able to produce 5 l/min hydrogen. A single cell of the stack was tested, and it was found that the degradation rate of the cell is acceptable [9]. The following assumptions (similar to the assumptions of the PEM fuel cell module) are made for the PEM electrolyzer module.

Assumptions of the PEM electrolyzer module:

- The membrane of the electrolyzer is assumed well hydrated.
- Temperature of the electrolyzer is assumed uniform throughout the cell. Thus, each cell of the stack has identical thermal characteristics.
- Electrolyzer is working in steady state. Following parameters are assumed as constant throughout the electrolyzer cell: open circuit voltage, heat capacities, molecular weights, densities and specific heat ratios of the reactants, and the lower heating value of hydrogen.
- Pressure effects are neglected. Pressure is assumed constant throughout the cell.
- Each cell in the stack is considered as one of identical cells connected in series.
- At the anode and the cathode inlets, stoichiometric coefficients of fluid flow are assumed constant.

Table 5 Technical data of the PEM electrolyzer.

Properties	Values
Effective area of each cell	100 cm ²
Number of stacks	5
Number of groups	2
Total number of cells per stack	10
Total effective area per stack	0.1 m ²
Max H ₂ production rate	5 lt/min
Max operating pressure	50 bars

2.1.6 Gas Storage Tanks

Three hydrogen tanks, each with a capacity of 10 m³, are used in the system. Total storage capacity of the hydrogen tanks is 30 m³. For safety reasons, the maximum pressure of the hydrogen tanks is limited to 55 bars. The produced oxygen is also stored to be used in the hospital; thus, an oxygen tank with a capacity of 1 m³ is included in the system. The maximum pressure of the oxygen tank is also limited to 55 bars.

2.2 System Simulations

The TRNSYS model of the system is presented in Figure 10. Typical Meteorological Year (TMY) data set that is available in TRNSYS is used in the simulations. The TMY data set is comprised of 12 meteorological months in a year. Likewise, TMY data set contains a complete year of hourly solar radiation, illuminance and meteorological elements. The data values for solar radiation and illuminance, which are antecedent to the indicated hour, represent the amount of energy received during the prescribed 60 minutes. Meteorological extremes are not provided in the TMY data set. Though, TMY data set has natural daily and seasonal fluctuations and represents a year of typical climatic conditions for a specific

location [113]. Second edition of TMY data set, “TMY2” is used in the system simulations. The weather data was collected between 1961 and 1990 for TMY2.

12 different forcing functions are defined to simulate the effects of monthly changing tilt angle of the PV panels. Each forcing function represents a single month with specified slope of the surface. By using an equation module, forcing functions are coupled with the weather data. Instead of the modules that are available in TRNSYS database, user defined modules are used for the PV panel module and the main controller module. These modules were also used by Uluoğlu [114]. By using the PV panel module, it is possible to define all the tabulated parameters in Table 2. The PV panel module calculates power, voltage and current data according to the defined parameters and TMY data, and sends the calculated data to the main controller. Output of the PV panels, as well as the emergency room demand and the hydrogen level in the tanks are provided to the controller as inputs. In the present study, first stage DC/AC inverters, which are located between the PV panels and the controller, is embedded into the controller.

System simulations are started with an initial level of 5% of hydrogen storage capacity. Simulations are performed for whole period of a year starting from 1st of March. This date is selected as the starting date of the simulations, because before this date the PV panels are not capable of both supplying the energy demand of the emergency room and filling the hydrogen tanks.

The PEM fuel cell, inverter of the PEM fuel cell, the PEM electrolyzer and the hydrogen tanks are defined by using the parameters that are provided in Section 2.1 with a single exception: the capacity of the hydrogen tanks is increased to 45 m³; since, it is not possible to meet the energy demand of the emergency room for whole period of a year with a hydrogen storage capacity of 30 m³.

In Figure 11, monthly electricity production of the PV panels is shown and daily power output of the PV panels is presented in Figure 12. It is observed that monthly electricity production of the PV panels is consistent with the daily power output. Total electricity production of the PV panels is 84.30 MWh, and the details of the energy analysis are discussed in Subsection 2.2.1. It can be said that the PV panels operate for long hours during the sunny summer days. On the other hand, the operating times are much shorter and the panels produce less energy on winter days, even though the peak power output is higher than summer days.

In Figure 13, the power profile of the system components for a typical sunny summer day is shown. For this day, until 5 am fuel cell supplies the necessary power to the user. Around 5 am, the PV panels start to operate. Until 6 am both the PV panels and fuel cell operates, then only the PV panels generate electricity. The excess power produced by the PV panels between 6 am and 6 pm is delivered to the PEM electrolyzer. Around 6 pm, the fuel cell starts up and generates electricity until next morning. In Figure 14, the power profile for a typical cloudy winter day is presented. It is observed that the electricity generated by the PV panels is not sufficient to meet the demand of the emergency room. Consequently, the PEM fuel cell runs for all day long. There is not adequate power to run the PEM electrolyzer.

Because of the inverter losses, fuel cell power (P_{fc}) is slightly higher than the load (P_{load}) in Figure 13 and Figure 14.

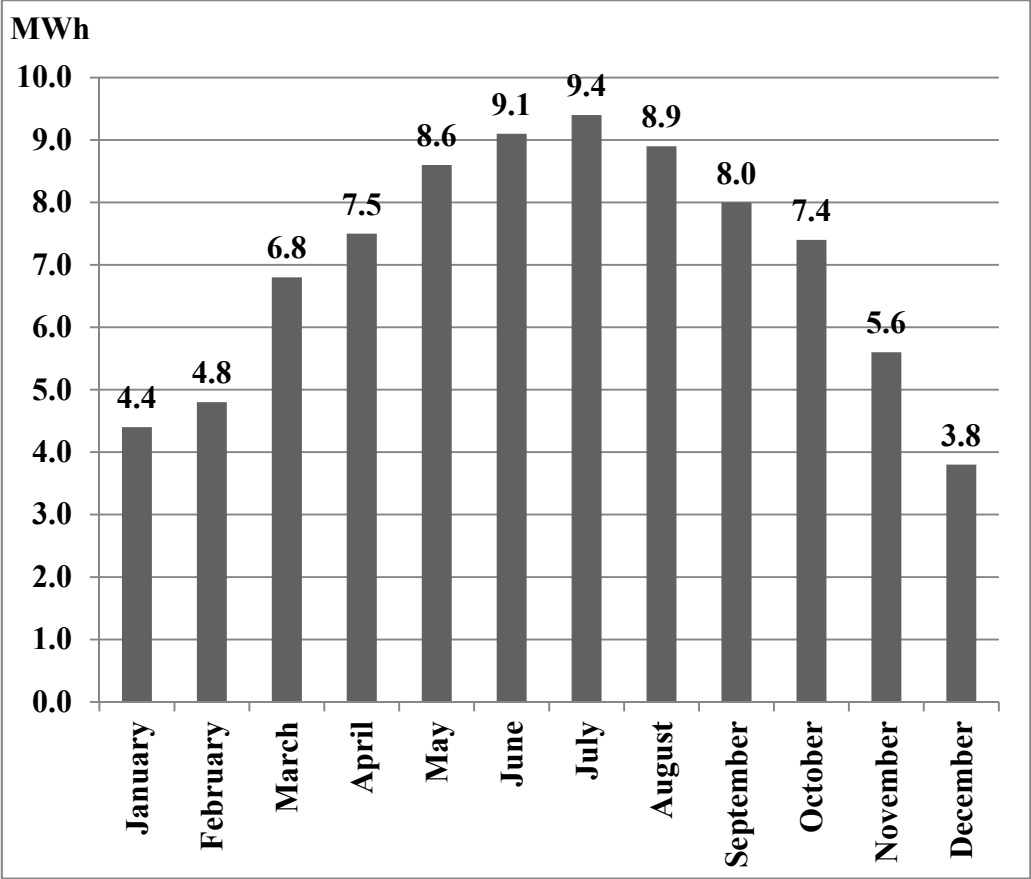


Figure 11 Monthly electricity production of the PV panels.

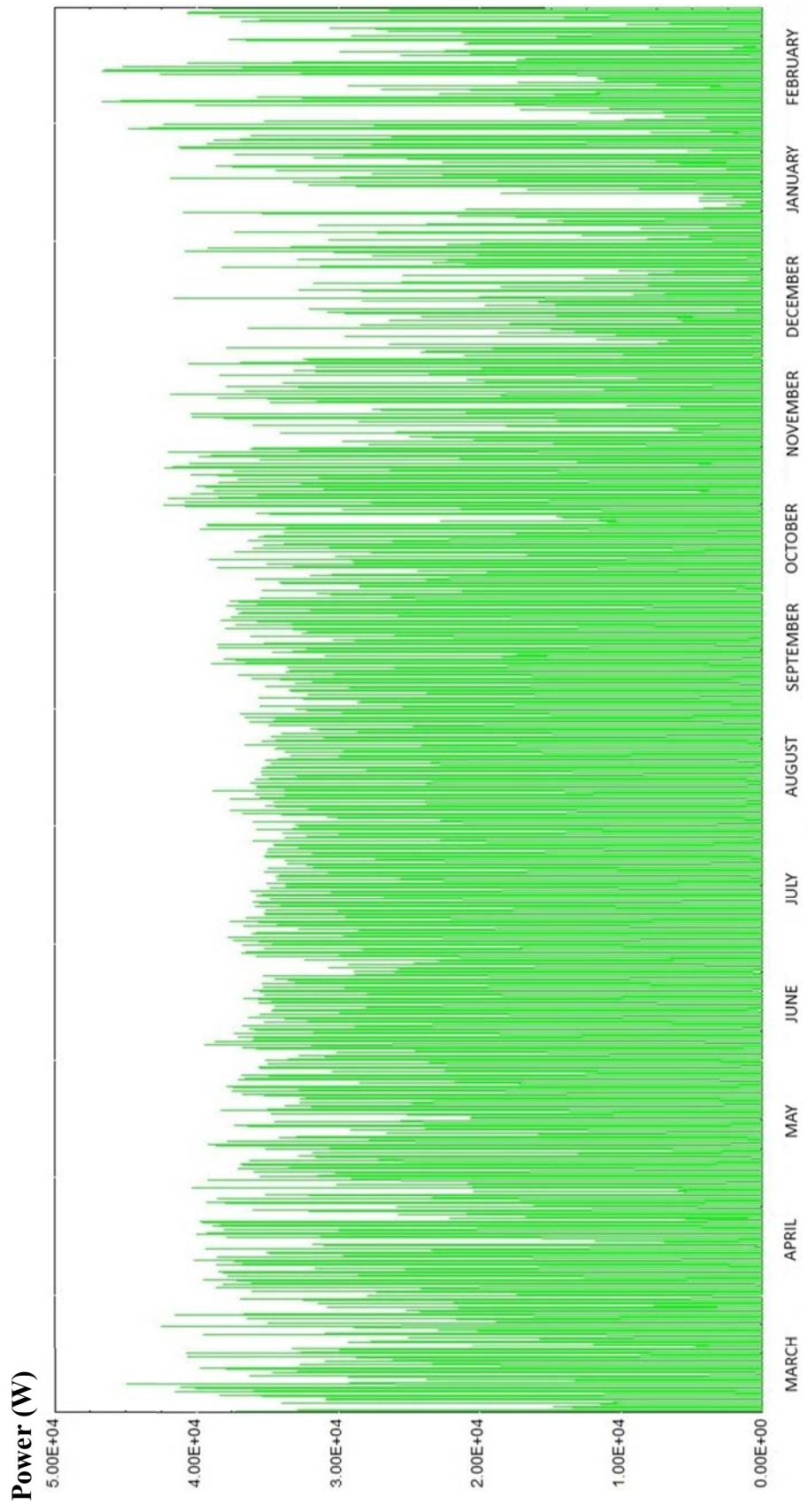


Figure 12 Daily power output of the PV panels.

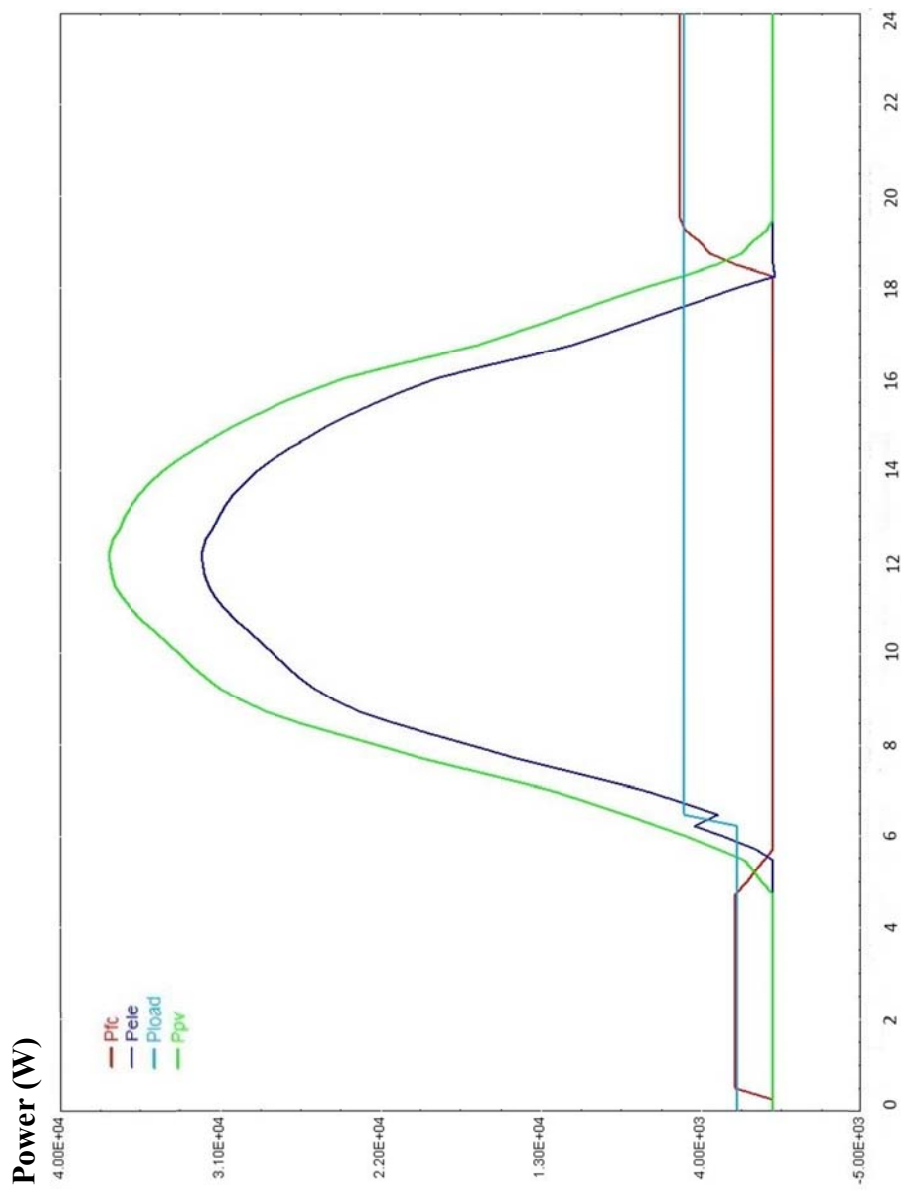


Figure 13 Power profiles of the components for a typical sunny summer day [time (hr)].

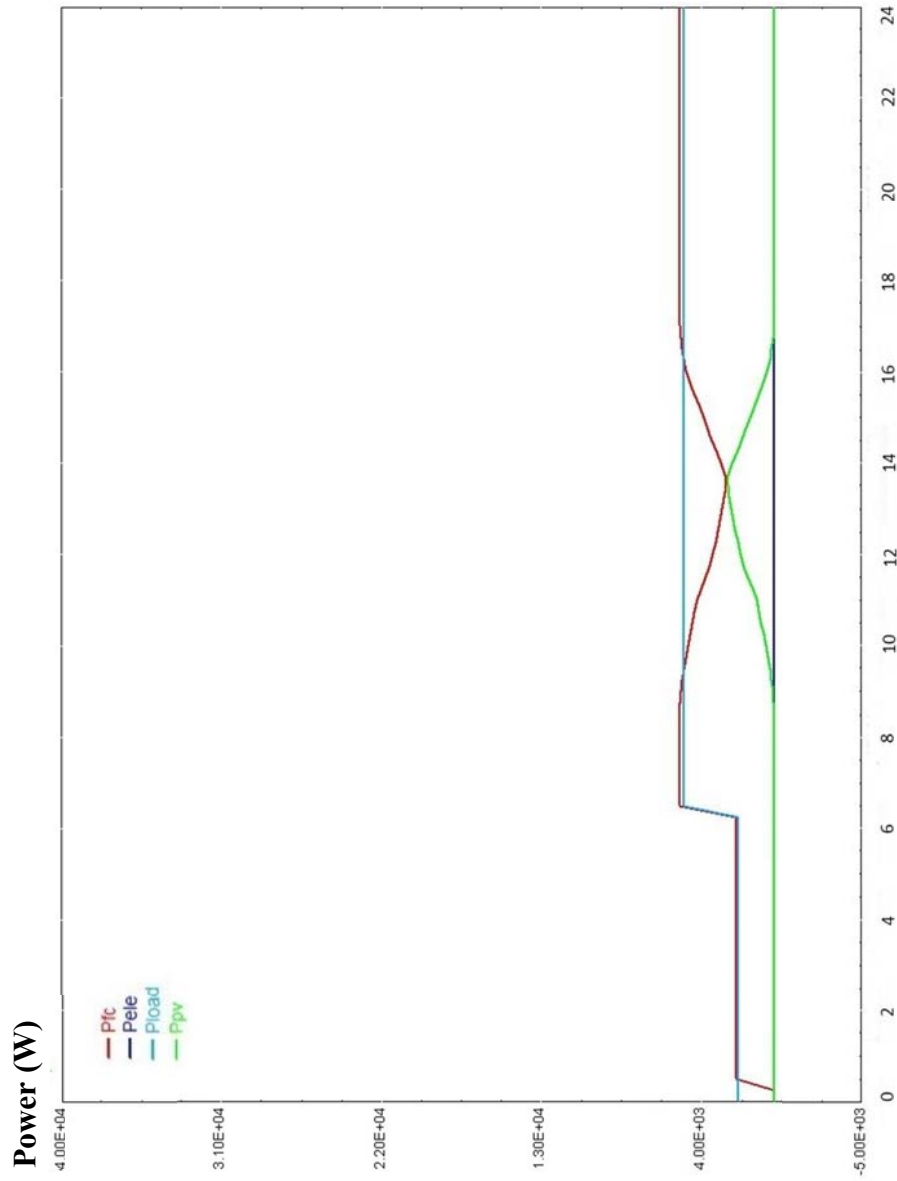


Figure 14 Power profiles of the components for a typical cloudy winter day [time (hr)].

In Figure 15, pressure level of the hydrogen tanks is presented for whole period of a year. 5% of relaxation is defined in the hydrogen storage; if the tanks are fully filled, then the system waits to fill until 5% of the stored gas is used. Thus, during the summer, the pressure level curve does not have a straight behavior. Initial pressure level of the hydrogen tanks is 5% (2.75 bars). After completing one year (starting from 1th of the March to 28th of February) simulation time, 2.42 bars (4.4%) hydrogen left in the hydrogen tanks. It can be concluded that, almost there is no change in the amount of the hydrogen level at the end of a simulation year. The difference between the pressure levels in the hydrogen tanks at the beginning of the simulation and at the end of the simulation can be defined as the hydrogen balance. When the final pressure level of the hydrogen tanks is not much less than the initial pressure level, it can be said that the system does not need an extra energy supply. Thus, it can be concluded that the hydrogen balance is a remarkable indicator of evaluating system performance in hydrogen based renewable energy systems.

Power consumed by the PEM electrolyzer is presented in Figure 16. It is observed that the electrolyzer does not continuously operate at maximum power, which also corresponds to the maximum operating temperature. Therefore, it can be said that the efficiency of the electrolyzer and the electrolyzer lifetime will not be affected from high operating cell temperatures.

Yearly operating time of the PEM fuel cell and the PEM electrolyzer is shown in Figure 17. The PEM fuel cell has an operating time of 5180 hours and the electrolyzer has an operating time of 4300 hours in a year. It is observed that, during the summer the PEM electrolyzer is used more than the PEM fuel cell. But, after November the PEM fuel cell is used more than the PEM electrolyzer, and the gap between the electrolyzer and the fuel cell opens up.

Total operating time of the PEM fuel cell and the PEM electrolyzer pair is 9480 hours in a year. Therefore, the PEM fuel cell and the PEM electrolyzer operate simultaneously for 720 hours in a year. The PEM fuel cell operates when the PV

panels are not operating or energy generation of the PV panels is lower than the demand. The PEM electrolyzers are activated when the energy generation of the PV panels is higher than the demand of the user. The energy generation of the PV panels is not constant and could not be limited to a certain value. Therefore, it is needed to activate the PEM electrolyzers when the PV panels start to generate energy to prevent consecutively start-stop. Because of this reason, in a typical day there is a certain period, in which the PEM fuel cell and the PEM electrolyzer operate simultaneously. This situation is illustrated in Figure 18, for a typical period of simulation time (23th and 24th of April). In this figure, daily operating period of the PEM based components are illustrated with power profiles of the components. Operating period of the PEM based components is indicated by on-off (0-1) logic. It is observed that the PEM based components are operating simultaneously during dawn and dusk period. It can be said that during partially cloudy days the concurrent operating time of the PEM based components would be higher than a typical day.

It is observed that hydrogen level drops to 3.8% (2.09 bars), when the system simulation is repeated for the second year starting with an initial hydrogen level of 4.4% (2.42 bars). Thus, the system is capable of operating for another whole year. Although, the system seems to continue working after two years operation, the hydrogen level will drop below 2 bars at the end of the third year. Even though, the degradation of the PEM based components is not taken into account, the system will not be stable after three years of operation, because of the low hydrogen level.

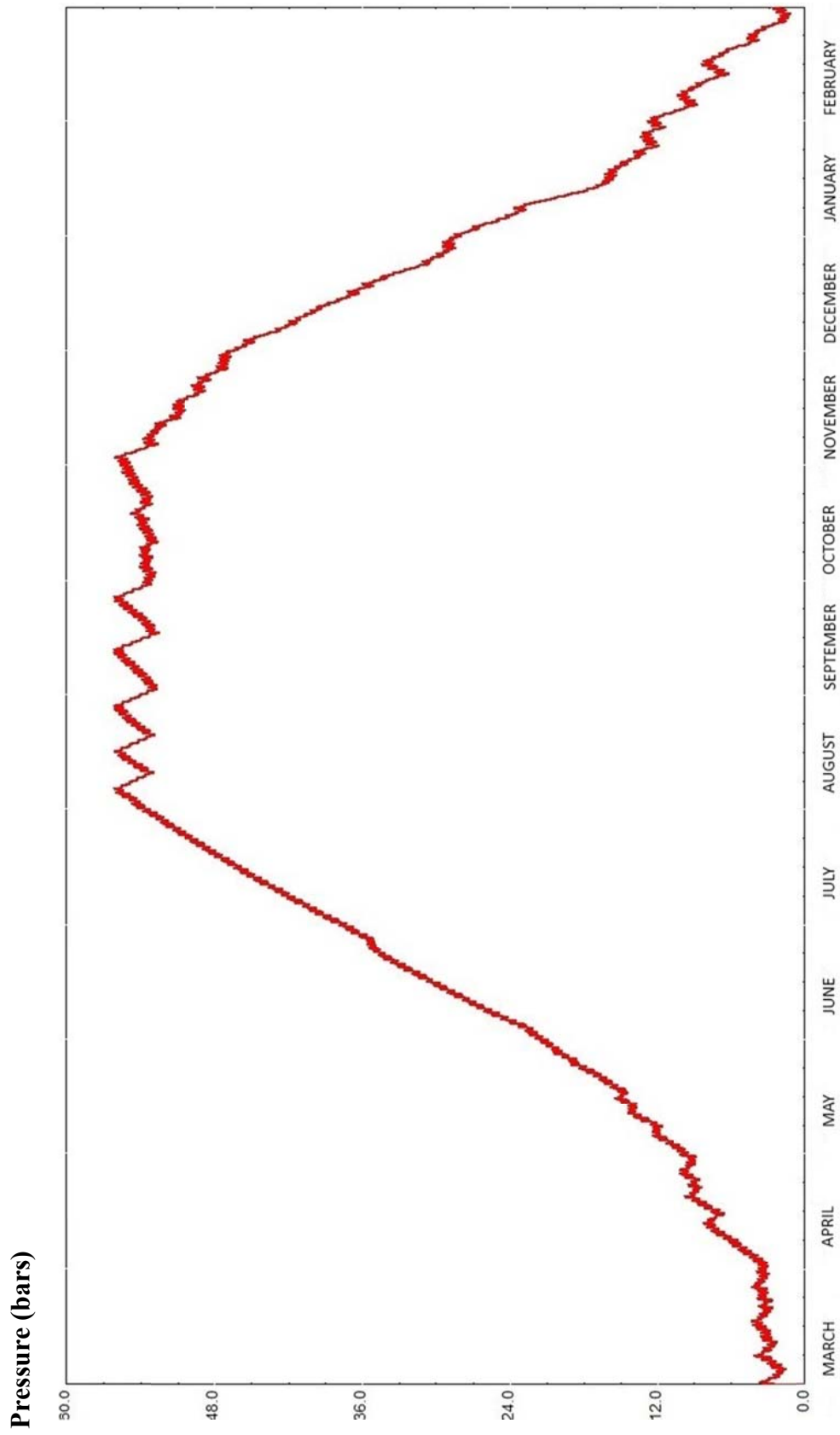


Figure 15 Pressure level of the hydrogen tanks.

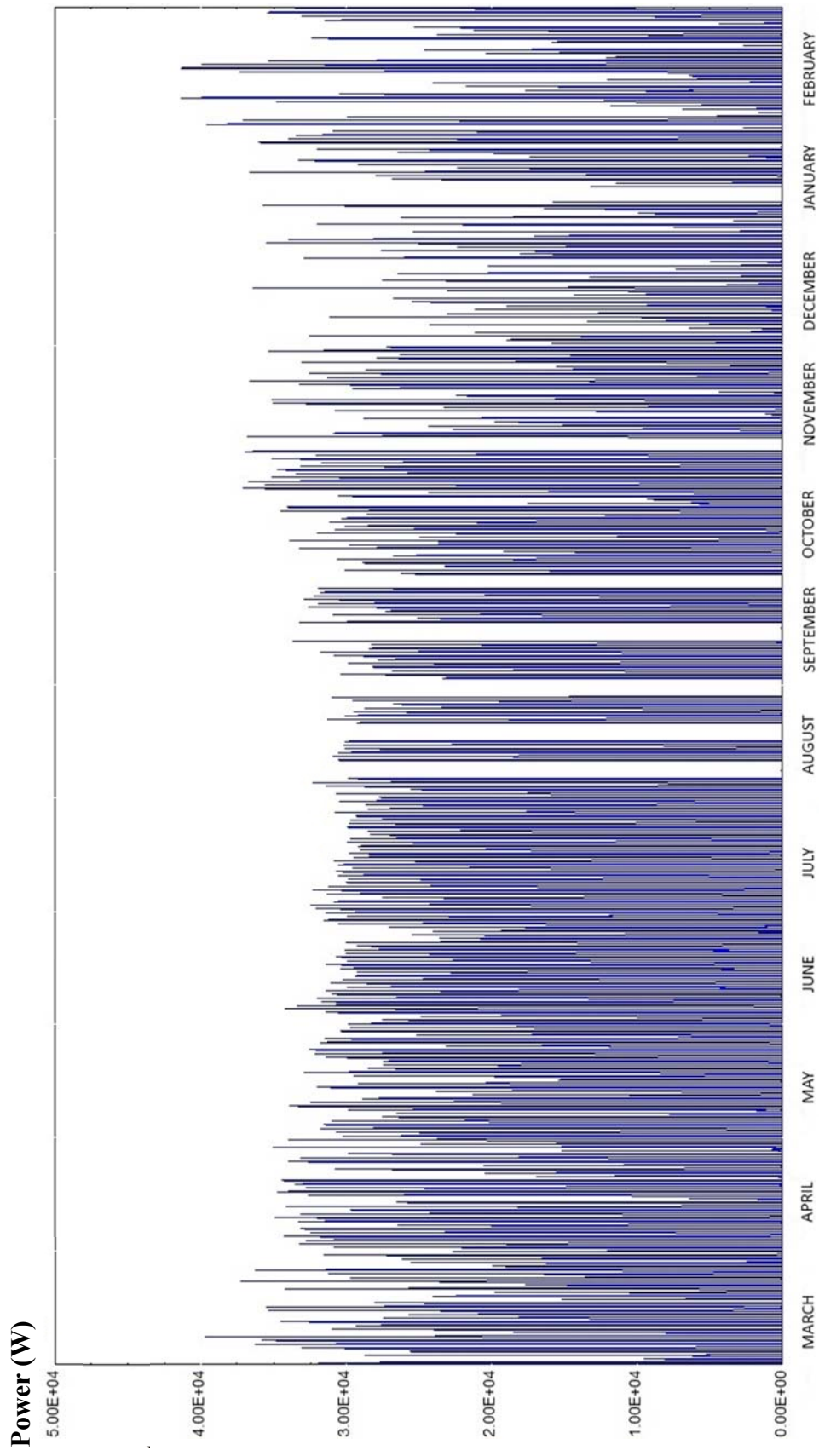


Figure 16 Power consumed by the PEM electrolyzer.

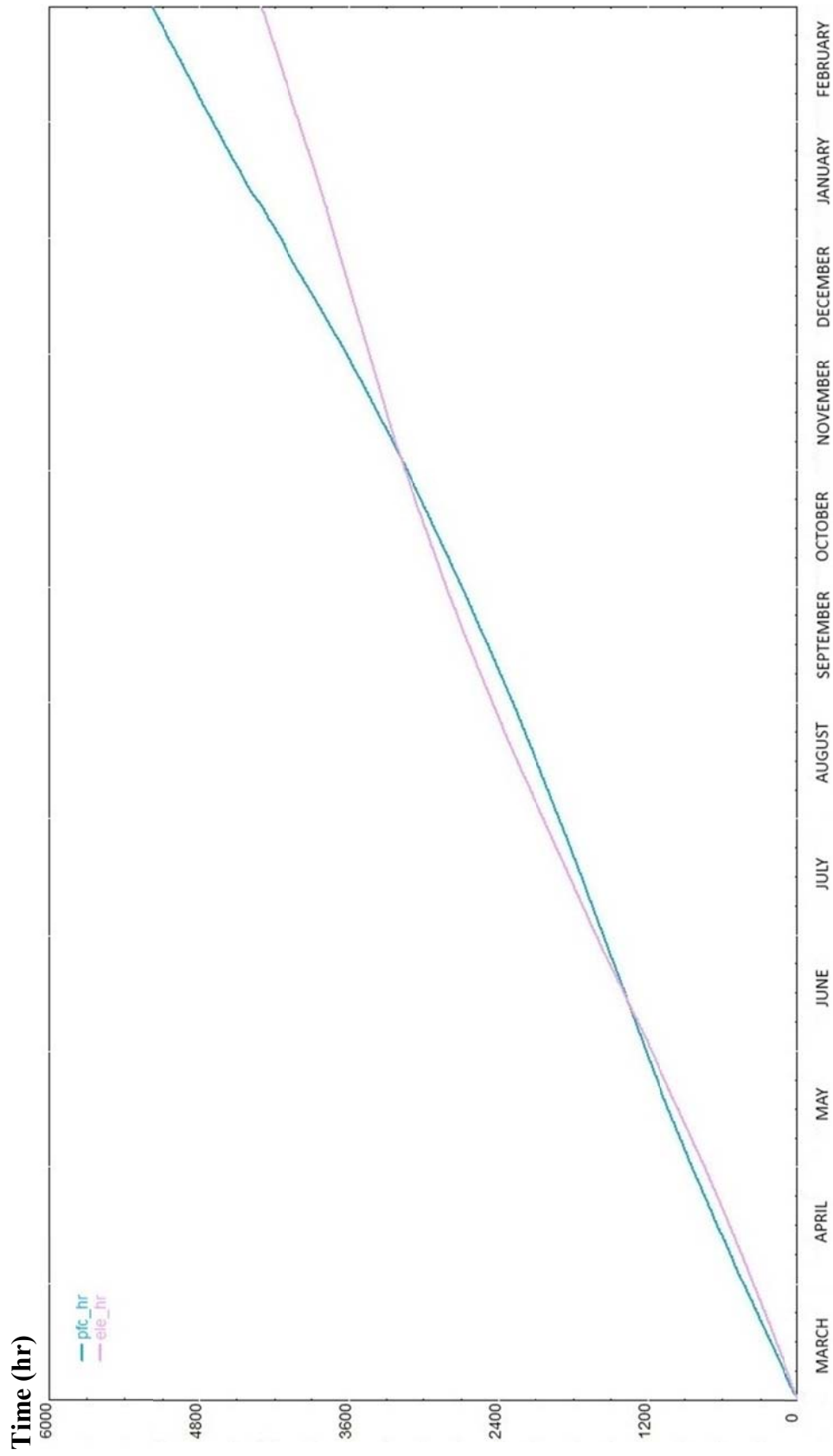


Figure 17 Yearly operating time of the PEM fuel cell and the PEM electrolyzer.

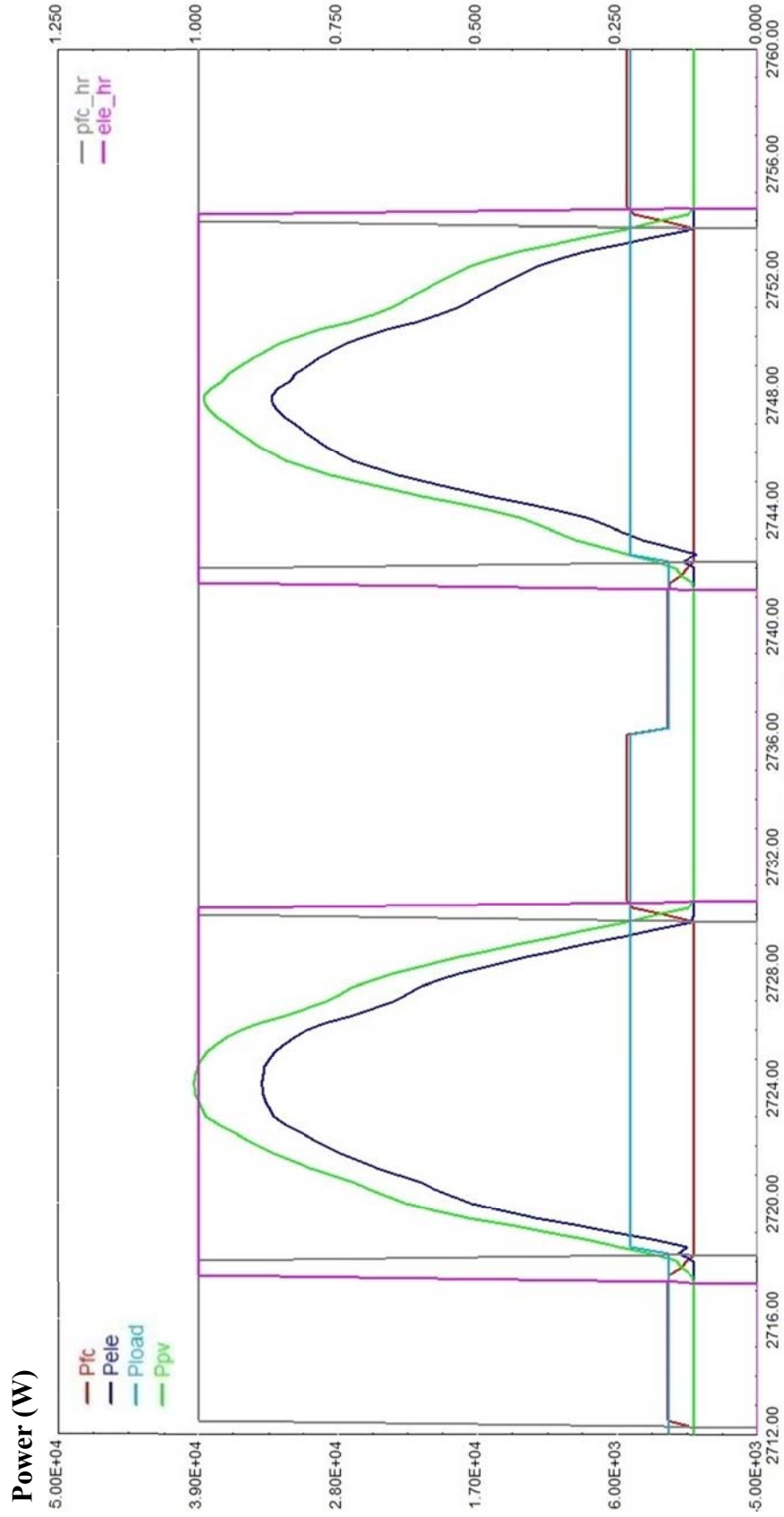


Figure 18 Power profiles of the components and operating time of the PEM based components for a typical period of simulation time (23th and 24th of April).

2.2.1 Energy Analysis of the System

In general, overall system energy efficiency can be defined as the ratio of the energy output to the energy input. In this study, solar energy is considered as the energy input and the energy supplied to the emergency room is the energy output. Based on this approach, overall system efficiency calculations are performed together with efficiency calculations of each component. Energy analysis is performed using TRNSYS.

In Figure 19, energy flow-chart of the system is presented. “E_Solar” is the solar irradiation on the PV panels; “E_PV” is the energy produced by the PV panels; “E_Inverter” is the energy directed to the inverter by the controller; “E_Elz” is the energy directed to the electrolyzer by the controller; “E_Dump” is the dumped energy by the controller; “E_H₂in” is the energy capacity of the generated hydrogen by the electrolyzer; “E_H₂out” is the energy capacity of the consumed hydrogen by the PEM fuel cell; “E_FC” is the energy generated by the PEM fuel cell; and “E_User” is the energy supplied to the emergency room.

The yearly energy flow values obtained from a year-long TRNSYS simulation is presented in Table 6. The overall system has an efficiency of 6.21%.

The overall system has an efficiency of 44.16% excluding the PV panels. The efficiency of the PV panels is calculated as 14.05%. The high performance Bosch Solar Panels are rated at an efficiency of 14.6% [115]. There is only 0.55% difference present between the rated and the calculated efficiency. The main reason of this difference is the angle of incidence of the PV panels, since the rated efficiency is defined for optimum angle of incidence. If it was possible to define the PV panel slope daily, this difference would decrease.

The first way of energy flow is the direct path from the PV panels to the user (see Figure 19). Through this path, 23.73% of the E_PV (20 MWh) is directed to the inverter from the controller. The second way of energy flow is from the PV Panels

to the user through the hydrogen cycle path including the PEM electrolyzer, the hydrogen tanks and the PEM fuel cells. 70.34% of the E_PV (59.3 MWh) is directed to the electrolyzer through the controller. Dumped energy from the controller E_Dump is calculated as 5.93% (5.0 MWh) of the E_PV. This value directly depends on the hydrogen storage capacity. During the summer, when the hydrogen tanks are fully filled, extra energy generated by the PV panels is dumped out. If the maximum pressure level of the hydrogen tanks or the total capacity of the hydrogen tanks is increased, less energy may be dumped out. However, due to safety limitations, initial investment cost and complexity of the system, the pressure level and the capacity of the hydrogen tanks are limited.

The PEM electrolyzer efficiency is calculated as 52.95%, and the PEM fuel cell efficiency is calculated as 61.15%. As a result, the second way of energy flow (the hydrogen cycle) has a total efficiency of 32.37%.

Table 6 Energy flow values of the system.

Components	Input	MWh	Output	MWh	Loss MWh	Efficiency
PV Panels	E_Solar	600.00	E_PV	84.30	515.70	14.05%
Controller	E_PV	84.30	E_Inverter	20.00	E_Dump 5.00	94.07%
			E_Elz	59.30		
PEM Electrolyzer	E_Elz	59.30	E_H ₂ in	31.40	27.90	52.95%
PEM Fuel Cell	E_H ₂ out	31.40	E_FC	19.20	12.20	61.15%
Inverter	E_FC	19.20	E_User	37.23	1.97	94.97%
	E_Inverter	20.00				
Overall System	E_Solar	600.00	E_User	37.23	562.77	6.21%
Overall System	E_PV	84.30	E_User	37.23	47.07	44.16%

20.0 MWh energy is directed to the inverter from the controller and 19.2 MWh energy is directed to the inverter from the hydrogen cycle. Both ways deliver similar amounts of energy, but the second way has an efficiency of 32.37% while there is no loss in the first way. However, the first way can only deliver energy when the solar energy is available.

Figure 20 shows comparison of the monthly engagement of the PEM fuel cells and the PV panels throughout the year. It can be said that, almost half of the energy demand of the emergency room is supplied by the hydrogen cycle of the system.

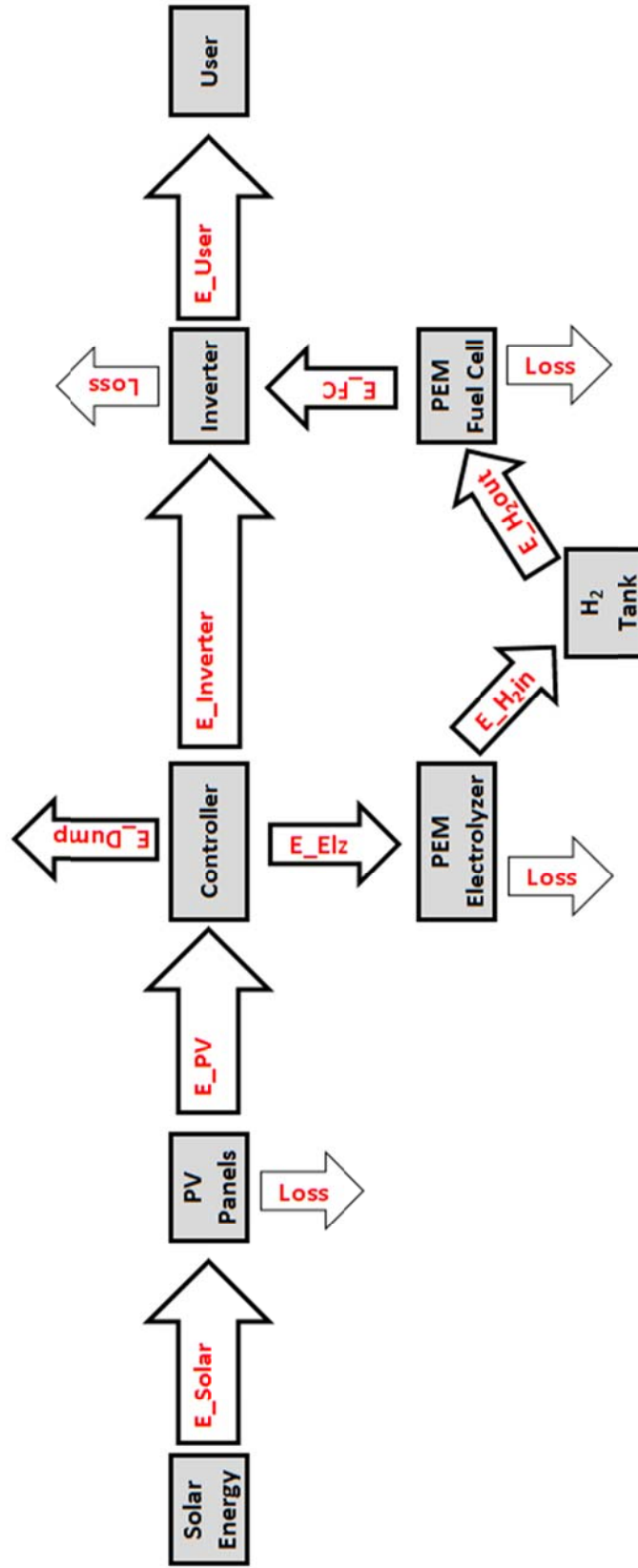


Figure 19 Energy flow-chart of the system.

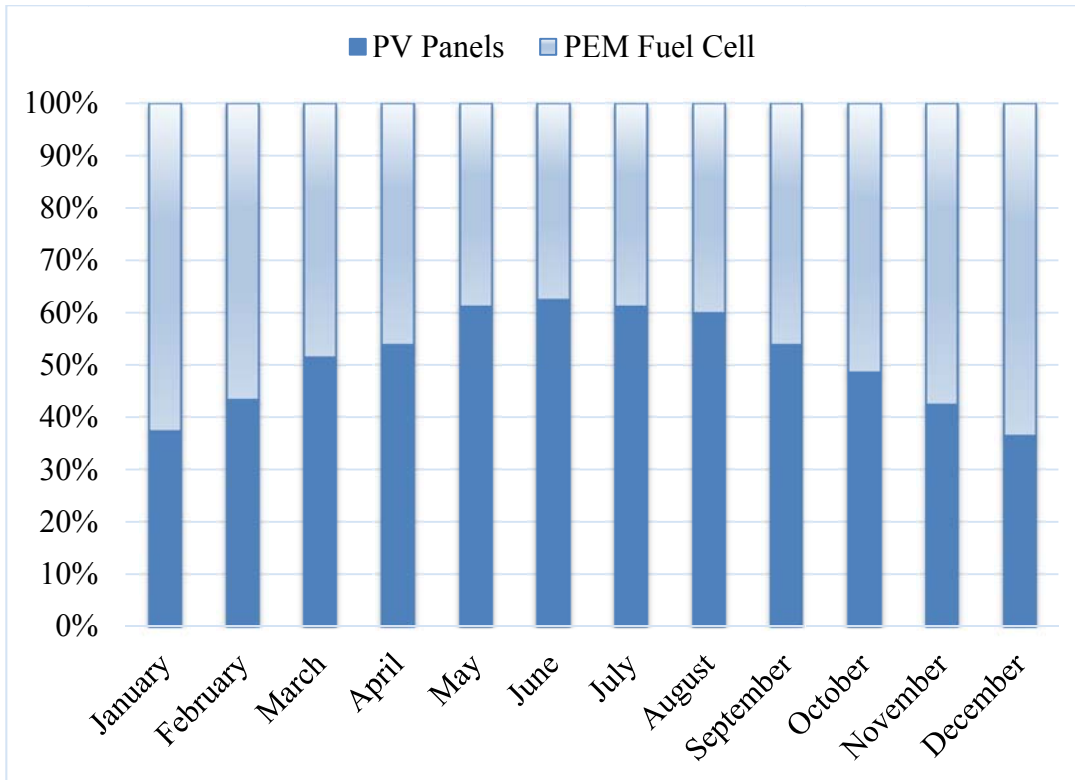


Figure 20 Comparison of the monthly electricity production of the PEM fuel cells and the PV Panels.

2.2.2 Exergy Analysis of the System

Exergy analysis, which is a commonly used thermodynamic investigation method, is mainly based on the 2nd law of thermodynamics. According to the exergy analysis, energy can be degraded in quality, even though it cannot be destroyed or created. Recently, exergy analysis is considered as an important method for evaluating thermal processes and their environmental effects (e.g. in [116]). Exergy analysis is commonly used for achieving effective energy utilization with reduced environmental impact and for obtaining optimal designs and operating systems [117]. Kazim [118] stated that through exergy analysis, it is also possible to obtain a true measure for a system performance. Therefore, an exergy analysis is performed together with an energy analysis to obtain a complete thermo-dynamical analysis related with the system. Ni et al. [119] mentioned that detailed thermodynamical

analysis is important for optimizing the performance of the PEM based components and identifying the major losses of the system. Thus, exergy analysis is performed for the hydrogen cycle of the system. In the following subsections the exergy analysis of each component of the system is discussed in detail.

2.2.2.1 Exergy Analysis of the PV Panels

The energy of a PV panel has two main components: electrical energy and thermal energy. During electricity generation process, PV panels are heated by the incident solar radiation. The thermal energy generated on PV panels can be considered as useless energy, since the generated heat is dissipated to the surroundings. In general, the energy efficiency of PV panels is considered simply as the ratio of the generated electricity to the solar irradiation. In this approach only the electricity generated by the PV panels is taken into account and the heat loss from the PV panels is neglected. Dinçer and Rosen [120] stated that some important parameters, which directly affect the efficiency of the PV panels, must be taken into account, such as temperature and pressure of the surroundings, temperature of the PV panels and chemical composition of the PV panels.

The electrical energy generated by the PV panels is the available energy that can be utilized by the user. In literature, the electrical energy is also called as “electrical exergy” [121].

The exergy balance of the PV panels can be expressed as:

$$\dot{E}\chi_{S,in} - \dot{E}\chi_{S,out,usf} - \dot{E}\chi_{S,loss} - \dot{E}\chi_{S,dest} = 0 \quad (2.5)$$

where $\dot{E}\chi_{S,in}$ is the exergy input, $\dot{E}\chi_{S,out,usf}$ is the net useful exergy output, $\dot{E}\chi_{S,loss}$ is the exergy loss and $\dot{E}\chi_{S,dest}$ is the exergy destruction rate of the PV panels [122].

Exergy input of the PV panels can be calculated with the following equation [123] [124]:

$$\dot{E}\chi_{S,in} = S_S A_{PV} \left[1 - \frac{4}{3} \left(\frac{T_{amb}}{T_{sun}} \right) + \frac{1}{3} \left(\frac{T_{amb}}{T_{sun}} \right)^4 \right] \quad (2.6)$$

where A_{PV} is the PV panel area, S_S is the solar irradiation on PV panels, T_{amb} is the ambient air temperature and T_{sun} is the sun temperature and taken as 6000 K [125] [126]. T_{amb} and S_S are obtained from TRNSYS simulations.

The net useful exergy output can be calculated using the following equation:

$$\dot{E}\chi_{S,out,usf} = V_m I_m \quad (2.7)$$

where V_m is the maximum voltage and I_m is the maximum current of the PV panels. These parameters are tabulated in Table 2.

The exergy loss can be calculated using the following equation:

$$\dot{E}\chi_{S,loss} = \dot{Q}_{S,loss} \left(1 - \frac{T_{amb}}{T_{PV}} \right) \quad (2.8)$$

where T_{PV} is the PV panel surface temperature obtained from TRNSYS simulations. $\dot{Q}_{S,loss}$ is the heat loss rate. It is given by the following equation [121] [127];

$$\dot{Q}_{S,loss} = h_{conv} A_{PV} (T_{PV} - T_{amb}) \quad (2.9)$$

where h_{conv} is the convective heat transfer coefficient from PV panels to the ambient. It is given by the following equation [128]:

$$h_{conv} = 2.8 + 3 V_w \quad (2.10)$$

where V_w is the wind velocity and obtained from TRNSYS simulations.

The exergy destruction rate of the PV panels is given by the following equation:

$$\dot{E}\chi_{S,dest} = \dot{E}\chi_{S,in} - \dot{E}\chi_{S,out,usf} - \dot{E}\chi_{S,loss} \quad (2.11)$$

The exergy efficiency of the PV panels is calculated using

$$\psi_s = \frac{\dot{E}\chi_{S,out,usf}}{\dot{E}\chi_{S,in}} \quad (2.12)$$

Substituting Equations 2.6 and 2.7 into Equation 2.12, the following equation is obtained:

$$\psi_s = \frac{V_m I_m}{S_S A_{PV} \left[1 - \frac{4}{3} \left(\frac{T_{amb}}{T_{sun}} \right) + \frac{1}{3} \left(\frac{T_{amb}}{T_{sun}} \right)^4 \right]} \quad (2.13)$$

Using TRNSYS, from Equation 2.12, the yearly exergy efficiency of the PV panels is calculated as 15.19%. In Figure 21, exergy analysis of the PV panels is illustrated by a Grassmann (or exergy flow) diagram. Hepbaşlı [129] defined the Grassmann diagram as a very useful way of representing exergy flows and exergy losses. The Grassmann diagram provides quantitative information about the amount of the exergy flows and exergy losses through each component of the system.

In Figure 22, the energy and the exergy efficiencies of the PV panels are presented for the period of a whole year. It is observed that the energy and the exergy efficiencies are decreasing until September. The system is more efficient in terms of energy and exergy efficiencies in the winter. The behavior of the exergy efficiency

curve is different from the energy efficiency curve. The seasonal effects are dominant on the exergy efficiency, because in the exergy calculations the electrical exergy is taken into account and the electrical exergy has its lowest value during the summer, as in [120]. After September a significant increase in the energy and the exergy efficiencies is observed. It can be concluded that the PV panels operate effectively in terms of energy and exergy during colder days.

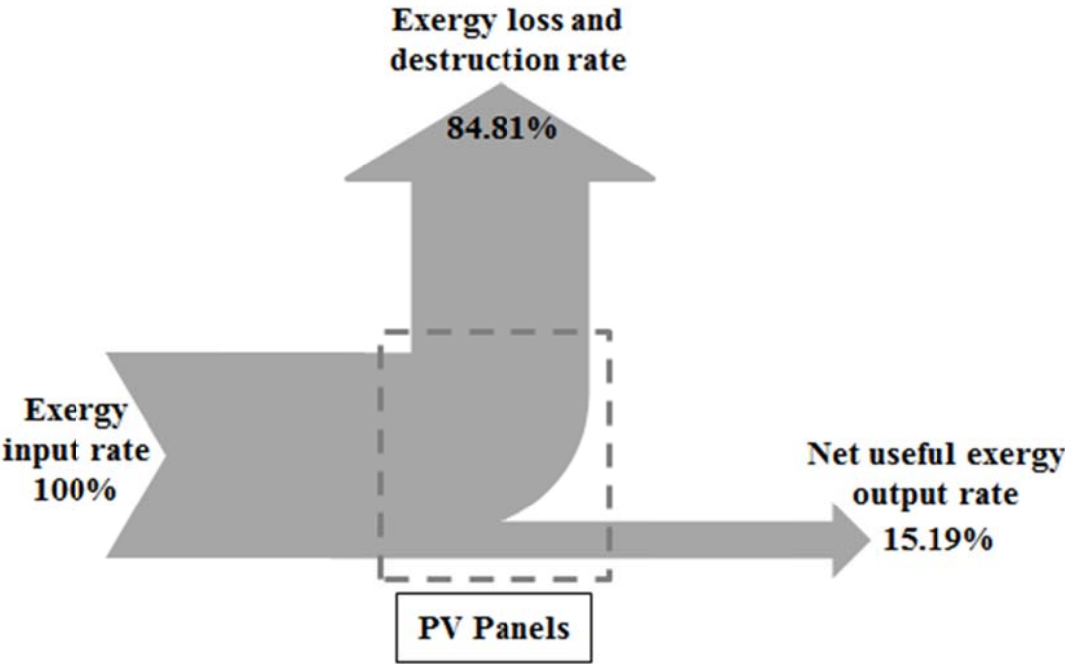


Figure 21 Grassmann diagram for the PV panels.

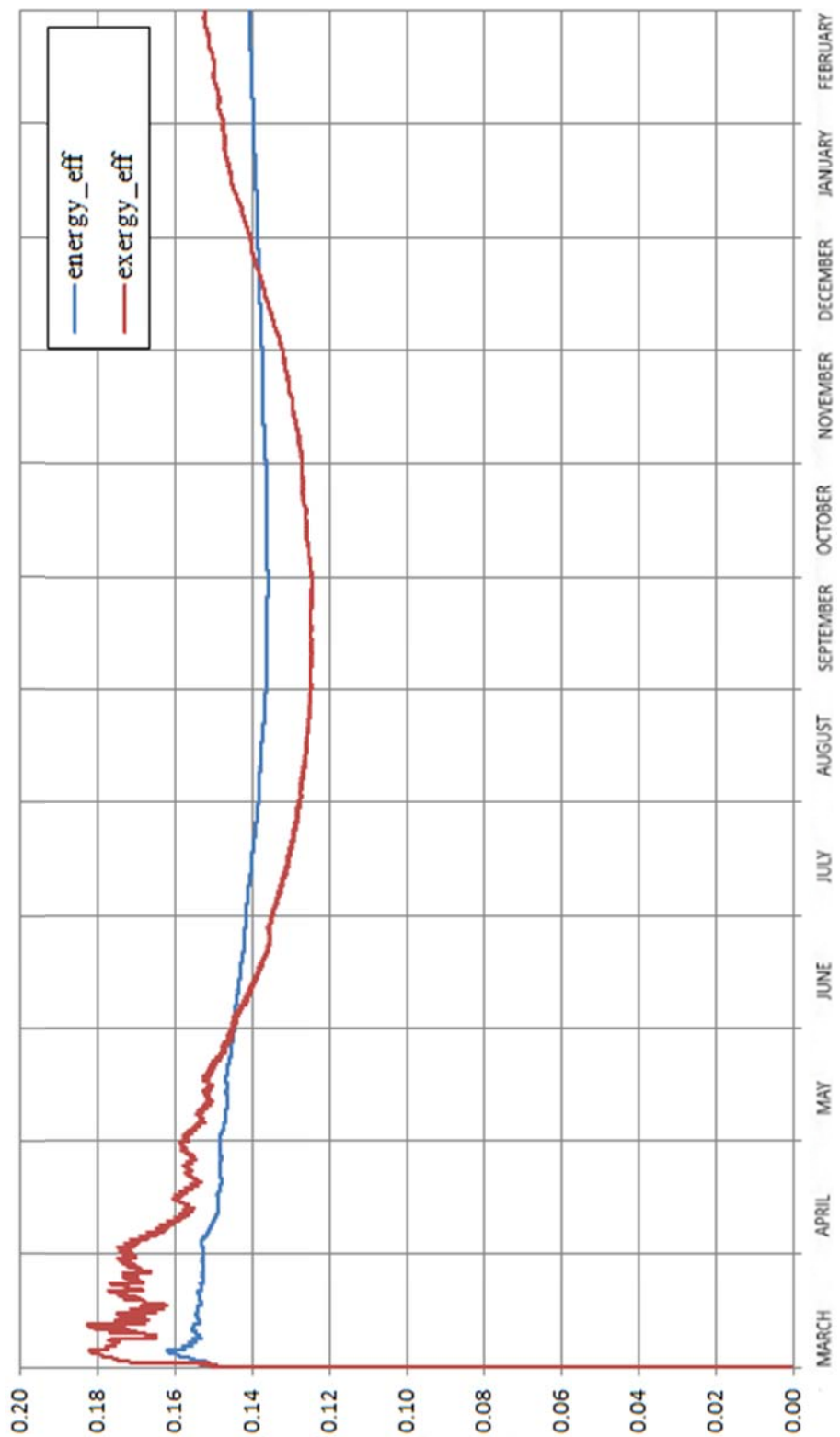


Figure 22 Energy end exergy efficiencies of the PV panels.

2.2.2.2 Exergy Analysis of the PEM Electrolyzer

In the exergy analysis of the PEM electrolyzer, the heating value of hydrogen is taken into account together with the capacity of hydrogen to do useful work, considering that hydrogen is not in equilibrium with the environment, as in [122].

The following assumptions are made for the exergy analysis of the PEM electrolyzer [123]:

- as the exergy input, only the electrical power input is taken into account;
- exergy of the water is not included in the exergy analysis of the electrolyzer;
- exergy of oxygen is neglected in exergy calculations;
- kinetic and potential energies of the reactants and products are neglected;
- hydrogen is taken as an ideal gas.

The exergy balance of the PEM electrolyzer can be expressed as

$$\dot{E}\chi_{Elz,in,el} - \dot{E}\chi_{Elz,out,H_2} - \dot{E}\chi_{Elz,dest} = 0 \quad (2.14)$$

where $\dot{E}\chi_{Elz,in,el}$ is the electrical exergy input to the electrolyzer; $\dot{E}\chi_{Elz,out,H_2}$ is the hydrogen exergy output of from the electrolyzer and $\dot{E}\chi_{Elz,dest}$ is the exergy destruction rate of the electrolyzer.

The electrical exergy input of the electrolyzer can be calculated using the following equation:

$$\dot{E}\chi_{Elz,in,el} = V_{Elz}I_{Elz} \quad (2.15)$$

where V_{Elz} is the voltage and I_{Elz} is the current of the electrolyzer. These parameters are obtained from TRNSYS simulations.

The hydrogen exergy output of the electrolyzer can be calculated using the following equation:

$$\dot{E}\chi_{Elz,out,H_2} = \dot{m}_{Elz,H_2}(ex_{ch} + ex_{ph})_{H_2} \quad (2.16)$$

where \dot{m}_{Elz,H_2} is the hydrogen production rate of the electrolyzer, which is obtained from TRNSYS simulations. ex_{ch} is the chemical exergy of the hydrogen and ex_{ph} is the physical exergy of the hydrogen. Chemical exergy of a substance can be defined as the deviation of the chemical composition of the material from its surroundings. In literature, chemical exergy of the hydrogen is reported as 117,113 kJ/kg [122]. Physical exergy of a substance can be defined as the maximum useful work available when the substance goes from its initial state to a reference state. The reference state is defined by the ambient temperature T_0 and pressure p_0 . Physical exergy of a substance is defined by the following equation:

$$ex_{ph} = \hat{h} - \hat{h}_0 - T_0(\hat{s} - \hat{s}_0) \quad (2.17)$$

where \hat{h}_0 and \hat{s}_0 represents the specific enthalpy and the specific entropy calculated with respect to the reference state. Equation 2.17 can be written for an ideal gas as follows:

$$ex_{ph} = c_p T_0 \left[\frac{T}{T_0} - 1 - \ln\left(\frac{T}{T_0}\right) + \ln\left(\frac{p_{H_2}}{p_0}\right)^{\frac{\varphi}{\varphi-1}} \right] \quad (2.18)$$

where φ is the adiabatic exponent and c_p is the heat capacity. In calculations, φ is taken as 1.4 and c_p is taken as 14.89 kJ/kg K for hydrogen. T_0 and p_0 are obtained from TRNSYS simulations.

The exergy destruction rate of the electrolyzer can be defined as

$$\dot{E}\chi_{ELz,dest} = \dot{E}\chi_{ELz,in,el} - \dot{E}\chi_{ELz,out,H_2} \quad (2.19)$$

The exergy efficiency of the PEM electrolyzer is calculated as

$$\psi_{ELz} = \frac{\dot{E}\chi_{ELz,out,H_2}}{\dot{E}\chi_{ELz,in,el}} \quad (2.20)$$

Substituting Equations 2.15, 2.16 and 2.18 into Equation 2.20, the following obtained:

$$\psi_{ELz} = \frac{\dot{m}_{ELz,H_2} \left(ex_{ch} + c_P T_0 \left[\frac{T}{T_0} - 1 - \ln \left(\frac{T}{T_0} \right) + \ln \left(\frac{T}{T_0} \right)^{\frac{\phi}{\phi-1}} \right] \right)_{H_2}}{V_{ELz} I_{ELz}} \quad (2.21)$$

Using Equation 2.21 (in TRNSYS), yearly exergy efficiency of the PEM electrolyzer is calculated as 53.51%. Exergy analysis of the PEM electrolyzer is illustrated by a Grassmann diagram in Figure 23.

In the energy analysis, efficiency of the PEM electrolyzer is calculated as 52.95%. For the PEM electrolyzer, the exergy efficiency is found slightly higher than the energy efficiency. This outcome is consistent with the literature [122] [123].

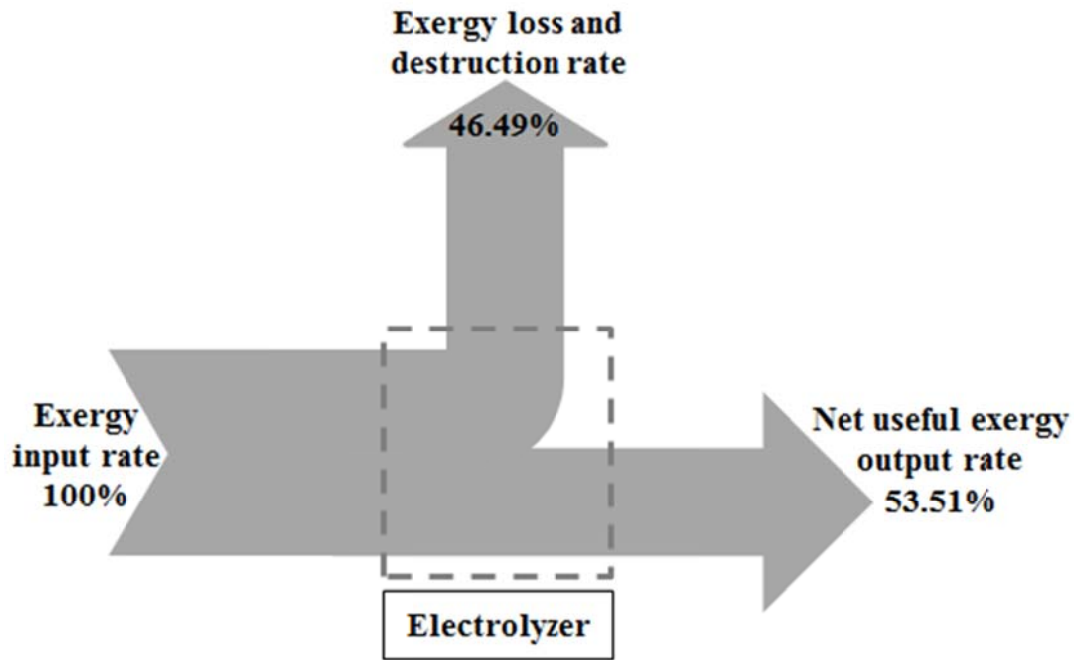


Figure 23 Grassmann diagram for the PEM electrolyzer.

2.2.2.3 Exergy Analysis of the PEM Fuel Cell

In the exergy analysis of the PEM fuel cell, a procedure similar to the one used in the exergy analysis of the PEM electrolyzer is followed with a difference in the reference state. Here, the reference state is defined by the temperature and pressure of the hydrogen fed into the fuel cell instead of the ambient values, as in [122].

The following assumptions (similar to the assumptions in the exergy analysis of the PEM electrolyzer) are made for the exergy analysis of the PEM fuel cell [130]:

- For the exergy input, only the exergy of hydrogen is assumed as the net exergy input;
- exergy of the water is not included in the exergy analysis of the fuel cell;
- exergy of oxygen is neglected in exergy calculations;
- kinetic and potential energies of the reactants and products are neglected;
- hydrogen is taken as an ideal gas.

The exergy balance of the PEM fuel cell can be written as

$$\dot{E}\chi_{FC,in,H_2} - \dot{E}\chi_{FC,out,usf} - \dot{E}\chi_{FC,dest} = 0 \quad (2.22)$$

where $\dot{E}\chi_{FC,in,H_2}$ is the exergy input rate of the PEM fuel cell; $\dot{E}\chi_{FC,out,usf}$ is the useful exergy output rate of the PEM fuel cell and $\dot{E}\chi_{FC,dest}$ is the exergy destruction rate of the PEM fuel cell .

The exergy input rate of the PEM fuel cell can be calculated using the following equation:

$$\dot{E}\chi_{FC,in,H_2} = \dot{m}_{FC,H_2}(ex_{ch} + ex_{ph})_{H_2} \quad (2.23)$$

where \dot{m}_{FC,H_2} is the hydrogen consumption rate of the fuel cell obtained from TRNSYS simulations. In the physical exergy calculations, the temperature T_{PEM} and the pressure p_{PEM} of the hydrogen fed into the fuel cell is used as the reference state. The physical exergy of hydrogen can be calculated using the following equation:

$$ex_{ph} = c_P T_{PEM} \left[\frac{T}{T_{PEM}} - 1 - \ln\left(\frac{T}{T_{PEM}}\right) + \ln\left(\frac{p_{H_2}}{p_{PEM}}\right)^{\frac{\varphi}{\varphi-1}} \right] \quad (2.24)$$

The definitions of ex_{ch} , φ and c_P values are given in Subsection 2.2.2.2. The exergy destruction rate of the fuel cell can be defined as

$$\dot{E}\chi_{FC,dest} = \dot{E}\chi_{FC,in,H_2} - \dot{E}\chi_{FC,out,usf} \quad (2.25)$$

The useful exergy output rate of the PEM fuel cell can be calculated using the following equation

$$\dot{E}\chi_{FC,out,usf} = V_{FC}I_{FC} \quad (2.26)$$

The voltage V_{FC} and the current I_{FC} of the fuel cell are obtained from TRNSYS simulations. The exergy efficiency of the PEM fuel cell is calculated by

$$\psi_{FC} = \frac{\dot{E}\chi_{FC,out,usf}}{\dot{E}\chi_{FC,in,H_2}} \quad (2.27)$$

Substituting Equations 2.23, 2.24 and 2.26 into Equation 2.27, the following is obtained:

$$\psi_{FC} = \frac{V_{FC}I_{FC}}{\dot{m}_{FC,H_2} \left(ex_{ch} + c_p T_{PEM} \left[\frac{T}{T_{PEM}} - 1 - \ln\left(\frac{T}{T_{PEM}}\right) + \ln\left(\frac{p_{H_2}}{p_{PEM}}\right)^{\frac{\varphi}{\varphi-1}} \right] \right)_{H_2}} \quad (2.28)$$

Using Equation 2.28 (in TRNSYS), the yearly exergy efficiency of the PEM fuel cell is calculated as 58.54%. Exergy analysis of the PEM fuel cell is illustrated by a Grassmann diagram in Figure 24.

In the energy analysis, efficiency of the PEM fuel cell is calculated as 61.15%. For the PEM fuel cell, the exergy efficiency is found slightly lower than the energy efficiency. This outcome is consistent with the literature [122] [123].

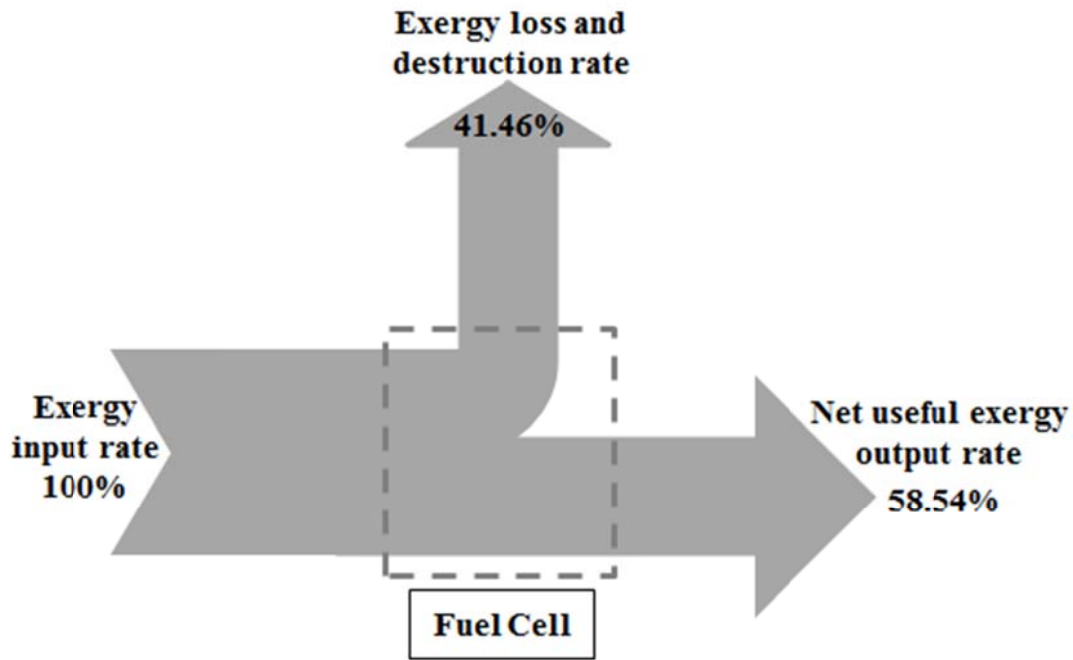


Figure 24 Grassmann diagram for the PEM fuel cell.

2.2.2.4 Exergy Analysis of the Inverters

Exergy efficiency of an inverter is assumed to be equal to its energy efficiency, since electrical energy is considered as completely useful work, as in [121]. The exergy efficiency of the DC/AC inverters can be defined as the ratio of the output power to the input power. Thus, exergy efficiency of a DC/AC inverter can be calculated using

$$\psi_{IN} = \frac{AC \text{ Power Output}}{DC \text{ Power Input}} \quad (2.29)$$

In the present study, the DC/AC inverters between the PV panels and the controller are embedded into the controller. Therefore, the exergy efficiency of the controller is equal to its energy efficiency, 94.07%. Similarly, the exergy efficiency of the inverter is equal to its energy efficiency, 94.97%.

2.2.2.5 Overall Exergy Analysis of the System

The exergy analysis is performed for a complete year. The exergy generated due to work and the exergy generated due to mass are neglected in the overall exergy calculations as suggested in [123]. Also, exergy analysis of the hydrogen storage system is not taken into account assuming that there is no leakage or loss from the hydrogen storage tanks (as it is done in [121]).

The overall exergy efficiency of the system is defined as follows [129]:

$$\psi_{sys} = \psi_s \psi_{ELZ} \psi_{FC} \psi_{IN} \quad (2.30)$$

Using Equation 2.31 the overall exergy of the hydrogen cycle of the system is calculated as 4.25 %.

Grassmann diagram for the hydrogen cycle of the hybrid renewable energy system is presented in Figure 25. It is observed that most of the exergy is lost or destroyed through the PV panels. Overall, only a small portion of the exergy input is converted to useful exergy output.

In Table 7, the average energy and exergy efficiencies of the system are summarized for the hydrogen cycle of the system. The energy efficiencies are obtained from the TRNSYS simulations. It can be said that the exergy efficiencies of the PV panels and the PEM electrolyzer are higher than their energy efficiencies. It can be further concluded that the system is more efficient in terms of exergy.

When the overall system is considered, it can be concluded that the energy and exergy efficiencies of the analyzed system are very low: The hydrogen cycle of the system has an energy efficiency of 4.06% and an exergy efficiency of 4.25%. The main reason for this is the low efficiency of the PV panels, since they only convert 14.05% of the incident solar energy to electricity. Also, destruction of the exergy in the PV panels is considerably high. The PV panels have an exergy efficiency value

of only 15.19%, as the PV panels convert high quality solar radiation to low quality waste heat.

Table 7 Average energy and exergy efficiencies of the system components.

Components	Energy Efficiency	Exergy Efficiency
PV Panels	14.05%	15.19%
Controller	94.07%	94.07%
PEM Electrolyzer	52.95%	53.51%
PEM Fuel Cell	61.15%	58.54%
Inverter	94.97%	94.97%
Overall System	4.06%	4.25%

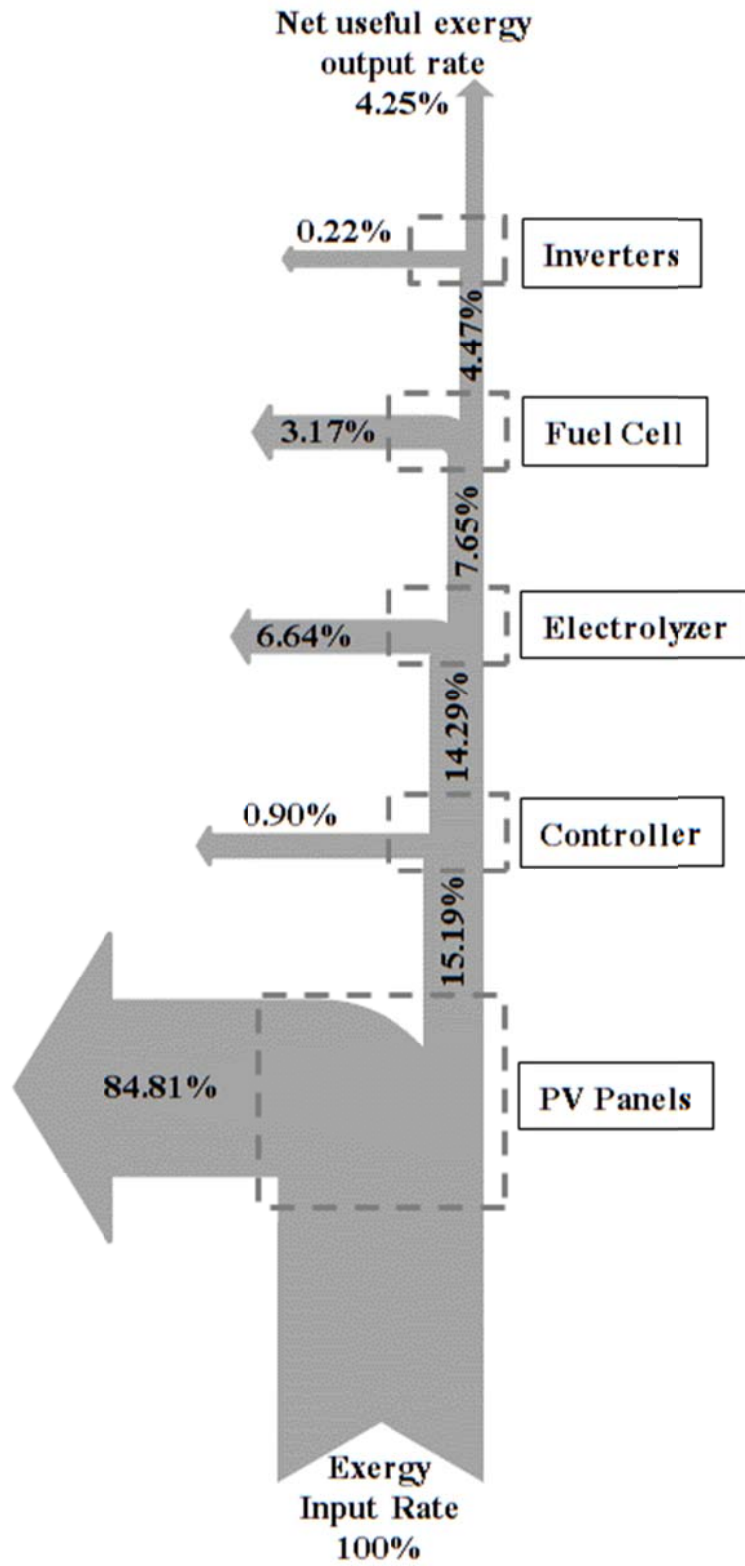


Figure 25 Grassmann diagram for the exergy losses of the system.

2.3 Economic Analysis of the System

A detailed economic analysis of the hybrid renewable energy system is performed in order to complement the energy and exergy analyses. An analysis method called as Levelized Cost of Electricity (LCE) is used. The levelized cost of electricity is defined in [131] as “*the constant price per unit of energy that causes the investment to just break even*”. LCE is an economic estimate of the generated energy. This method is commonly used in the literature for similar systems (among others, in [4] [8] [131] [132] [133] [134]). It is also used in designing and sizing of the hybrid renewable energy systems. LCE analysis includes all of the costs related with the system throughout its lifetime. Details of the LCE analysis method and the assumptions are presented as Appendix A.

LCE analysis is performed for the system lifetime of 25 years and annual interest rate is assumed as constant namely 6%, which is a commonly used value in similar studies [8] [135] [136]. LCE of the analyzed system is calculated as 0.626 \$/kWh. Bezmalinovic et al. [8] found LCE as 0.828 \$/kWh for a similar solar-hydrogen based hybrid renewable energy system. However, the mentioned study was performed for a base-station of mobile communications. This is a very small application as compared to the present one. In the base-station, the electrolyzer cost dominates the overall system cost because of the size of the system. In the present system, PV panels cost dominates the overall system cost; thus, LCE value is approximately 0.2 \$/kWh less than the base-station in [8].

For comparison, the LCE analysis is repeated for a pure PV/battery energy system and a pure diesel generator system.

In the pure PV/battery system only batteries are used instead of the hydrogen cycle of the system. Details of this analysis are presented as Appendix A.3. LCE of the PV/battery system is calculated as 0.687 \$/kWh. Approximately 0.06 \$/kWh difference exists between the PV/hydrogen based system and the PV/battery based

system. The PV/battery system is calculated to be more expensive than the PV/hydrogen system. This is because the required number of batteries is high, the service life of the batteries is short, and the replacement cost of the batteries is high. Generally in the literature, pure battery solutions are rejected due to the requirement of high number of batteries [137].

In the pure diesel generator system only a diesel generator is used instead of the complete system. This analysis is conducted for two different fuel price scenarios and the details are presented as Appendix A.4. LCE values of the pure diesel generator system are calculated as 0.221 \$/kWh and 0.359 \$/kWh for the fuel price scenarios of 1.5 \$/l and 2.5 \$/l, respectively. As expected, the diesel generator system is calculated to be more economical than the PV/hydrogen system. However, as stated before, fossil fuels have several undesirable impacts on environment, and they may be hard to continuously obtain during a long-term emergency blackout.

2.4 Discussions

System modeling study shows that the stand-alone hybrid renewable system is capable of satisfying the electricity demand of the emergency room up to one year with a single exception. Only insufficient equipment is the hydrogen tanks. If the capacity of the tanks is increased from 30m³ to 45m³, the system could provide uninterrupted electricity to the system for a whole year during a long term emergency blackout. On the other hand, if the hydrogen tank capacity does not increased to 45m³, the system could provide continuous energy to the system for 316 days with a 30m³ hydrogen storage capacity. This means, if the system starts to operate at the 1th of March with an initial level of 5% of hydrogen storage capacity, it would be capable of providing electric to the system until 10th of January.

The average energy-exergy efficiency values of the various components of the system are determined. When the overall system is considered, it can be concluded

that energy and exergy efficiencies of the analyzed system is very low. The hydrogen cycle of the system has an energy efficiency of 4.06% and exergy efficiency of 4.25%. The main reason of this is the low efficiency of the PV panels, since only 14.05% of the solar energy is utilized by PV panels for electricity generation and the exergy destruction rate of the PV panels is considerably high.

Among the system components taken into account, the maximum exergy efficiency is obtained for the inverters. The second highest exergy efficiency is obtained for the PEM fuel cell and the third highest exergy occurs for the PEM electrolyzer. The least exergy efficiency is observed for the PV panels.

It is observed that the exergy efficiency of the PV panels is higher than the energy efficiency due the analysis of the solar radiation. In the solar radiation analysis, the solar energy contribution is higher than the solar exergy contribution; this is because, the effects of the sun and the dead state temperature are considered in the exergy analysis (See Equation 2.6).

According to the LCE analysis, PV/hydrogen based renewable energy system is found slightly economical than the PV/battery based system. Rapidly advancing PEM fuel cell and PEM electrolyzer technologies could improve this trend in the near future. On the other hand, LCE analysis of the pure diesel generator system shows that diesel generator system is more economical than the PV/hydrogen system. However, in this study, the main goal is to show that a solar-hydrogen based renewable energy system can be a possible alternative to fossil fuel based energy systems especially in long-term emergency blackout conditions.

Main difficulty of the LCE analysis is obtaining real market values of the system components, since the hydrogen technology is not fully commercialized so far. There is still no mass production for the PEM fuel cells and the PEM electrolyzers yet. Thus, PEM based equipment commonly sold by individual arrangements with

user-defined specifications. This issue makes unit prices of the PEM based components quite high.

CHAPTER 3

CFD MODELING

Single cell of a PEM fuel cell with serpentine type flow channels is modeled using CFD. CFD simulations are conducted for this model and compared with a similar study that is available in the literature. After successfully modeling the single cell, stack modeling is investigated. In this chapter, results of the CFD simulations are discussed for a complete cell and simplified 2-cell, 3-cell and 4-cell stacks.

3.1 PEM Fuel Cell Model

A complete, single-cell PEM fuel cell model with serpentine type flow channels is analyzed using CFD. The model has 10 cm² active area and 20 serpentine passes. The MEA, the GDL and the bipolar plates are modeled in detail. The single-cell PEM fuel cell model is presented in Figure 26. The model used in this study is available in the literature. Jeon et al. [138] studied the influences of serpentine flow-field designs on PEM fuel cell performance, and compared four different serpentine geometries. One of the serpentine geometries from Jeon et al. [138] is investigated in this study. The same serpentine geometry is successfully modeled and CFD simulations are performed for this model for two cases, low inlet humidity and high inlet humidity boundary conditions.

Jeon et al. have several published work related with PEM fuel cell modeling by using CFD. In these studies, different aspects of the PEM fuel cell modeling were analyzed in detail. For instance, Jeon et al. investigated the transient performance of PEM fuel cells in detail [73] [74] [75]. They also investigated mass transport

phenomenon inside PEM fuel cells [50], water and current distribution through PEM fuel cells [139] [140] and temperature distribution inside PEM fuel cells [141] [54]. Similarly, they investigated the effects of the channel geometry [55] [142] [143] and the humidity [144] [145] [146] on the performance of PEM fuel cells. Gas diffusion media (GDL) of PEM fuel cells was also analyzed by Jeon et al. considering the flooding effect [147] [148] [149].

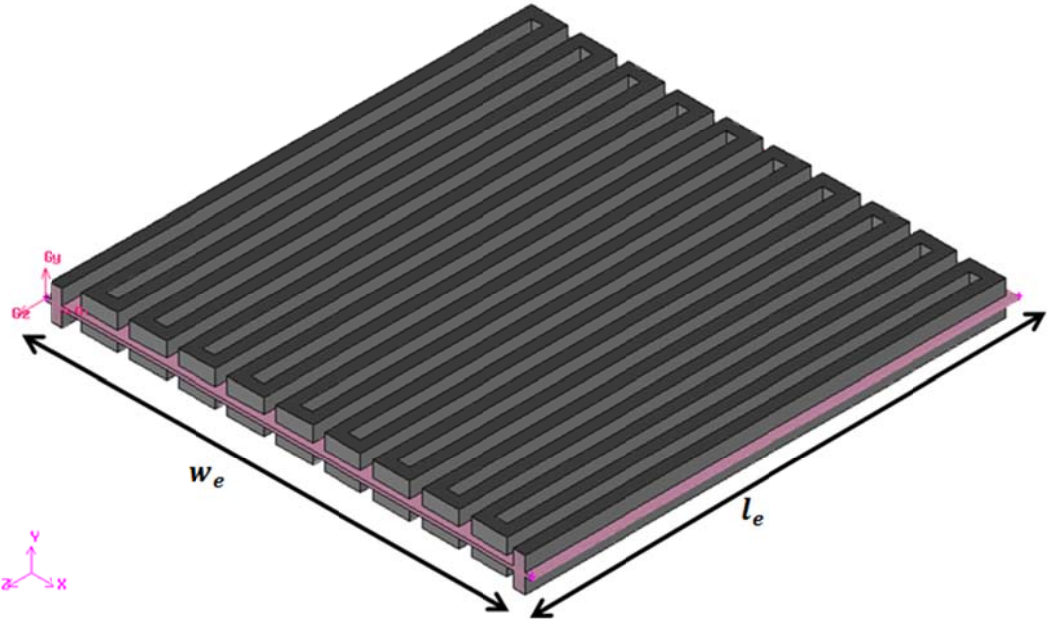


Figure 26 PEM fuel cell model.

3.1.1 Boundary and Operating Conditions

The geometrical parameters and the material details of the CFD model are tabulated in Table 8. The tabulated data is adapted from the literature [138] [139] [143]. Simplified representation of the solution domain is presented in Figure 27. Geometrical parameters of the PEM fuel cell model are shown in Figure 26 and Figure 27. Boundary and operating conditions of the simulated PEM fuel cell model are presented in Table 9 (tabulated data is adapted from [138]). The operating

conditions presented in this table are the optimized values obtained from experimental studies in the literature.

Simulations are performed for high inlet humidity and low inlet humidity boundary conditions with corresponding inlet velocity boundary conditions tabulated in Table 10. For the high inlet humidity boundary condition, inlet humidity values of the anode and cathode corresponds to 80°C (353.15K) and 70°C (343.15K) dew point temperatures, respectively. Governing equations of the model are modified according to the conditions of the simulated case and presented as Appendix B. CFD modeling details are explained in Subsections 3.1.1, 3.1.2 and 3.1.3.

Table 8 Geometrical parameters and material details of the CFD model.

Symbols	Properties	Values
w_c	Flow channel width (mm)	0.8
h_c	Flow channel height (mm)	1.0
d_c	Distance between channels (mm)	0.8
w_e, l_e	Electrode width, length (cm)	3.2
A_r	Reaction area (cm ²)	10
t_{GDL}	GDL thickness (micron)	250
ε_{GDL}	GDL porosity	0.7
K_{GDL}	GDL permeability (m ²)	$1.0e^{-12}$
k_{GDL}	GDL thermal conductance (W/m K)	0.21
t_{MEA}	MEA thickness (micron)	50
k_{MEA}	MEA thermal conductance (W/m K)	0.15
M_m	Dry membrane equivalent weight (g/mol)	1100
ρ_m	Dry membrane density (g/cm ³)	2.0
k_{bp}	Bipolar plate thermal conductance (W/m K)	5.7

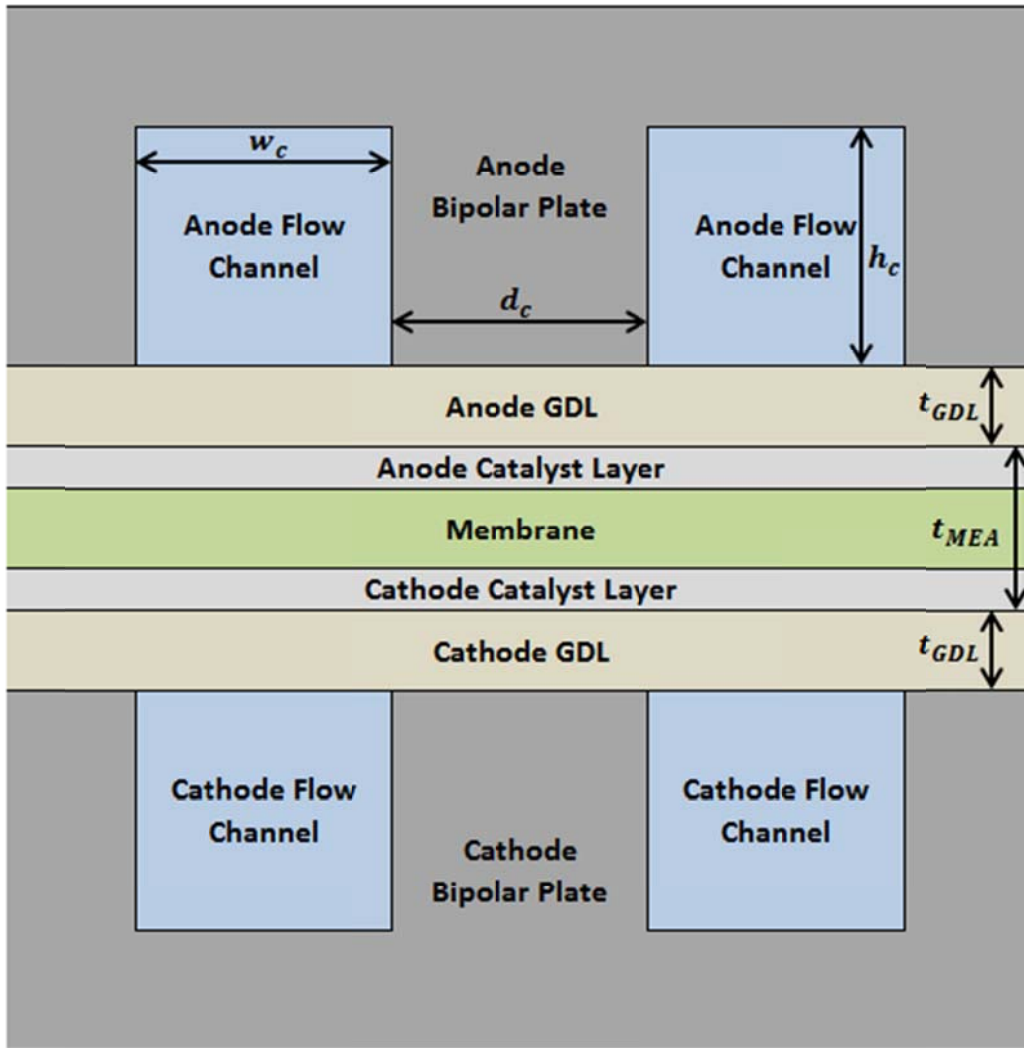


Figure 27 Simplified representation of the solution domain (not to scale).

Table 9 Boundary and operating conditions of the CFD model.

	High inlet humidity BC	Low inlet humidity BC
Anode		
Mass fraction of H ₂ (%)	11.5	25.7
Mass fraction of H ₂ O (%)	88.5	74.3
Stoichiometry	1.2	1.2
Inlet temperature (°C)	80 (353.15K)	80 (353.15K)
Dew point (°C)	80 (353.15K)	65 (338.15K)
Relative humidity (%)	100	53
Inlet flow velocity (m/s)	2.582	1.833
Cathode		
Mass fraction of O ₂ (%)	18.3	20.2
Mass fraction of H ₂ O (%)	21.5	13.1
Stoichiometry	2.0	2.0
Inlet temperature (°C)	70 (343.15K)	70 (343.15K)
Dew point (°C)	70 (343.15K)	60 (333.15K)
Relative humidity (%)	100	64
Inlet flow velocity (m/s)	7.678	6.629
Operating Conditions		
Open circuit voltage (V)	0.95	
Operating pressure (atm)	1	
Cell temperature (°C)	70 (343.15K)	
Outlet pressure (kPa)	101	

Table 10 Inlet velocities.

	High inlet humidity BC	Low inlet humidity BC
Anode (m/s)	2.582	1.833
Cathode (m/s)	7.678	6.629

3.1.2 Model Domain

Top view of the model domain is presented in Figure 28. As seen on the figure, cross-section of the model domain is constant throughout the channel. Only the inlet, the outlet and the u-turn parts of the model domain is critical. Thus, mesh density is increased in these regions. Cross-section of the domain for a single channel is presented in Figure 29. Blue region represents the flow channels of the anode and the cathode. The MEA and the GDL regions are also critical regions in terms of mesh density, since these regions are very thin compared to the other regions of the domain. Same mesh size is applied for the flow channels and the bipolar plates. In the catalyst layers and the membrane 4 elements are used with equal size. In the GDL 8 elements are used with a size function of 1.15. In this layer size function is applied from the catalyst layer to the membrane.

Optimum mesh size for the cross section of the domain is applied, as suggested in [36]. Additionally, the mesh size is compared with the literature: [50] [141] [54] [55] [146]. Consequently, it was decided that the applied mesh is suitable for the current PEM fuel cell model. In Table 11 mesh details of the CFD model are tabulated. Total number of the cells in the model is 2,649,600. Prismatic-hexagonal elements are used in the model.

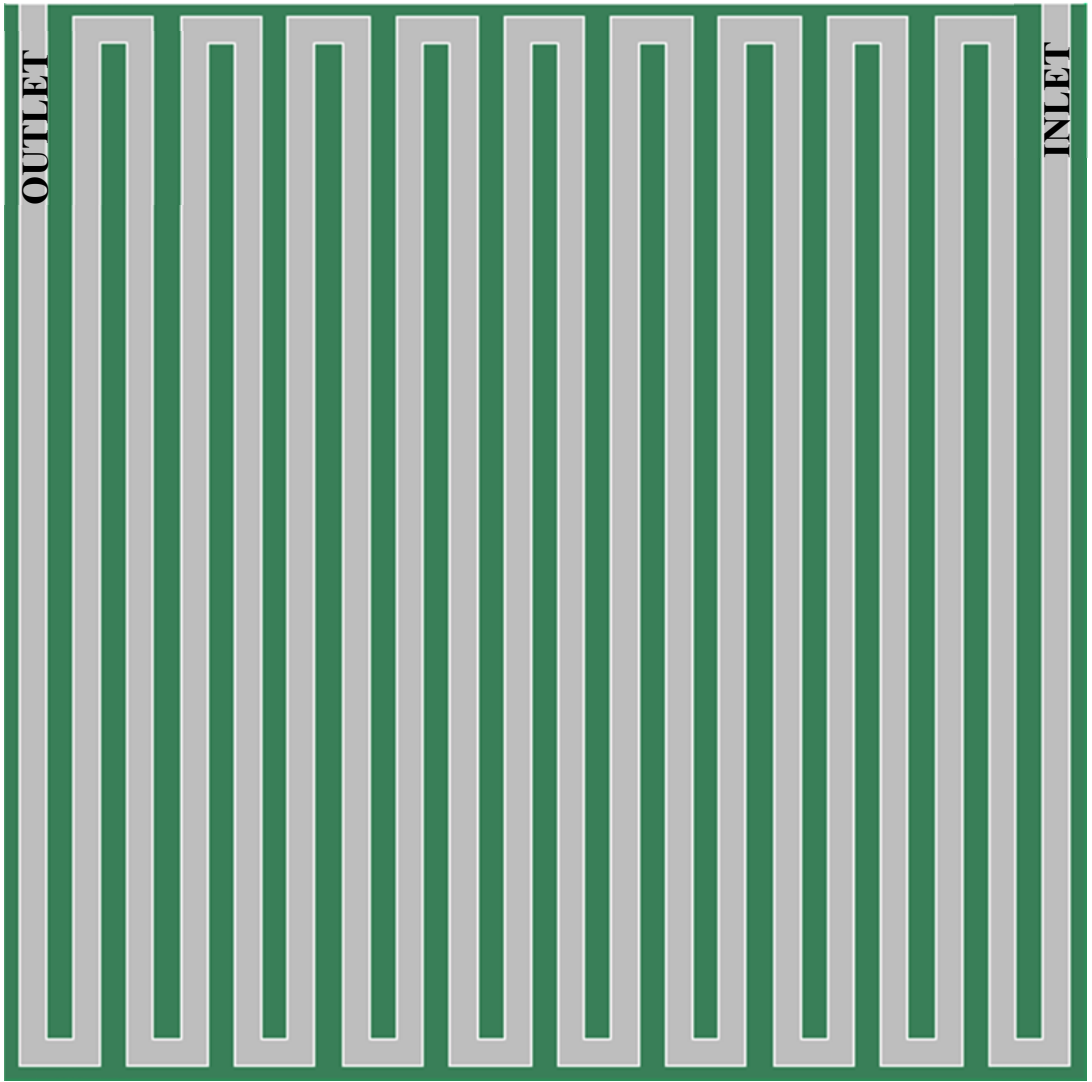


Figure 28 Model domain.

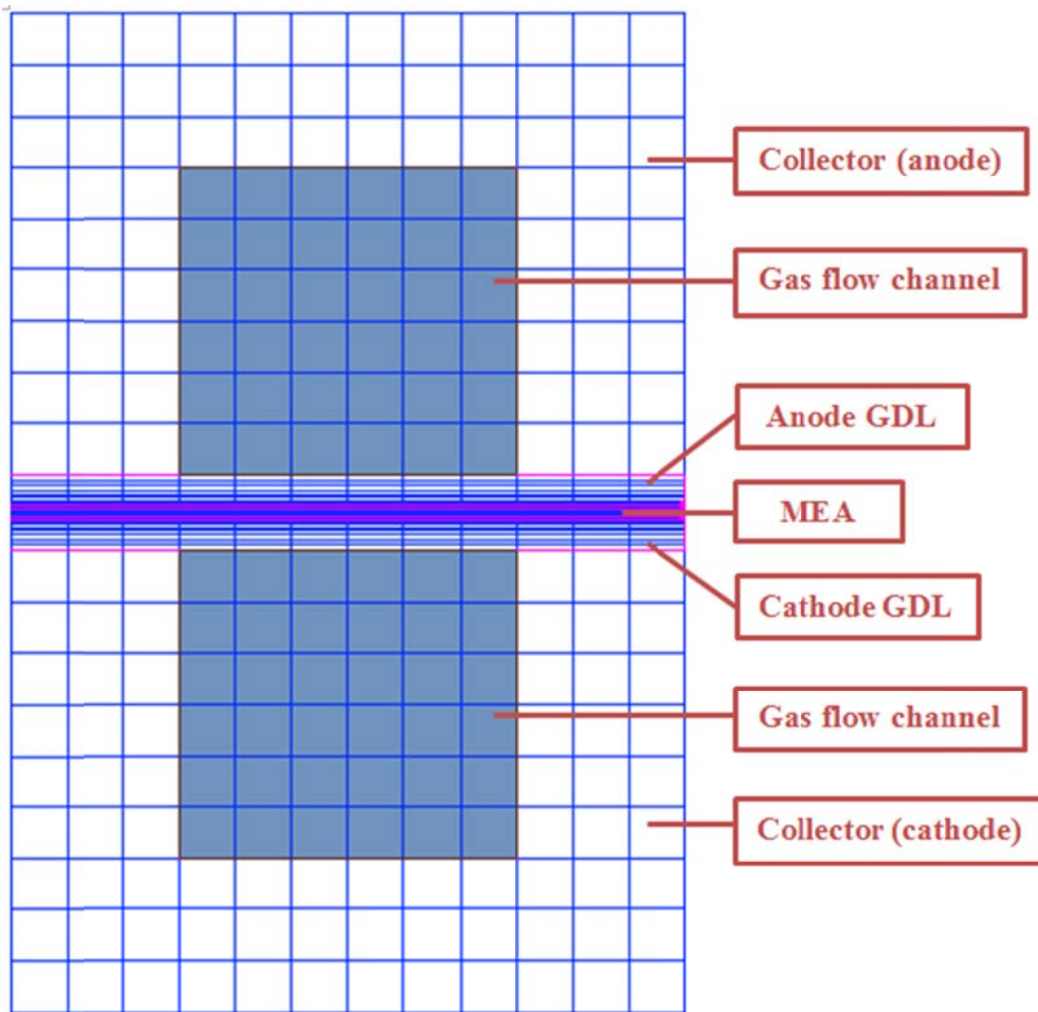


Figure 29 Cross-section of the single channel of the domain.

Table 11 Mesh details.

	Mesh Density	Mesh type	# Mesh
Anode			
Bipolar plate	12 x 9	hex-submap	345,600
Flow channel	6 x 6	hex-submap	172,800
GDL	8	hex-map	460,800
Catalyst	4	hex-wedge cooper	230,400
Cathode			
Bipolar plate	12 x 9	hex-submap	345,600
Flow channel	6 x 6	hex-submap	172,800
GDL	8	hex-map	460,800
Catalyst	4	hex-wedge cooper	230,400
Membrane			
	4	hex-wedge cooper	230,400
		Total	2,649,600

3.1.3 ANSYS Fluent Solver

Parallel solver of the ANSYS Fluent version 14.5 [150] is used with Fuel Cell and Electrolysis add-on Module [36]. Liquid water saturation (phase change) is considered by using under-relaxation in the solver. Water amount, water saturation level and potential rates are solved by using user defined scalars in the solution domain. Discrete solver is used to improve the convergence of the simulations. Multi-grid cycle is changed to F-cycle with BCGSTAB (bi-conjugate gradient stabilized method) as the stabilization method for the species and the two potential equations. In addition, multi-grid cycle tolerances are decreased to 0.001 for some of the numerical equations, as suggested in [37].

3.2 Simulation Results

Simulations are performed for the prescribed operating and boundary conditions (in Section 3.1) for the serpentine type PEM fuel cell model. Mass flow rates for the anode and cathode sides are calculated for the prescribed velocity inlet boundary conditions for the anode and the cathode side (Table 10). Because, in the literature [150], it is suggested that velocity inlet boundary conditions are not appropriate for some complex flow problems. It is advised that mass flow inlet boundary conditions should be used in such complex flows to define an inlet boundary condition. Simulations are performed for both velocity inlet boundary and the calculated mass flow rates. Nevertheless, the results of the mass flow rate and velocity inlet boundary condition simulations successfully match with each other. Thus, it is concluded that velocity boundary condition assignment is appropriate for PEM fuel cell modeling.

In the following subsections, mainly results of the high inlet humidity boundary condition case are presented. The main reason for this is explained by Jeon et al. [138]; high inlet humidity boundary conditions are generally applied in stationary applications, whereas low inlet humidity boundary conditions are usually used in transportation applications.

3.2.1 Velocity Distribution

For the high inlet humidity boundary condition, velocity distributions for the anode and cathode sides are presented in Figure 30 and Figure 31, respectively. In the first flow channel velocity distribution is different from the other channels, since uniform velocity BC is defined for the anode and the cathode sides. It is observed that flow speed is high at the u-turn regions because of the sharp turns of the channel geometry. It is better to have tapered turns instead of sharps turns. However, because of the very thin flow channels, machining process of the flow channels on the bipolar plates is very difficult and costly, when tapered turns are

used. Therefore, flow channels are usually machined on the bipolar plates with sharp turns.

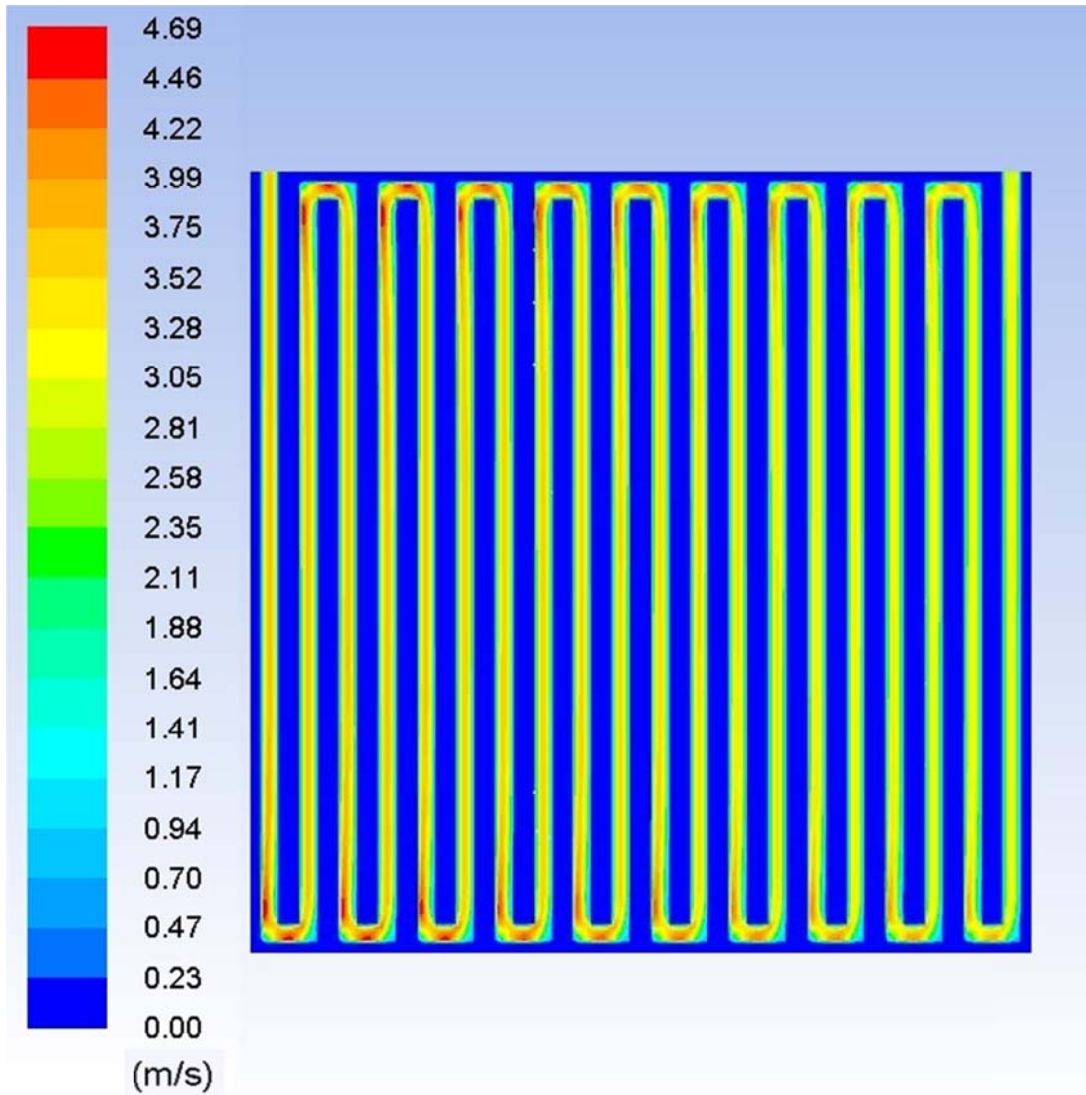


Figure 30 Velocity distribution in the anode channel (high inlet humidity BC).

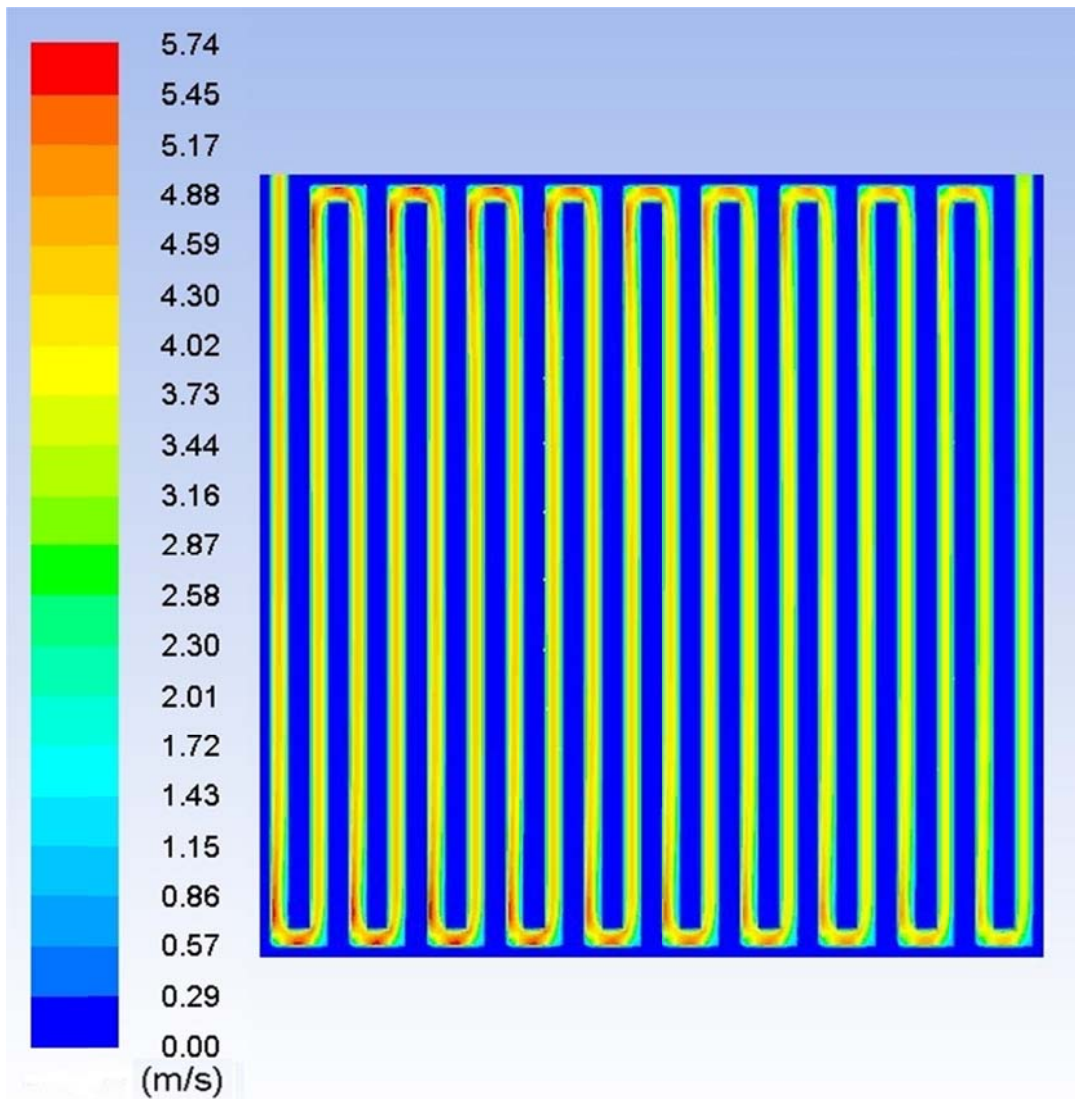


Figure 31 Velocity distribution in the cathode channel (high inlet humidity BC).

3.2.2 Species Distribution

Mass fraction of H_2 for the high inlet humidity boundary condition is presented in Figure 32. Right top of this figure is the anode side inlet of the model and this figure is obtained from the middle of the anode flow channel. It is observed that most of the supplied H_2 gas is used throughout the cell. Only a small portion of the H_2 gas is leaving the anode flow channel.

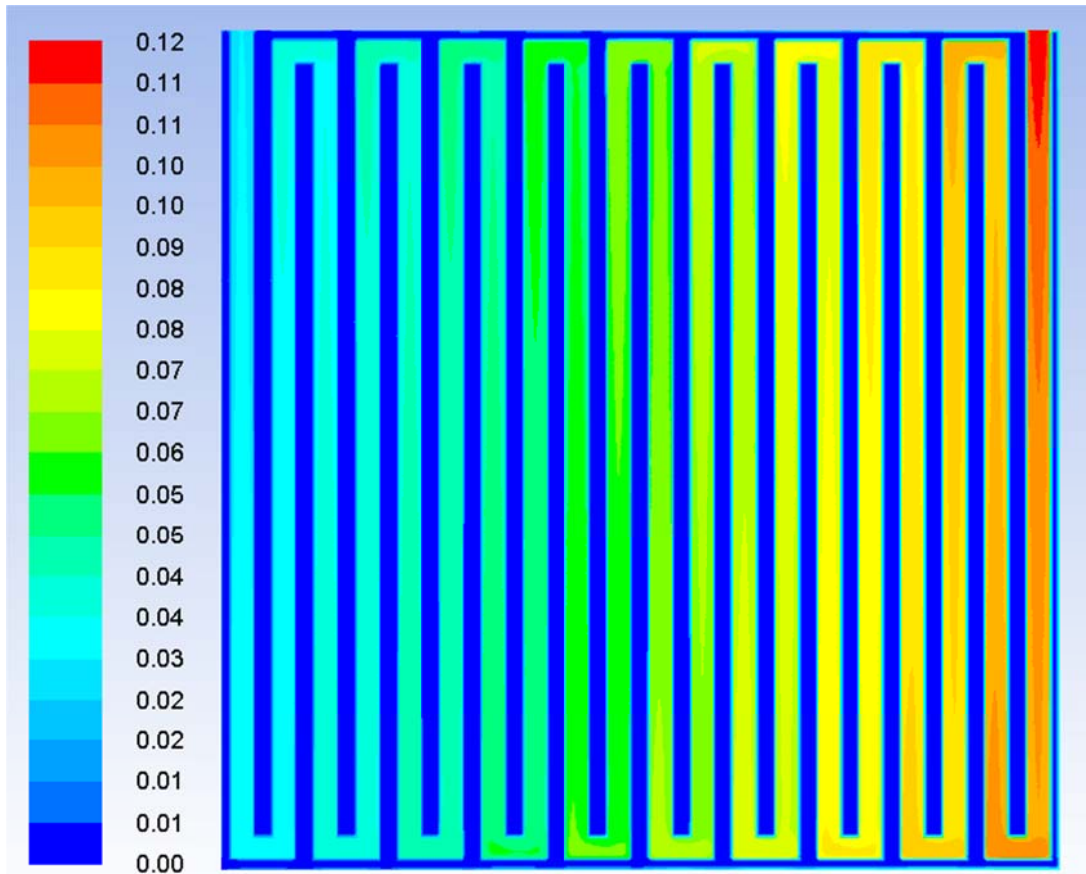


Figure 32 Mass fraction of H₂ (high inlet humidity BC).

Mass fraction of H₂O for the high inlet humidity boundary condition is presented in Figure 33. This figure is obtained from the middle of the membrane. It is observed that the membrane active area is used efficiently. It can be said that membrane is kept humid, since the mass fraction of the H₂O is not below 0.40 through the membrane. Mass fraction of H₂O is increasing through the channel. Therefore, membrane dry out problem is not expected for the simulated case. It can be concluded that the simulated serpentine geometry is a proper cell design, since H₂ gas is used effectively.

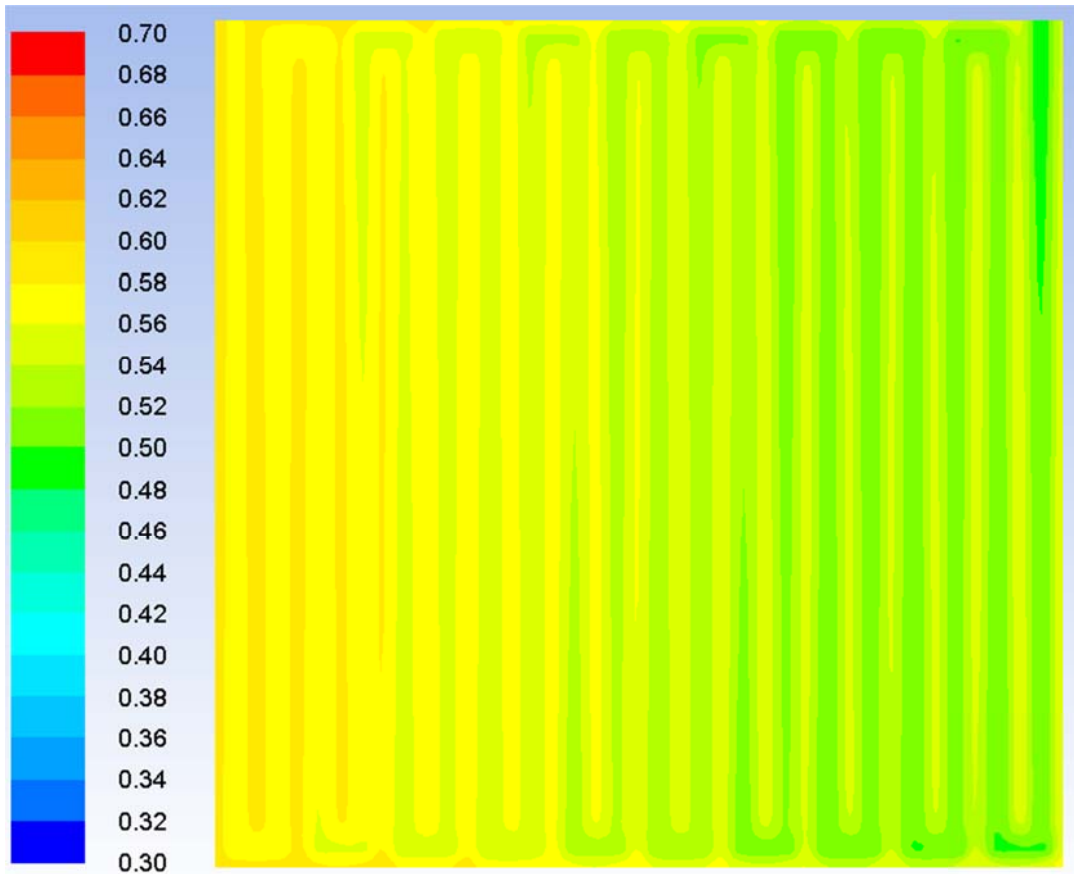


Figure 33 Mass fraction of H₂O (high inlet humidity BC).

3.2.3 Current Density Distribution

Current density distribution on the MEA surface for the high inlet humidity boundary condition for current density boundary condition of 0.35 A/cm² is presented in Figure 34. It is observed that the local current density is higher around the inlet region and lower around the outlet region because of the concentration of the reactants. In serpentine type flow channels it is normal to obtain such a current density distribution, since uniformity of the current density distribution is directly related with the length of the flow channels. In literature, it was reported that shorter flow channel length results in more uniform current density distribution than the longer flow channel length [142].

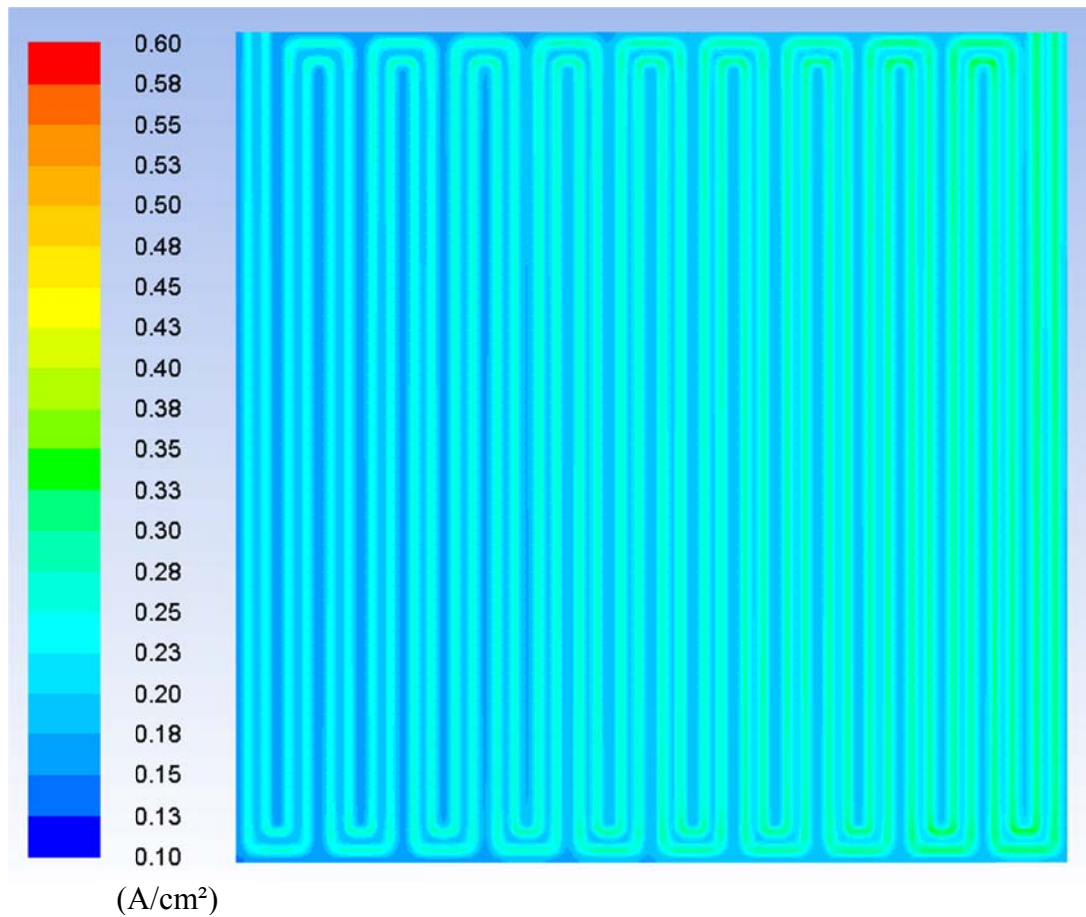


Figure 34 Current density distribution on the MEA surface for high inlet humidity BC (for 0.35 A/cm² current density).

3.2.4 Temperature Distribution

Thermal management is an important phenomenon in PEM fuel cells. Thermal management is needed to remove the excess heat produced as a result of electrochemical reactions. Without a successful thermal management, the membrane of the fuel cell becomes vulnerable to thermal stresses and drying out phenomenon [151].

Operating temperature of the cell is defined as 70°C (343.15K). Cathode side inlet temperature is assumed same as operating temperature, 343.15K. Whereas, anode side inlet temperature is 80°C (353.15 K). In Figure 35, temperature distribution of the membrane for the high inlet humidity boundary condition is presented. In Figure 36, temperature distribution at the mid-plane of the membrane (for $l_e/2$) is shown on a virtual line. This virtual line and the direction of the virtual line are shown on Figure 35. It is observed that the maximum temperature of the membrane is 346.15K and there is only a 3K temperature difference exists through the membrane. Also, it can be said that the temperature of the cell is decreasing from inlet to outlet. Thus, it can be concluded that the fuel cell is in stable operating condition. As explained above, the membrane is very vulnerable to high temperature differences. Hence, the selected operating conditions for the fuel cell are reasonable.

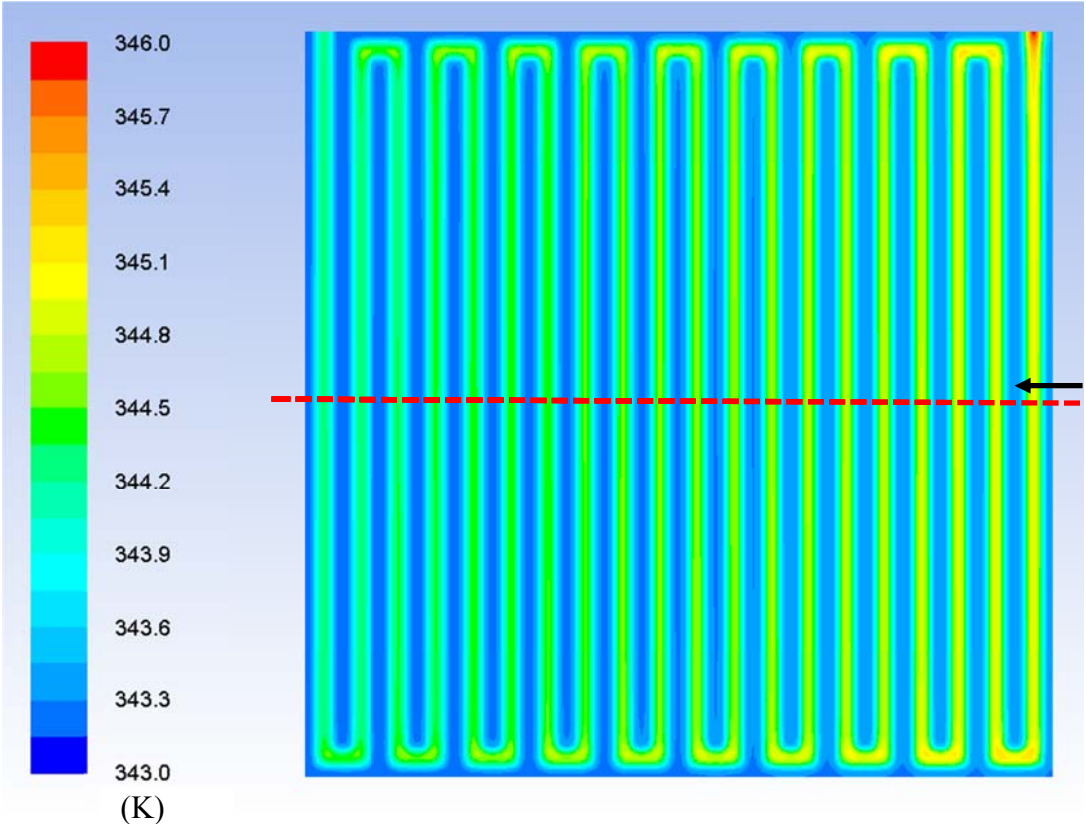


Figure 35 Temperature distribution of the membrane (high inlet humidity BC).

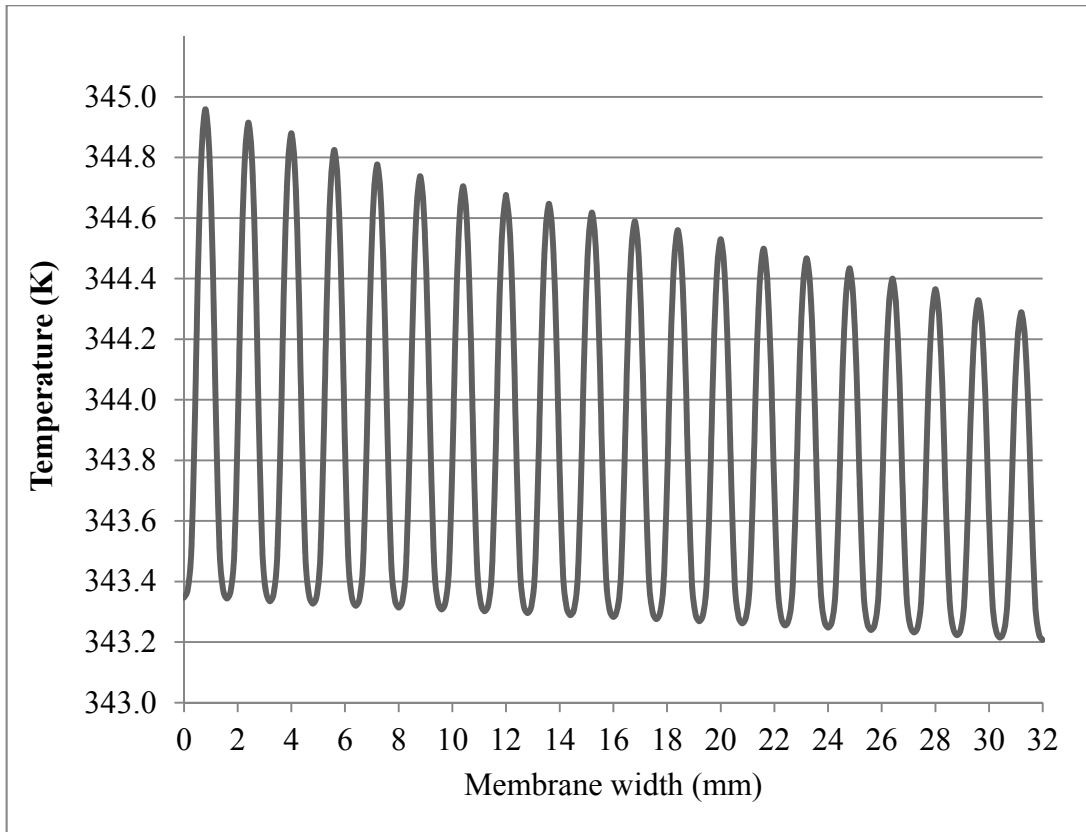
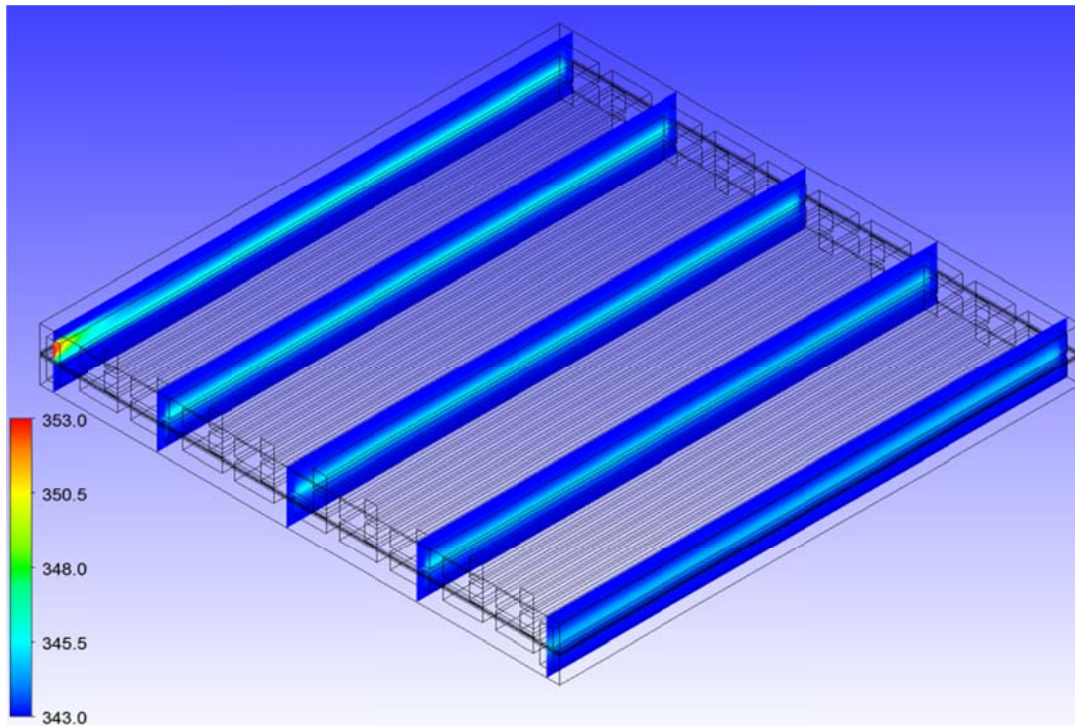


Figure 36 Temperature distribution at the mid-plane of the membrane (for $l_e/2$).

In Figure 37, axial temperature distributions inside 1st, 5th, 15th and 20th flow channels are shown for the high inlet humidity boundary condition. Because of the 10°C temperature difference between the anode inlet and the cathode inlet boundary conditions; temperature distribution is different only in the 1st channel. For other channels the observed temperature distribution is similar to each other. Therefore, it can be said that the temperature distribution of the flow channels is consistent with the temperature difference of the membrane.



(K)
 Figure 37 Temperature distributions inside 1st, 5th, 15th and 20th flow channels (high inlet humidity BC).

In Figure 38, section view of temperature distributions inside 9th, 10th and 11th flow channels is shown for the high inlet humidity boundary condition. This section view is created at the middle of the fuel cell. As explained before, the flow characteristics and the temperature distribution inside the flow channels are similar to each other, except from the 1st flow channel. It is observed that the MEA and the GDL are the hottest regions in the fuel cell because of the exothermic reactions. The temperature distribution throughout the membrane is consistent with the similar studies available in the literature [50] [152].

The anode side inlet temperature is assigned higher than the cathode side inlet temperature, because electrochemical reactions take place at the cathode catalyst layer. According to Al-Baghdadi [152], due to the reversible and irreversible

entropy production inside cathode catalyst layer, the temperature at the anode side is normally lower than the cathode side. In a PEM fuel cell, the maximum temperature location coincides with the highest electrochemical activity region. The peak temperature is observed in the cathode catalyst layer, showing that major heat generation takes place at this region.

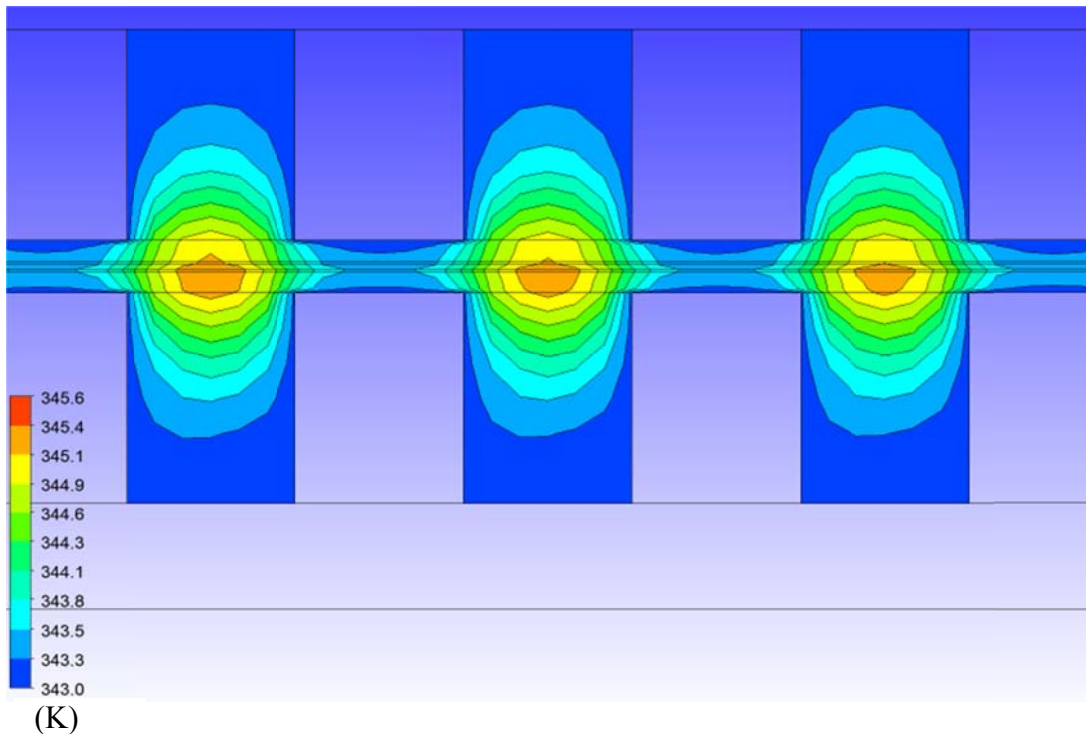


Figure 38 Section view of temperature distributions inside the 9th, 10th and 11th flow channels (high inlet humidity BC).

3.2.5 Pressure Distribution

For the high inlet humidity boundary condition, pressure distribution inside the cathode flow channel is presented in Figure 39 and pressure distribution inside the anode flow channel is presented in Figure 40. The pressure distribution

characteristics inside the flow channels are as expected. For both sides, pressure drop has a linear characteristic throughout the flow channels. “Zero gage pressure” boundary condition is applied for the outlets of the anode and the cathode flow channels. However, it is observed that at the outlet region of the anode flow channel, very small negative pressure values are present. Because of the characteristics of the flow inside the channel, water is present in the channel with gases. Thus, it is possible to have negative pressure values. But the observed negative value is very small and negligible.

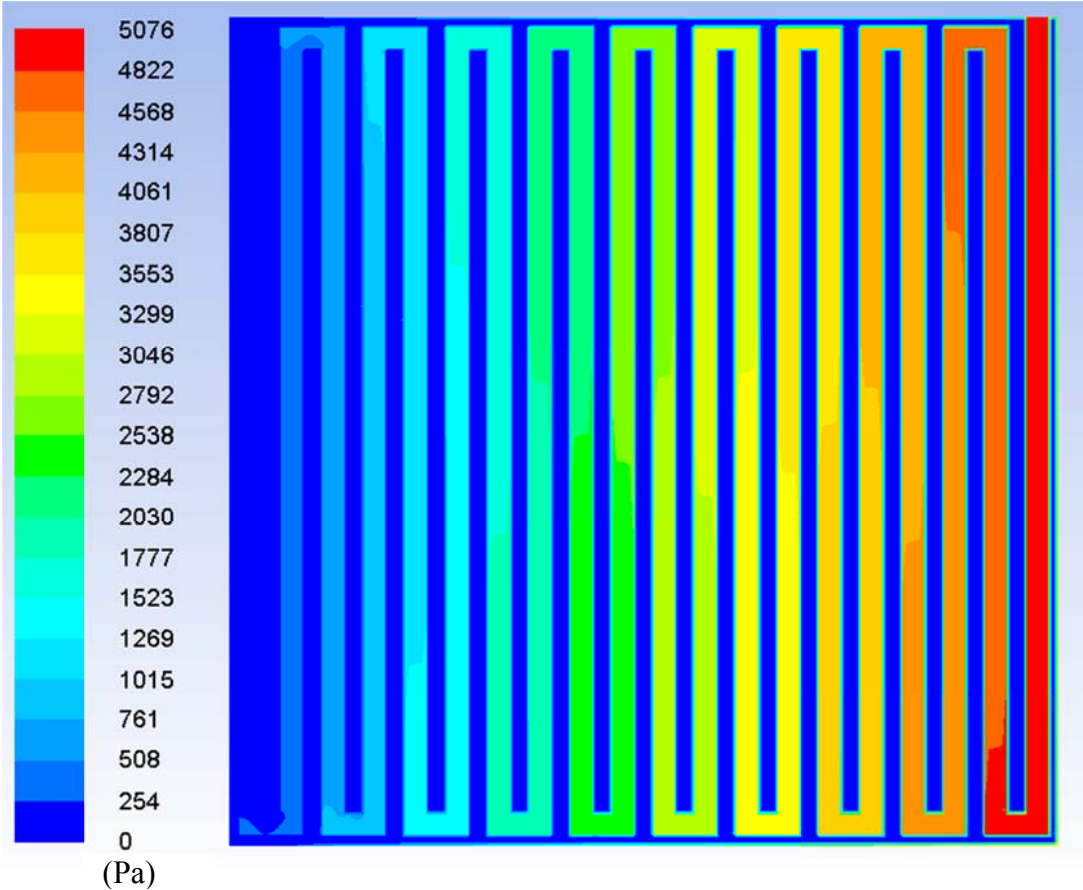


Figure 39 Pressure distribution inside the cathode flow channel (high inlet humidity BC).

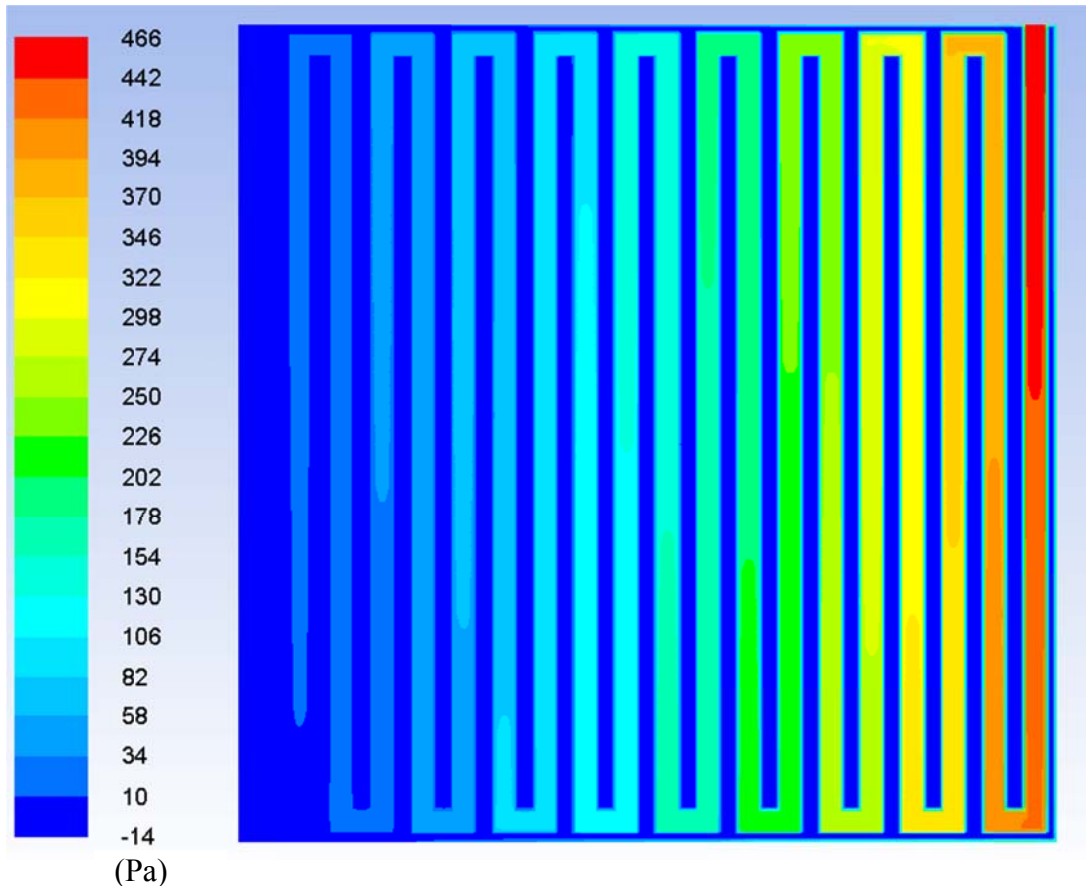


Figure 40 Pressure distribution inside the anode flow channel (high inlet humidity BC).

3.2.6 Fuel Cell Performance

In this part of the study, fuel cell polarization curve is drawn for a serpentine type single cell PEM fuel cell using the simulation data. The polarization curve is compared with the theoretical polarization curve and the literature [138]. To draw a current density versus cell potential (I-V) polarization curve by using ANSYS Fluent, the electric potential for the cathode should be varied starting from a voltage near the open circuit voltage and then, it should be gradually decreased.

The current supplied by a fuel cell is directly proportional with the amount of the fuel consumed. Therefore, when the cell voltage decreases, the produced electrical power per unit amount of fuel is also decreases. In other words, the fuel cell voltage axis can be called as an “efficiency axis” of the fuel cell, as in [153].

The theoretical potential value of a typical hydrogen fuel cell is 1.23V. However, in practice open circuit potential, which is called the maximum potential, is considerably lower than the theoretical potential, typically less than 1.0 V.

There are different kinds of voltage losses present in a PEM fuel cell; activation polarization losses, ohmic losses, concentration polarization losses and crossover losses. These voltage losses are caused by several factors. In Figure 41, voltage losses observed in a PEM fuel cell and the resulting polarization curve are presented. It is observed that, for a typical fuel cell when more current is drawn from the fuel cell, these losses become greater.

Activation polarization losses occur in a fuel cell, since some voltage difference from equilibrium is necessary to get the electrochemical reactions start and continue. Ohmic losses are mainly caused by the resistance to the flow of ions and electrons in the membrane and conductive parts of the fuel cell. Concentration polarization losses observed when a reactant is quickly consumed at the catalyst layer. Due to the electrochemical reactions, concentration gradients are formed, resulting in concentration losses. Although the membrane is not electrically conductive and is almost impermeable to reactants, a little quantity of hydrogen may diffuse from the anode side to the cathode side. Also, some electrons may catch a "shortcut" through the membrane causing cross-over losses.

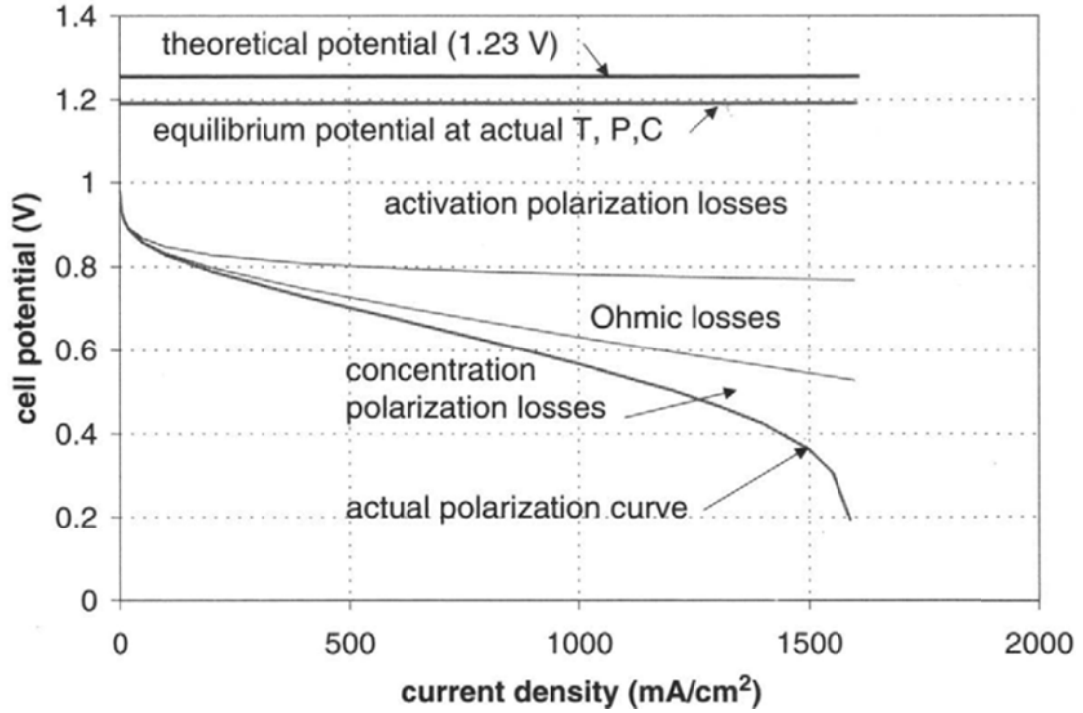


Figure 41 Voltage losses in the fuel cell and resulting polarization curve (adapted from Barbir [32]).

The most significant characteristic of a fuel cell and its performance is the polarization curve. The real voltage output for a fuel cell is written by the difference of the thermodynamically predicted voltage output and the voltage drops due to the described losses. By the following equation, an adequately precise approximation of the fuel cell polarization curve can be found:

$$E_{cell} = E_{r,T,P} - \frac{RT}{\alpha F} \ln \left(\frac{i + i_{loss}}{i_o} \right) - \frac{RT}{nF} \ln \left(\frac{i_L}{i_L - i} \right) - iR_i \quad (3.1)$$

Equation 3.1 is an approximation of the Equation 2.1 and this equation is commonly used in the literature [32]. In Equation 3.1, $\frac{RT}{\alpha F} \ln \left(\frac{i + i_{loss}}{i_o} \right)$ represents activation losses, $\frac{RT}{nF} \ln \left(\frac{i_L}{i_L - i} \right)$ represents the concentration losses and iR_i represents ohmic losses.

The open circuit voltage of the PEM fuel cell is taken as 0.95 V in CFD simulations. The electric potential for the cathode is varied starting from a voltage near the open circuit voltage (0.85 V). Then, the electric potential is gradually decreased to 0.35 V. In Figure 42, the polarization curve, which is obtained from the CFD simulations, is presented for the high inlet humidity boundary condition. The obtained polarization curve is compared with the theoretical polarization curve and literature [138] for the high inlet humidity case. The general behavior of the numerical polarization curve is acceptable when compared with the theoretical one. It is also observed that, there is no considerable difference exists between the CFD results and the literature. Thus, it can be concluded that the CFD results match well with the literature.

The theoretical polarization curve is an ideal curve for the selected operating conditions. Up to a cell potential value of 0.55V, the general behavior of numerical cell potential graph well fits the theoretical one. But, for the cell potential value below 0.55V, the difference between the numerical and the theoretical potential values increase. The main reason of this is the overall potential loss mainly caused by concentration losses. As the current density increases, the concentration losses also increase and become significant in numerical calculations. On the other hand, in practical applications, current density and cell potential values are limited to certain values. De Bruijn et al. [154] stated that higher degradation and hydrogen cross-over rates are observed in PEM fuel cells, when the fuel cell is exposed to higher current conditions, in which concentration losses are dominant. Because of this reason, higher current densities are generally avoided in PEM fuel cell systems, as in [155]. In the system modeling study, the minimum allowable cell voltage is limited to 0.7 V and maximum allowable current density is limited to 700 mA/m² in the fuel cell module.

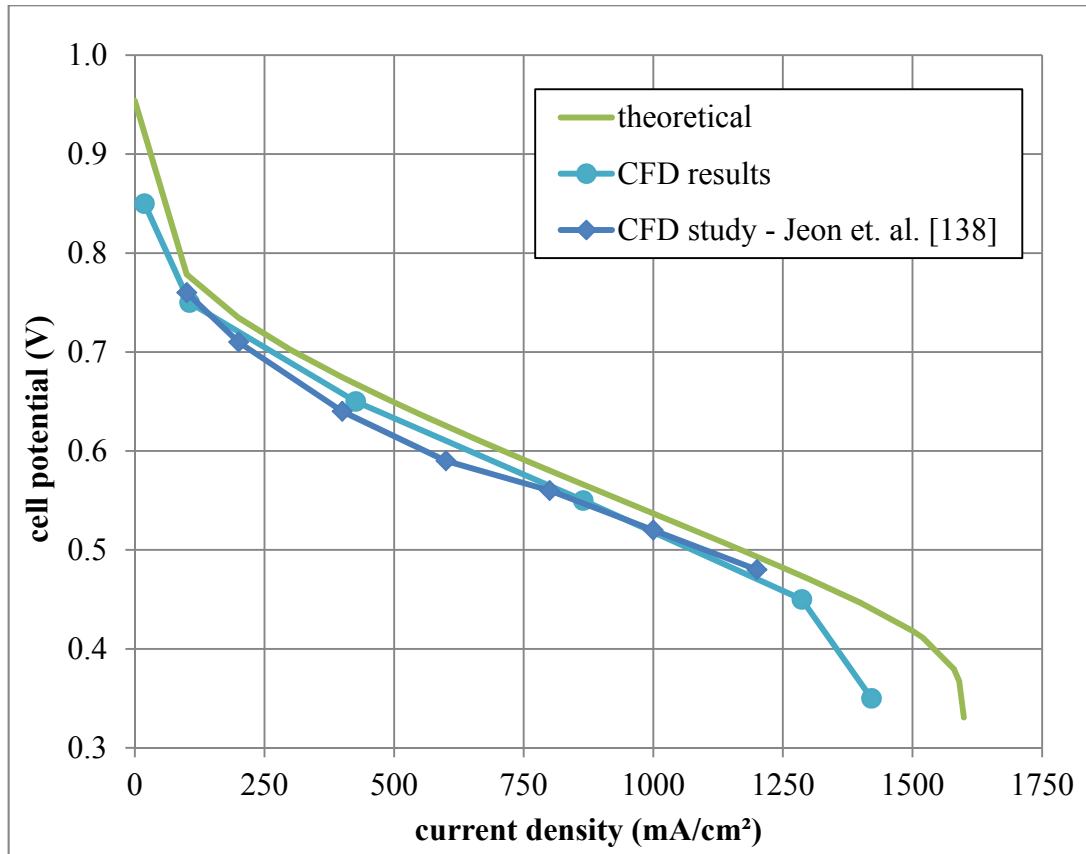


Figure 42 Comparison of the theoretical and numerical polarization curves (high inlet humidity BC).

In Figure 43, comparison of the polarization curves for the high inlet humidity and the low inlet humidity boundary conditions are shown. The polarization curves are compared with the literature [138]. It is observed that the performance of the high inlet humidity condition is better than the low inlet humidity boundary condition for both studies. The difference in results between the current study and [138] is higher for the high inlet humidity BC. For the low inlet humidity BC, current study gives lower current density values when compared with the literature. On the other hand, for the high inlet humidity BC, current study gives higher current density values.

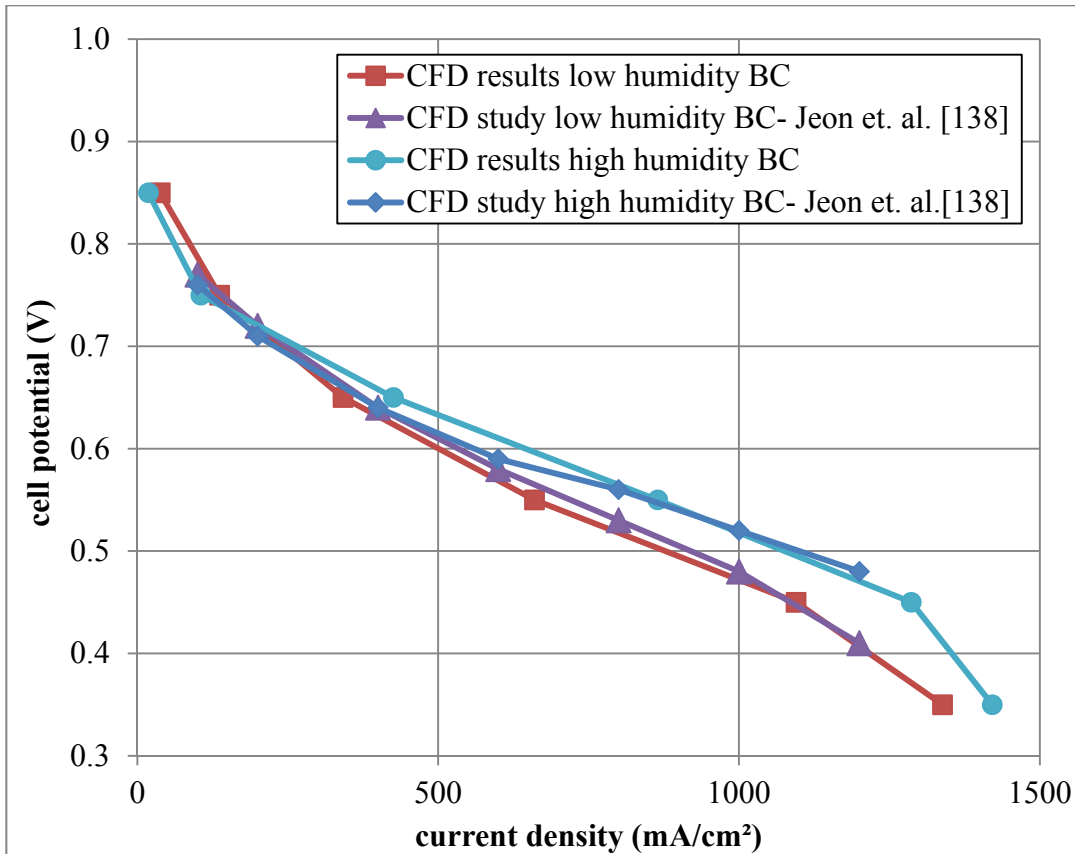


Figure 43 Comparison of polarization curves for high inlet humidity and low inlet humidity boundary conditions.

3.3 Stack Modeling

In this part of the study, stack management is investigated in PEM fuel cells. 2-cell, 3-cell and 4-cell stacks are modeled and compared with the single channel PEM fuel cell model.

The voltage of a single cell fuel cell is limited with 1 V. However, 1 V is not sufficient for real-life applications. Generally, multiple fuel cells are interconnected in series to increase the voltage output of the fuel cells. This method is called as

“stacking”. Fuel cell stacks are developed to meet any voltage requirement of real-life applications. In Section 3.3.1, details of the fuel cell stack sizing are discussed. The bipolar configuration is the most commonly used stack configuration. A single cell is separated from the adjacent cell in the stack by a bipolar separator plate. This makes possible to connect the surface of one anode and the cathode of the following cell. The bipolar plate also serves as a means of supplying oxygen to the cathode side and hydrogen to the anode side.

In Figure 44, typical PEM fuel cell stack configuration is presented for a two-cell stack. Each cell and each MEA are separated by a plate with flow fields on both sides to distribute the reactants. Fuel cell stacks are mainly held together by using bolts and rods. End plates of the fuel cell stacks have only single-sided flow fields.

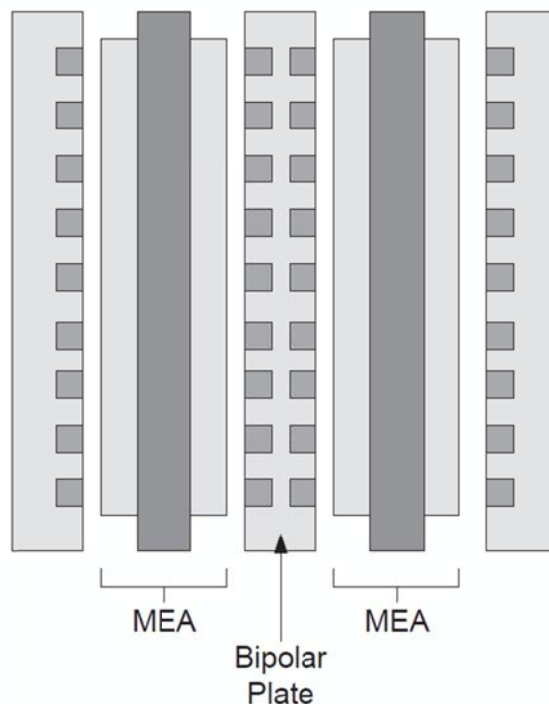


Figure 44 Typical fuel cell stack configuration (adapted from Spiegel [156]).

In Figure 45, arrangement of the major cell components in a fuel cell stack is presented in detail. In this arrangement fuel flow and the oxidant flow are arranged in cross-flow configuration. The end plates serve for current collection in fuel cell stacks. The fuel and oxidant flow channels may be part of the bipolar plate. The bipolar plates serve as a part of the electron conduction path through the fuel cell stack; thus, they must be electronically conductive, but they must not permit gas permeation.

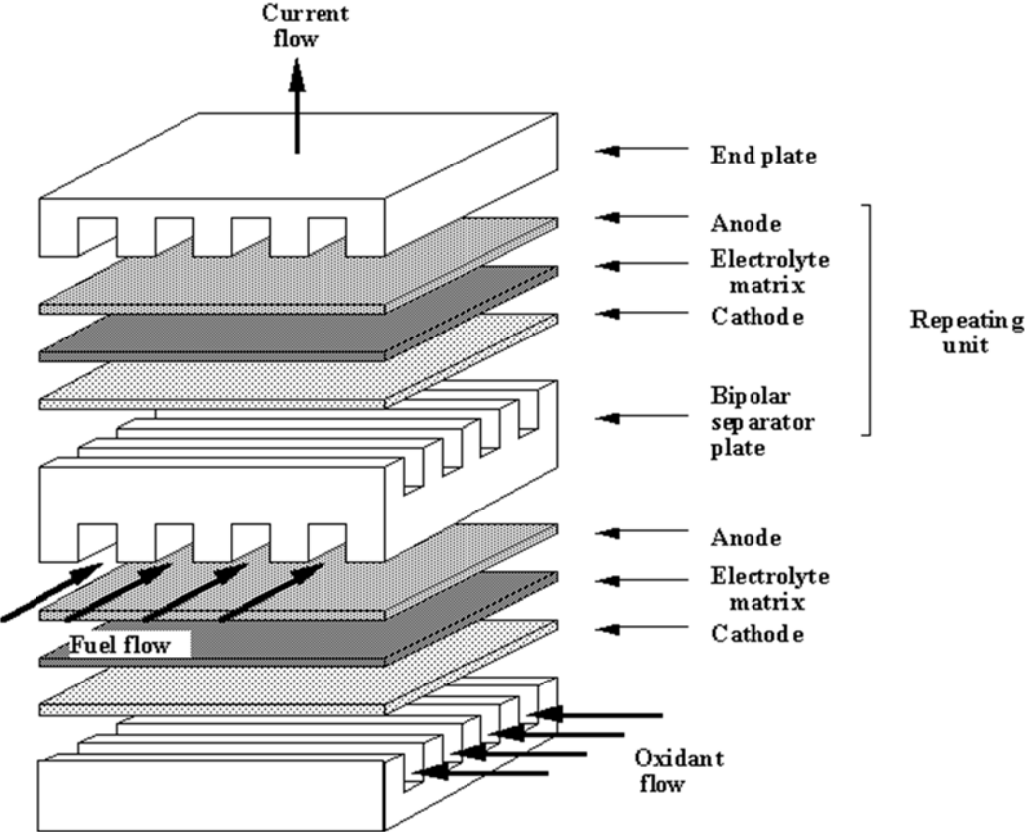


Figure 45 Arrangement of the major cell components in a fuel cell stack (adapted from internet source [157]).

The following issues should be taken into account in fuel cell stack design [156]:

- Reactants should be distributed homogeneously throughout every cell of the stack.
- The temperature should be uniform through each cell.
- Resistive forces between the components should be kept as low as possible.
- Gas leakage should be prevented by proper sealing.
- The membrane should not dry out or become flooded with water.
- The stack should be strong enough to withstand environmental conditions.

In Figure 46, 2-cell stack PEM fuel cell model is presented. In this model, anode collector plate of a single PEM fuel cell is connected by a cathode collector plate of another PEM fuel cell, by forming a bipolar plate. It is a simplified PEM fuel cell stack design, since it is assumed that the two cells have the same inlet and exit boundary conditions. Thus, the effects of the inlet and exit manifolds are neglected. For the 3-cell and 4-cell stack, similar CFD models are formed by connecting bipolar plates. CFD simulations are performed for the multi-cell CFD models. Single cell stack simulation parameters are used. Simulations are performed for the cell potential value of 0.35 V.

Fuel cell performance is strongly dependent upon the flow rate of the reactants. Irregular flow characteristic can result in unequal performance between cells. Reactant gases need to be supplied to each cell in the stack by using flow distribution manifolds [156]. However, in present study inlet and exit manifolds are not modeled to simplify the geometry. It is assumed that, all the cells have the same inlet and exit boundary conditions for the anode and cathode sides.

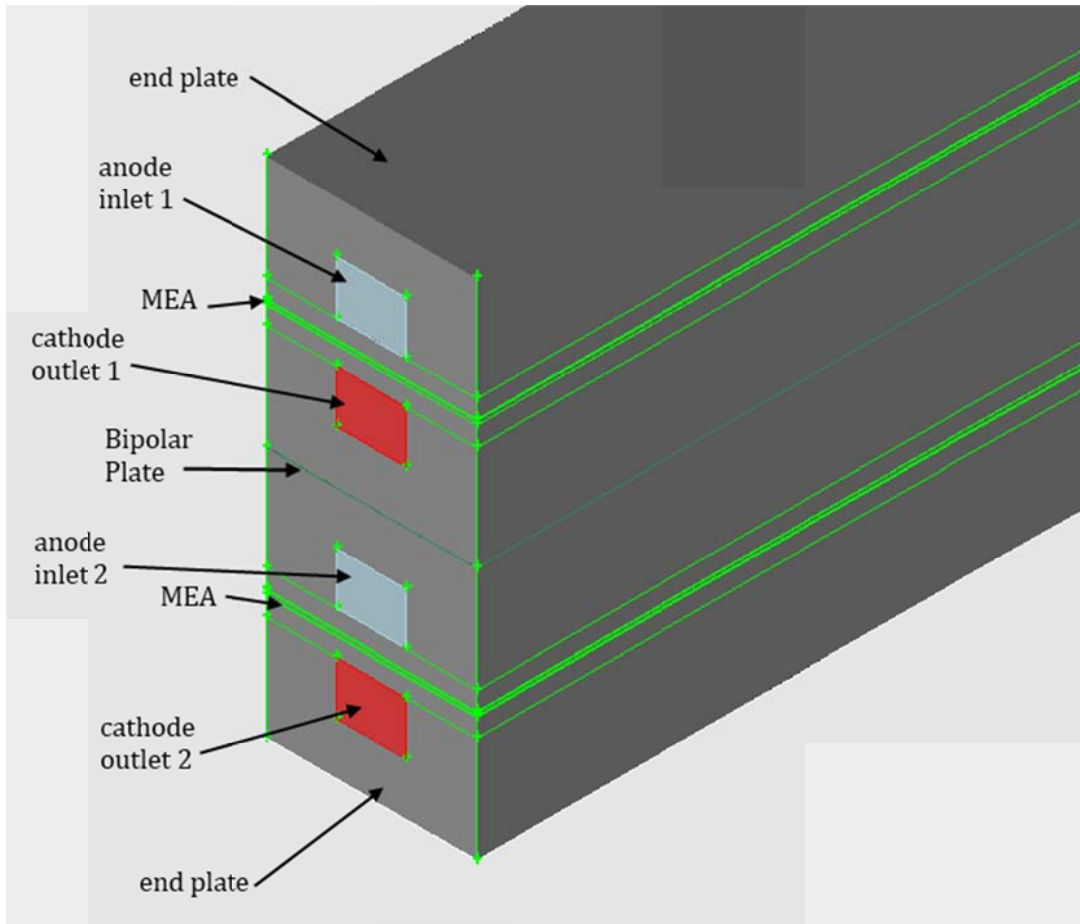


Figure 46 2-cell stack PEM fuel cell model.

3.3.1 Sizing of a Fuel Cell Stack

There are two independent variables must be considered in fuel cell stack sizing; voltage and current. The stack power output is simply a product of the voltage and the current:

$$W_{FC} = V_{st} I \quad (3.2)$$

where V_{st} is the total stack potential and defined by multiplication of the average of the each cell potential values and number of cells in the stack.

$$V_{st} = \bar{V}_{cell} N_{cell} \quad (3.3)$$

The current I is a product of the current density and cell active area, and can be calculated using the following equation.

$$I = i A_{cell} \quad (3.4)$$

The cell potential and the current density are directly related by the I-V curve. Thus, the cell potential is a function of the current density:

$$V_{cell} = f(i) \quad (3.5)$$

The fuel cell stack efficiency can be estimated by a simple equation [32] [156]:

$$\eta_{stack} = \frac{V_{cell}}{1.482} \quad (3.6)$$

where 1.482 V corresponds to the higher heating value of the hydrogen.

3.3.2 Stack Performance

The results of the CFD simulations for the multi-cell stacks are tabulated in Table 12. It is observed that, by using additional cells, the performance of the fuel cell is improved when compared with a single cell fuel cell. If the current density values are compared, it is observed that, the effective fuel cell is the 2-cell stack fuel cell. The reason for this is that the side cells of a fuel cell stack have the highest performance. Shimpalee et al. [158] performed similar numerical studies on a portable PEM fuel cell stack, which has six cells, and it was decided that the middle cells of the fuel cell show the lowest performance, while side cells show the highest

performance. Additionally, it is observed that, hydrogen consumption per cell is directly related to the cell performance or the current density of the cell.

It can be said that, when the number of cells in a fuel cell stack increases, the average performance of the cells in the fuel cell stack decreases. The main reason for this is the increase of temperature in the middle cells. Average outlet temperature values for the anode and cathode sides are tabulated in Table 13. It is observed that the side cells have lower temperature than the middle cells, since the side cells are exposed to natural convection. The anode side temperature is lower than the cathode side temperature, for all of the cells.

Table 12 Comparison of performance of single cell fuel cell with multi-cell fuel cells.

# cells in stack	current density (mA/cm²)	total hydrogen consumption (kg/s)	hydrogen consumption per cell (kg/s)
1-cell stack	1387	8.69E-08	8.69E-08
2-cell stack	1486	1.87E-07	9.35E-08
3-cell stack	1482	2.78E-07	9.27E-08
4-cell stack	1408	3.52E-07	8.80E-08

Table 13 Average outlet temperatures of the anode and the cathode sides.

Cell Number / Side		Single Cell (K)	2-Cell Stack (K)	3-Cell Stack (K)	4-Cell Stack (K)
1	anode	344.22	344.58	344.73	344.79
	cathode	345.02	346.05	346.32	346.37
2	anode	-	344.83	345.68	345.76
	cathode		345.72	346.80	346.89
3	anode		345.12	345.93	
	cathode		345.94	347.02	
4	anode		-	345.24	
	cathode		-	346.02	

As discussed in Section 2.1.4, the cathode outlet temperature is slightly lower than the temperature of the cell and can be assumed as equal to the operating temperature of the cell. According to Riascos and Pereira [159], the optimal operating temperature of a typical PEM fuel cell should be lower than 76°C (349.15K). Similarly, Hamelin et al. [160] stated that the optimal operating temperature range of PEM fuel cells is between 72-75°C (345.13 - 348.15K). By analyzing Table 13, it can be said that, when the number of cells in a fuel cell increases, operating temperature of each cell also increases. Therefore, it can be concluded that when the number of cells increases, the operating temperature of each cell deviates more from the optimum operating temperature. Also, it can be said that increasing the cell temperature may result in dehumidification, which also decreases the cell performance.

In Figure 47, comparison of the stack performances with the single cell case is presented. It is observed that, the 2-cell stack has the highest performance in terms of current density. Therefore, it can be said that the optimal operating temperature for the model investigated in this study is around 72.90°C (346.05K). Barbir [32] reported that operation above optimum cell temperature results in performance loss.

This issue explains why the 2-cell stack has higher performance than the 3-cell and 4-cell stack configurations. In general, it is accepted that a single cell has the highest performance when compared with stacks. However, due to the operating conditions, which are closer to the optimum operating temperature, the 2-cell stack gives the highest performance in the analyzed case.

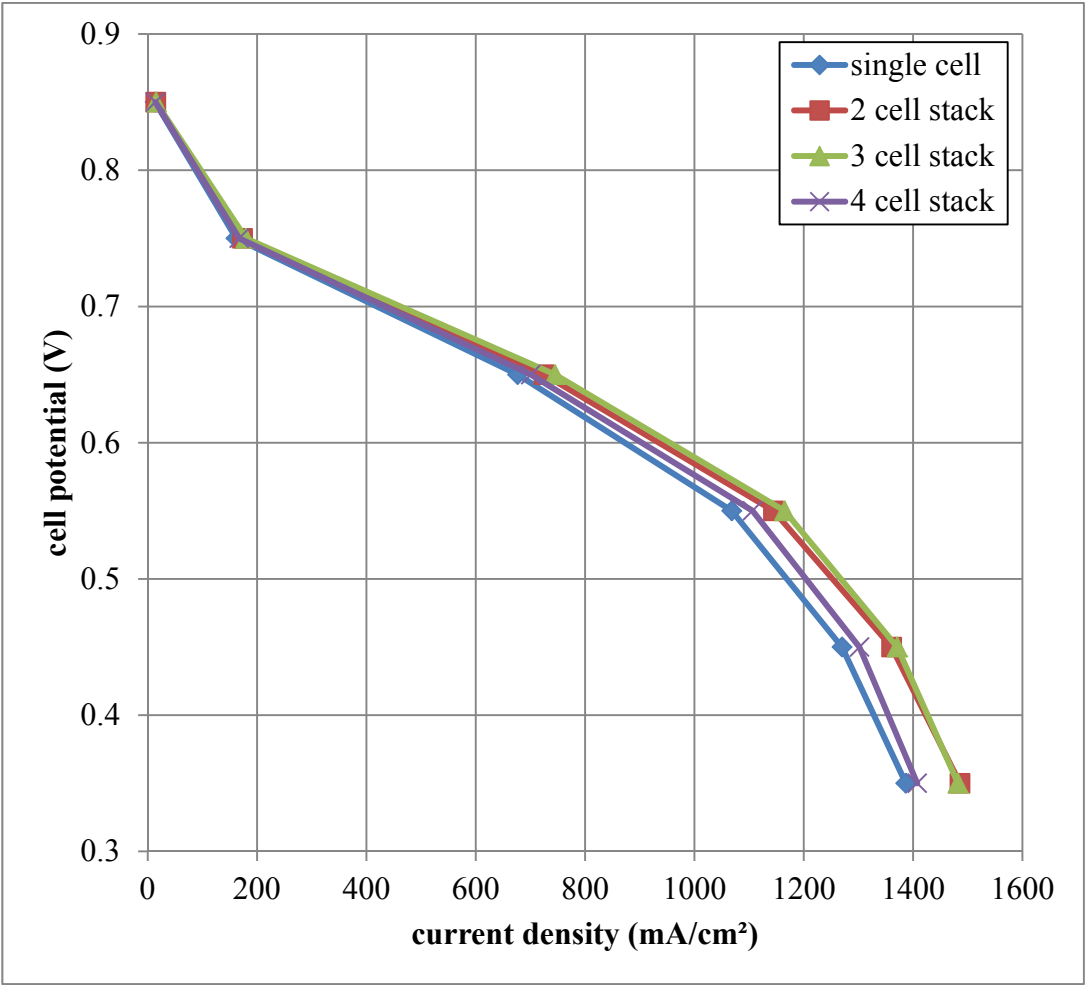


Figure 47 Comparison of stack performances with the single cell case.

3.4 Discussions

In this chapter a complete three-dimensional CFD model of a PEM fuel cell with serpentine type flow channels has been investigated. The CFD model is developed to expand fundamental understanding of the electro-chemical and physical phenomena in PEM fuel cells. The CFD model explicates the transport phenomena in the cell, including diffusive and convective heat transfer, electro-chemical reactions, transport mechanisms throughout the cell and phase change of water inside the cell.

CFD simulations are performed for a single cell and multi-cell stacks. Results of the CFD simulations are compared with theoretical calculations and a similar study from the literature. It is observed that the results of CFD simulations match with the theoretical calculations and the results from literature. Then, CFD simulations are performed for multi-cell stacks and the stack performances are evaluated.

Additionally, a separate CFD modeling study was completed in University of Split by using ANSYS Fluent [161]. It was focused on designing a heat exchanger with variable surface area for passive cooling of PEM fuel cells. That work is presented as Appendix C.

CHAPTER 4

FUEL CELL DEGRADATION

The target life time for a fuel cell vary significantly for different types of applications, ranging from 5000 hours for mobile to 40,000 hours for stationary applications [100]. In Chapter 2, yearly operating time of the fuel cell stack in the stand-alone solar-hydrogen hybrid system is calculated as 5180 hours. Therefore, being a stationary power system, the system is expected to operate at least 8 years without changing sub-parts of the PEM based components.

It is hard to evaluate long-term performance and durability of the PEM fuel cells, since all degradation mechanisms for the components of the PEM fuel cells are not completely figured out yet [100]. In this chapter, a degradation study is performed for the complete cell model and the fuel cell stacks using a variety of observed degradation patterns reported in the literature. Additionally, the degraded PEM fuel cell is parametrically analyzed by using ANSYS Fluent. This chapter is concluded with system simulations for degraded PEM based components and the economical analysis for the degraded system.

4.1 Degradation Modes

As the PEM fuel cell operates, the carbon particles and PTFE of the cell are exposed to chemical attack and electrochemical oxidation. The loss of carbon particles and PTFE leads to changes in physical characteristics of the cell components. The performance of the cell decreases as a result. Wu et al. [162]

stated that durability of the fuel cell is negatively affected by degradation mechanisms.

General information about PEM fuel cell degradation was presented in Chapter 1. In the following subsections degradation modes of PEM fuel cells are discussed for each component in detail.

4.1.1 Membrane Degradation

Fuel cell is assumed to be in on-off operating condition with its maximum available capacity to prevent the membrane degradation. The membrane experiences hydration and temperature variations, when fuel cell operates in fluctuating operating conditions. Thus, fuel cell degradation from hydro-thermal fatigue loading is reduced by assuming on-off operating condition [163].

Performance of a PEM fuel cell is directly related to the membrane. The membrane is modeled by the equations presented below.

The membrane phase conductivity is modeled using the following equation [164].

$$\sigma_{mem} = \beta(0.514\lambda - 0.326)\omega e^{1268\left(\frac{1}{303} - \frac{1}{T_{cell}}\right)} \quad (4.1)$$

where λ designates the water content of the membrane and defined by Equation 4.2, which is obtained using the correlation suggested by Springer et al. [164]. Here, two model constants, ω and β are introduced by ANSYS Fluent for generality [36].

$$\lambda = 0.043 + 17.18a - 39.85a^2 + 36a^3 \quad (a < 1) \quad (4.2)$$

$$\lambda = 14 + 1.4(a - 1) \quad (a > 1) \quad (4.3)$$

where a is the water activity that is given by the following equation:

$$a = \frac{P_{wv}}{P_{sat}} + 2s \quad (4.4)$$

where s is the water saturation ratio (water volume fraction) [165].

From Equations 4.1 – 4.4, it is observed that the membrane performance is directly related with the water content and the water activity. However, degradation of the membrane can be directly observed from one of the physical characteristics of the membrane, which is called the equivalent weight. Equivalent weight is a parameter of the back diffusion flux equation given by the following equation:

$$J_w^{diff} = -\frac{\rho_m}{M_m} M_{H_2O} D_l \nabla \lambda \quad (4.5)$$

where ρ_m and M_m are the density and the equivalent weight of the membrane. M_m is valid for dry a membrane. Equivalent weight is the inverse of the ion-exchange capacities (IEC). IEC are given in units of moles of titratable protons per gram of the dry ionomer [166]. Equivalent weight changes as a function of degradation time and can be taken as 1132 kg/kmol for a degraded membrane [167], whereas fresh membrane has an equivalent weight value of 1100 kg/kmol.

4.1.2 Catalyst Layer Degradation

Schmittering and Vahidi [100] stated that catalyst layer properties, output voltage and performance of the cell are negatively influenced by the carbon corrosion of the catalyst layer. According to Madden et al. [83], high relative humidity across the cell leads to an increase in the catalyst dissolution rate, which also results in higher rate of radical attack inside the MEA. Catalyst layer porosity is an important parameter in fuel cell modeling, which directly affects the performance of the cell [168]. Viscous resistance is also affected by changing porosity. The porosity of the cathode catalyst layer can be calculated by the following equation [169]:

$$\varepsilon_{cat} = 1 - \varepsilon_S - \varepsilon_N \quad (4.6)$$

where ε_N is the volume fraction of the polymer electrolyte in the cathode and ε_S is the volume fraction of platinum to carbon in the cathode, and defined by the following equations:

$$\varepsilon_N = \hat{n}V_{nuc}\varepsilon_{agg} + V_{ctg} \quad (4.7)$$

$$\varepsilon_S = \hat{n} [V_{nuc}(1 - \varepsilon_{agg})] \quad (4.8)$$

where \hat{n} is the number of agglomerates per unit volume, V_{nuc} is the volume of the agglomerate nucleus, ε_{agg} is the volume fraction of the polymer in agglomerate nucleus and V_{ctg} is the volume of the polymer coating around the agglomerate nucleus. In a real fuel cell, \hat{n} value increases with operating time, which causes a decrease in the catalyst layer porosity value.

4.1.3 GDL Degradation

Paimushin et al. [170] stated that functional performance of a fuel cell is affected by a change in material properties of the GDL. According to Williams et al. [171] for an operating fuel cell, when the GDL permeability decreases over time, the fuel cell performance and durability are negatively affected. Lee et al. [172] studied various materials and physical properties including electrical resistivity, bending stiffness, surface contact angles, porosity and water vapor diffusion. And it was concluded that cell performance is only affected by a change in porosity. Porosity of the GDL has an important effect on the limiting current density. For instance, Berning and Djilali [47] stated that a decrease in porosity from $\varepsilon = 0.5$ to $\varepsilon = 0.3$ can decrease current density by a ratio of 1/3. Decreasing porosity also affects the viscous resistance of the GDL. For a fresh PEM fuel cell $\varepsilon = 0.5$ [147] and a degraded fuel cell $\varepsilon = 0.3$ [173] [169] for the GDL. The porosity and viscous resistance values of degraded and fresh cells are summarized in Table 14.

4.1.4 Bipolar Plate Degradation

Nishith [174] stated that contact between the bipolar plate and the GDL, and between the GDL and the catalyst layer is not perfect even under compression, due to the rough nature of these materials. Interfacial gaps are formed with the uneven compression pressure between the bipolar plate and the GDL, and between the GDL and the catalyst layer, which leads to a decrease in the electrochemical active surface area. Contact resistance is controlled by the surface topography of contacting pairs and it is directly affected by the contamination that is resulted from degradation. At the contacting surfaces, the actual area in contact decreases, which results in a voltage drop [175]. As shown in Figure 48, a bulk electrical junction formed at the contact region, and the electrical lines bundle together to pass through certain regions.

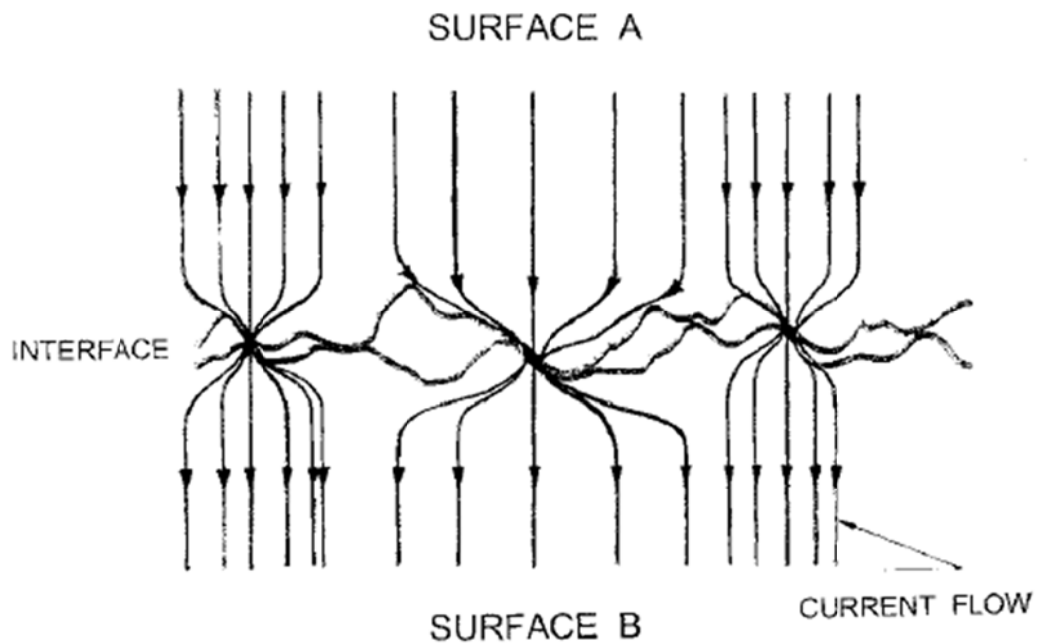


Figure 48 Schematic diagram of a bulk electrical interface (adapted from Timsit [176]).

Berning and Djilali [47] assumed the contact resistance as $50 \text{ m}\Omega\text{cm}^2$. Barbir et al. [177] measured contact losses and found that the contact resistance of a standard cell can be as high as $150 \text{ m}\Omega\text{cm}^2$ for an old fuel cell. Dandekar and Mendoka [178] conducted an experimental and theoretical study on contact resistance. They calculated contact resistance theoretically as $68 \text{ m}\Omega\text{cm}^2$ and experimentally as $108 \text{ m}\Omega\text{cm}^2$ for a degraded cell. Consequently, in the present study contact resistance is assumed as $108 \text{ m}\Omega\text{cm}^2$ for a degraded cell.

4.2 Degraded Single Cell

Summary of the degraded parameters used in the degraded PEM fuel cell model is tabulated in Table 14. CFD simulations are performed for the degraded PEM fuel cell by using the values tabulated in this table. The results of the CFD simulations are compared with the results that are presented in Chapter 3.

Table 14 Summary of the degraded parameters used in the degraded PEM fuel cell model.

Component	Parameter	Fresh Value	Degraded Value
Membrane	Equivalent weight (kg/kmol)	1100 [167]	1132 [167]
Catalyst Layer	Porosity	0.5 [147]	0.2 [173] [169]
	Viscous resistance ($1/\text{m}^2$)	1.0×10^{12} [147]	4.0×10^{12} [173]
GDL	Porosity	0.5 [147]	0.3 [179] [72]
	Viscous resistance ($1/\text{m}^2$)	1.0×10^{12} [147]	2.0×10^{12} [180]
Bipolar Plate	Contact resistance ($\text{m}\Omega\text{cm}^2$)	Neglected	108 [178]

In Figure 49, comparison of performances of the fresh cell and the degraded cell is presented. It is observed that the degradation is more significant below the cell potential value of 0.65 V. However, as stated in Chapter 2, PEM fuel cells mainly operate above the cell potential value of 0.7 V and below the current density value of 700 mA/cm². Therefore, it is decided to concentrate on the cell potential values over 0.65V in the fuel cell degradation study.

For cell potential values of 0.85 V, 0.75 V and 0.65 V; the calculated performance loss is 14.6%, 16.9% and 16.6%, respectively. It is observed that a maximum performance loss of approximately 17% exists between the fresh cell and the degraded cell. Therefore, it can be concluded that degradation is a very important phenomenon which strongly affects the overall performance of a PEM fuel cell.

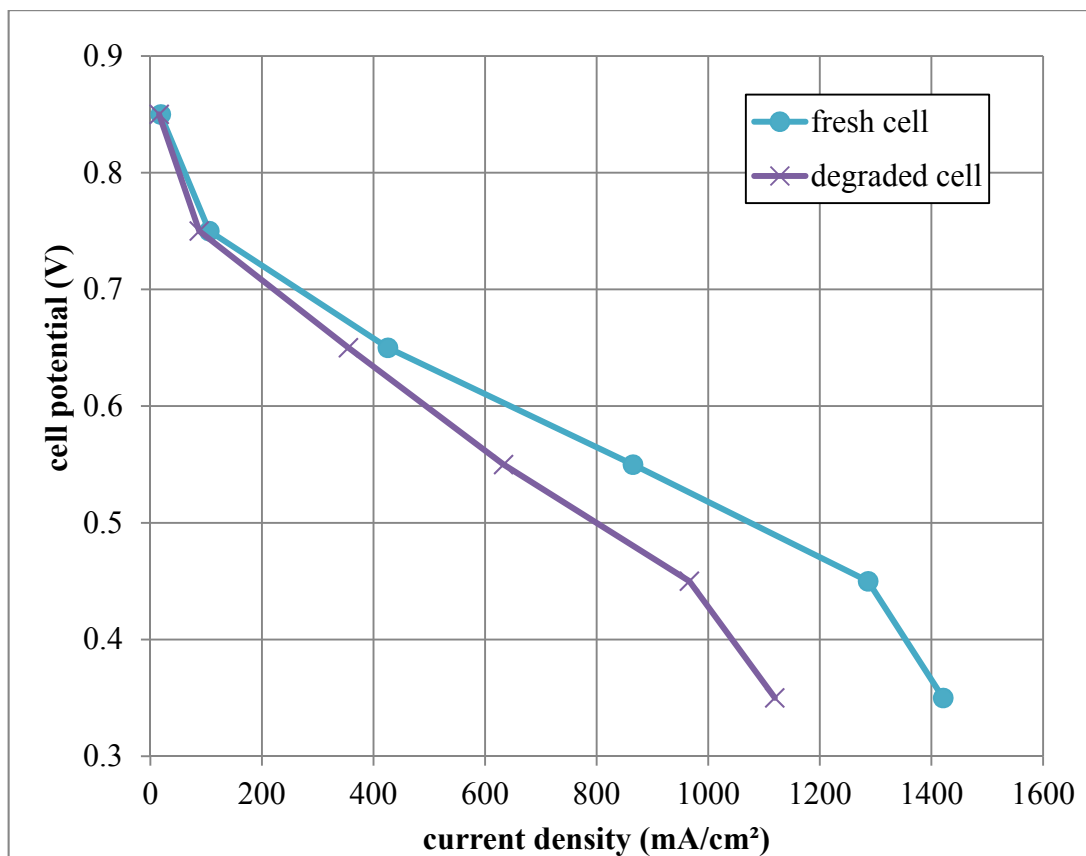


Figure 49 Comparison of performances of the fresh cell and the degraded cell (after 2 years).

Temperature contours of the degraded cell and the fresh cell is presented in Figure 50, for a cell potential value of 0.65V. The location of the presented temperature contours is shown in Figure 35. In Figure 51, comparison of the temperature distribution of the membrane for the degraded cell and the fresh cell is shown. After examining Figure 50 and Figure 51, it can be asserted that the operating temperature of the degraded cell is higher than that of the fresh cell. Therefore, it can be concluded that the performance of the degraded fuel cell is lower than the fresh cell due to the higher operating temperature caused by degradation.

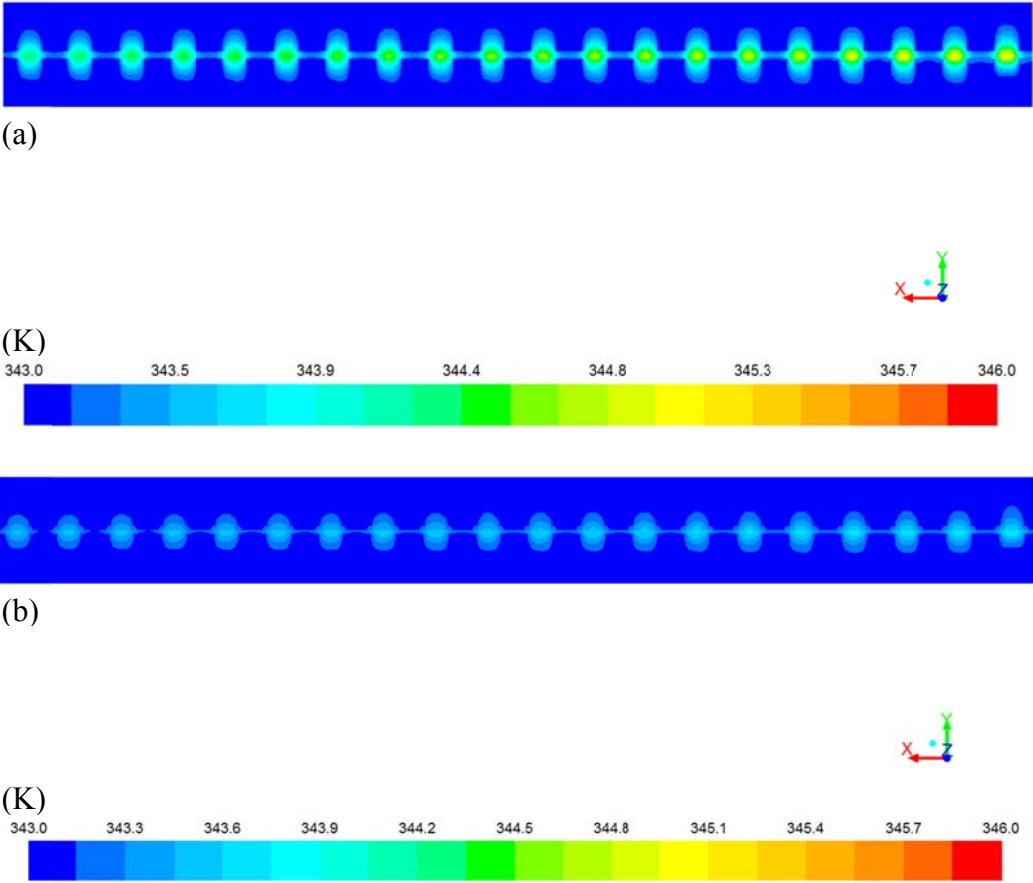


Figure 50 Comparison of temperature contours of; (a) degraded cell (after 2 years), (b) fresh cell.

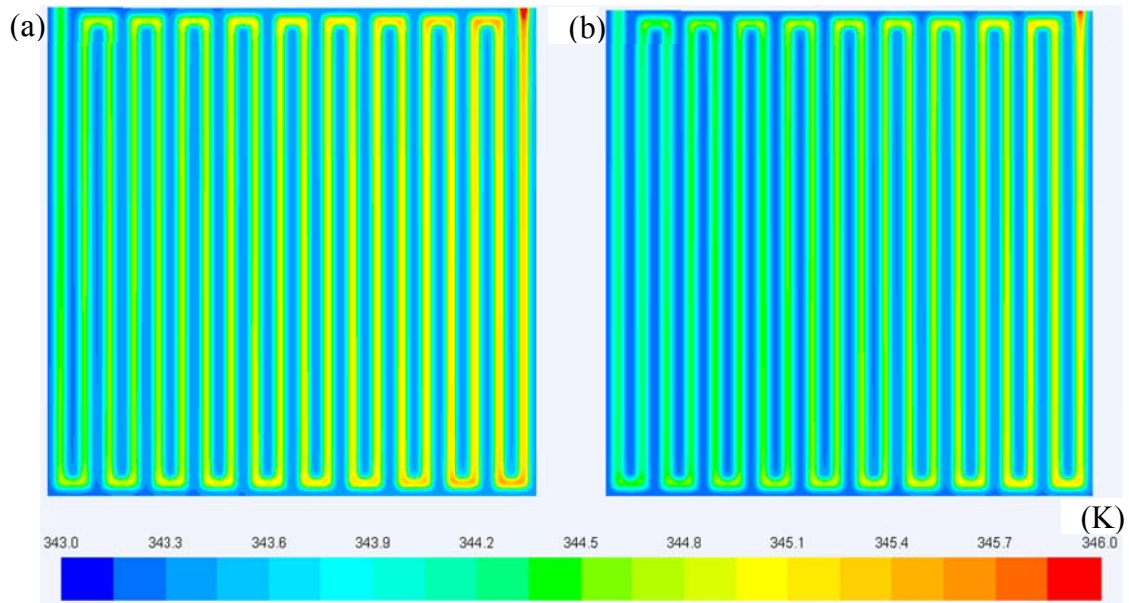


Figure 51 Comparison of temperature distribution of the membrane for: (a) degraded cell (after 2 years), (b) fresh cell.

4.3 Parametric Analysis

The results of the parametric study conducted with parameters discussed in Section 4.2. As presented here, the effects of the parameters, which are summarized in Table 14, are investigated individually. The details of the parametric analysis are presented in Table 15. Total 114 simulations are performed for different components of the fuel cell. In the parametric analysis, only the investigated parameter is changed and all of the other parameters are kept as “fresh value”, which is presented in Table 14.

First, the effect of membrane degradation is investigated by assigning two different values for the equivalent weight. The degraded value of the equivalent weight is compared with a different value, which is assigned between the fresh and the degraded values. Similar approach is used for the other investigated parameters. Then, the effect of the catalyst layer degradation is examined by investigating the

effects of the porosity and the viscous resistance on the cell performance by assigning three different values for each. Next, the GDL degradation is simulated similar to the catalyst layer analysis by assigning two different values for the porosity and the viscous resistance. Also, accumulated effect of the porosity and the viscous resistance is examined for the catalyst layer and the GDL. Finally, the effect of bipolar plate degradation is examined by assigning four different values for the contact resistance.

Results of the parametric analysis are tabulated Table 16. In this table, the results of the parametric analysis are compared with the fresh cell and percent differences from the fresh cell results are calculated for each simulation. Also, percent differences between the fully degraded cell and the fresh cell results are given in the “Fully Degraded Cell” column of this table. For the catalyst layer and GDL, accumulated effect of the porosity and the viscous resistance is tabulated in the “Total Effect” column.

Table 15 Details of the parametric analysis.

Analysis No:	Investigated Component	Investigated Parameter		Cell Potential (V)
1	None	-	-	0.35
2				0.45
3				0.55
4				0.65
5				0.75
6				0.85
7	Membrane	Equivalent Weight	1116 kg/mol	0.35
8				0.45
9				0.55
10				0.65
11				0.75
12				0.85
13	Membrane	Equivalent Weight	1132 kg/mol	0.35
14				0.45
15				0.55
16				0.65
17				0.75
18				0.85
19	Catalyst Layer	Porosity	0.4	0.35
20				0.45
21				0.55
22				0.65
23				0.75
24				0.85
25	Catalyst Layer	Porosity	0.3	0.35
26				0.45
27				0.55
28				0.65
29				0.75
30				0.85
31	Catalyst Layer	Porosity	0.2	0.35
32				0.45
33				0.55
34				0.65
35				0.75
36				0.85
37	Catalyst Layer	Viscous Resistance	2.0E+12 1/m ²	0.35
38				0.45
39				0.55
40				0.65
41				0.75
42				0.85

Analysis No:	Investigated Component	Investigated Parameter		Cell Potential (V)
43	Catalyst Layer	Viscous Resistance	3.0E+12 1/m²	0.35
44				0.45
45				0.55
46				0.65
47				0.75
48				0.85
49	Catalyst Layer	Viscous Resistance	4.0E+12 1/m²	0.35
50				0.45
51				0.55
52				0.65
53				0.75
54				0.85
55	Catalyst Layer	Porosity & Viscous Resistance	0.2 & 4.0E+12 1/m²	0.35
56				0.45
57				0.55
58				0.65
59				0.75
60				0.85
61	GDL	Porosity	0.4	0.35
62				0.45
63				0.55
64				0.65
65				0.75
66				0.85
67	GDL	Porosity	0.3	0.35
68				0.45
69				0.55
70				0.65
71				0.75
72				0.85
73	GDL	Viscous Resistance	1.5E+12 1/m²	0.35
74				0.45
75				0.55
76				0.65
77				0.75
78				0.85
79	GDL	Viscous Resistance	2.0E+12 1/m²	0.35
80				0.45
81				0.55
82				0.65
83				0.75
84				0.85

Analysis No:	Investigated Component	Investigated Parameter		Cell Potential (V)
85	GDL	Porosity & Viscous Resistance	0.3 & 2.0E+12 1/m²	0.35
86				0.45
87				0.55
88				0.65
89				0.75
90				0.85
91	Bipolar Plate	Contact Resistance	27 mΩcm²	0.35
92				0.45
93				0.55
94				0.65
95				0.75
96				0.85
97	Bipolar Plate	Contact Resistance	54 mΩcm²	0.35
98				0.45
99				0.55
100				0.65
101				0.75
102				0.85
103	Bipolar Plate	Contact Resistance	81 mΩcm²	0.35
104				0.45
105				0.55
106				0.65
107				0.75
108				0.85
109	Bipolar Plate	Contact Resistance	108 mΩcm²	0.35
110				0.45
111				0.55
112				0.65
113				0.75
114				0.85

Table 16 Results of the parametric analysis (details are tabulated in Table 15).

Cell Potential (V)	Membrane		Catalyst Layer										Degraded Cell
	Equivalent Weight (kg/mol)		Porosity			Viscous Resistance (l/m ²)			Total Effect				
	1116	1132	0.4	0.3	0.2	2.0E+12	3.0E+12	4.0E+12					
0.35	0.10%	0.23%	0.35%	0.72%	0.95%	0.20%	0.32%	0.43%			1.07%	21.24%	
0.45	0.22%	0.39%	0.52%	1.01%	1.31%	0.34%	0.51%	0.70%			1.47%	24.89%	
0.55	0.14%	0.33%	0.47%	0.83%	1.23%	0.30%	0.41%	0.55%			1.39%	26.80%	
0.65	0.32%	0.76%	1.23%	2.02%	2.49%	0.59%	1.16%	1.63%			2.91%	16.58%	
0.75	1.03%	1.65%	1.96%	2.89%	3.30%	1.24%	1.86%	2.27%			3.71%	16.91%	
0.85	1.22%	1.95%	1.71%	2.44%	3.66%	1.46%	1.83%	2.44%			3.90%	14.60%	
Cell Potential (V)	GDL										Degraded Cell		
	Porosity		Viscous Resistance (l/m ²)			Total Effect		Bipolar Plate					
	0.4	0.3	1.5E+12	2.0E+12		27	54	81	108				
0.35	1.84%	4.65%	0.18%	0.49%	4.75%	3.17%	6.29%	9.65%	12.81%		21.24%		
0.45	3.06%	5.14%	0.29%	0.80%	5.29%	5.34%	9.71%	13.91%	17.62%		24.89%		
0.55	2.54%	5.82%	0.25%	0.64%	5.96%	6.52%	11.97%	17.25%	22.43%		26.80%		
0.65	2.66%	4.29%	1.16%	3.42%	4.43%	7.27%	9.19%	11.38%	13.50%		16.58%		
0.75	4.23%	5.05%	1.03%	1.34%	5.26%	4.43%	8.04%	11.75%	14.64%		16.91%		
0.85	4.88%	6.10%	1.10%	3.17%	6.34%	1.34%	2.44%	4.39%	6.22%		14.60%		

It is observed that, among the parameters taken into account, membrane degradation is the least effective factor in terms of fuel cell degradation. The effect of membrane equivalent weight on the cell performance loss is below 0.4%. The second lowest effective component is the catalyst layer. Total effect of the porosity and the viscous resistance of the catalyst layer are below 4%. The catalyst layer analysis shows that the porosity is more effective on the cell performance than the viscous resistance.

It can be said that, the GDL degradation has a considerable effect on the cell performance. The effect of the GDL on the cell performance is around 6%. Similar to the catalyst layer, it is observed that the porosity is more effective than the viscous resistance.

According to the parametric analysis, it can be concluded that bipolar plate degradation is the most effective component on the fuel cell performance. In other words, when the contact resistance of the bipolar plate increases, performance of the fuel cell decreases remarkably. For a cell potential value of 0.55V, 21.4% percent performance loss is observed for a fully degraded bipolar plate with a contact resistance value of $108\text{m}\Omega\text{cm}^2$.

Maximum performance loss is observed for a cell potential value of 0.55V for the degraded bipolar plate analysis and the fully degraded cell. However, PEM fuel cells mainly operate at the cell potential values above 0.7V and at the current density values below 700 mA/cm^2 . To sum up, according to parametric analysis on fuel cell degradation, it is expected a performance loss above 14% for the fully degraded cell.

4.4 Degraded Stack Simulations

Degradation study is repeated for the fuel cell stacks that are discussed in Chapter 3. As stated above, PEM fuel cells mainly operate at the cell potential values above

0.7 V and at the current density values below 700 mA/cm². Thus, this study is concentrated on the performance of the PEM fuel cell stack in the mentioned range.

In Figure 52, comparison of the performances of the fresh 2-cell stack and the degraded 2-cell stack is presented. For cell potential values of 0.85 V, 0.75 V and 0.65 V, it is observed that maximum performance loss of 19% exists between the fresh 2-cell stack and the degraded 2-cell stack. In Figure 53, comparison of the performances of the fresh 3-cell stack and the degraded 3-cell stack is presented. It is observed that the maximum performance loss of 18% exists between the fresh 3-cell stack and the degraded 3-cell stack, for same cell potential values. In Figure 54, comparison of the performances of the fresh 4-cell stack and the degraded 4-cell stack is presented. For the same cell potential values, it is also observed that the maximum performance loss of 18% exists between the fresh 4-cell stack and the degraded 4-cell stack.

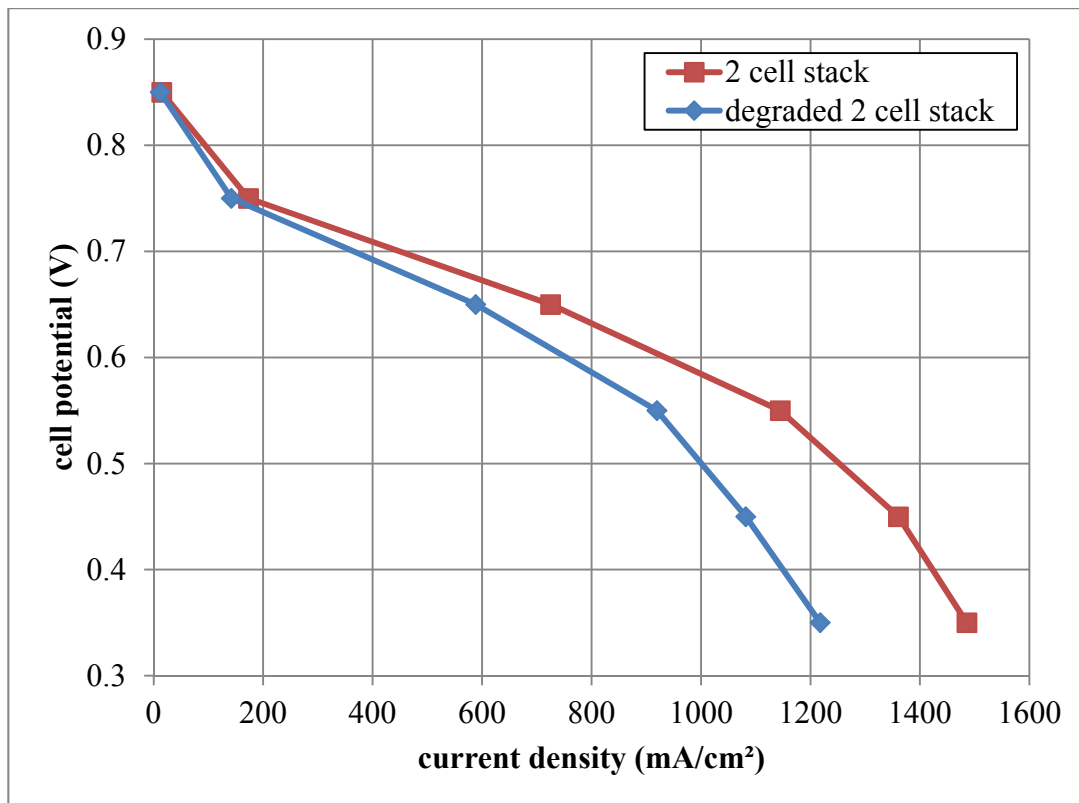


Figure 52 Performances of the fresh stack and the degraded stack (2-cells, after 2 years).

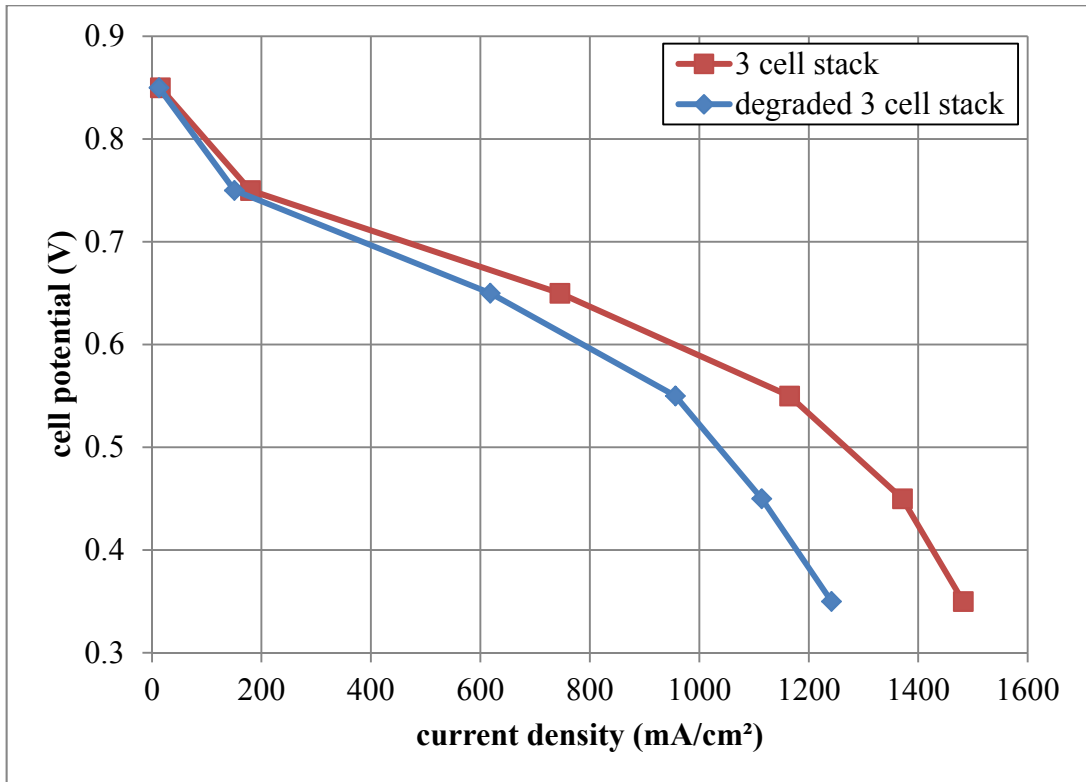


Figure 53 Performances of the fresh stack and the degraded stack (3-cells, after 2 years).

To sum up, maximum performance loss of 19% is observed between fresh and degraded fuel cell stacks. For the single cell, a performance loss of 17% is observed. Thus, it can be assumed that there is a performance loss of approximately 20% exists between the fresh and the degraded cells. Consequently, it is decided to perform system simulations using the degraded parameters used in this part of the study for the PEM based components in the following section.

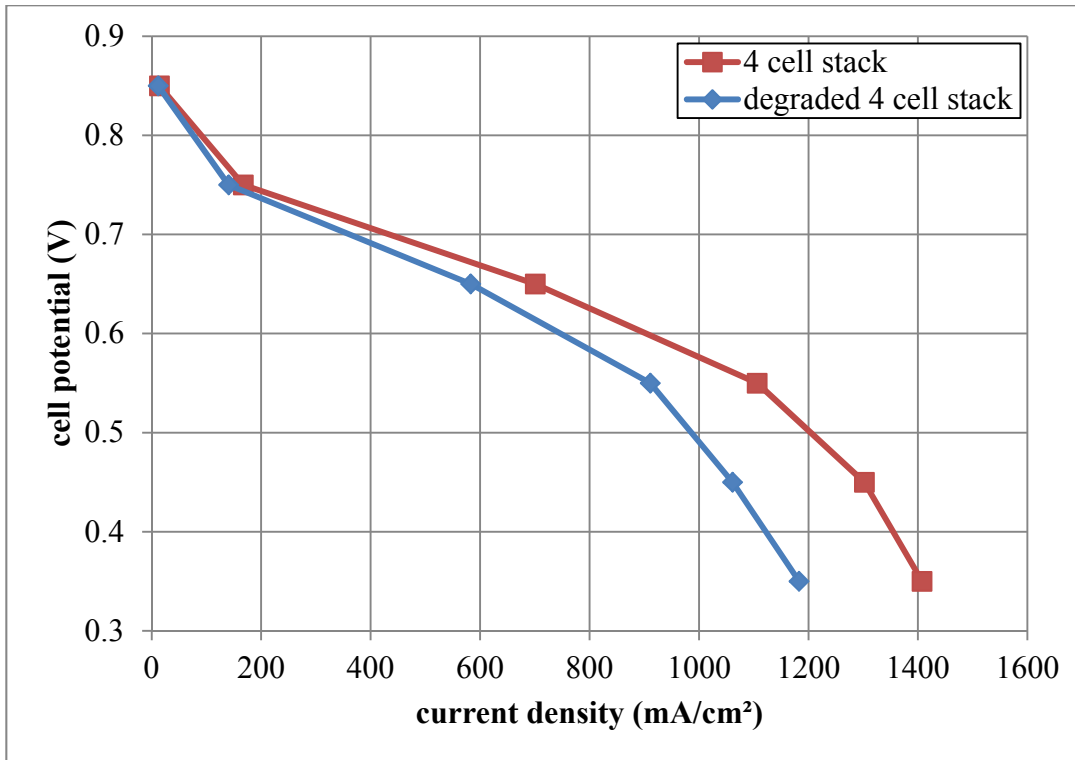


Figure 54 Performances of the fresh stack and the degraded stack (4-cells, after 2 years).

4.5 System Simulations with Degraded PEM Fuel Cells

System simulations are repeated for the degraded PEM based components. The simulations are started with 3.8% of hydrogen level. This is the hydrogen level at the end of the two years of simulation time. After two years of operation, it is expected to see the effects of degradation both on PEM based components and on the overall system. In the simulated system, the PEM fuel cell yearly operating time is 5180 hours and in two years it exceeds 10,000 hours of operation time. According to Zhang et al. [181] voltage degradation rate curve of a typical PEM fuel cell seems like the profile of a bathtub, which is comprised of three parts: infant degradation, steady degradation, and accelerated degradation. The infant degradation part of the voltage degradation rate curve is very short compared to the

other parts of the curve. Also, infant degradation is a running-in phenomenon. The steady degradation part of the voltage degradation rate curve characteristically results in a steady voltage degradation rate. Likewise, the steady degradation is attributed to former service life of a PEM fuel cell. In the accelerated degradation part of the voltage degradation curve, the effects of degradation are forceful. In the literature, 10,000 hours is reported as the critical time, after which accelerated degradation effects are observable [182].

In Figure 55, the comparison of the pressure levels in the hydrogen tanks is presented for the fresh and the degraded system. It is observed that the system is not capable of supplying energy demand of the emergency room for the whole year when the PEM based components are degraded. After simulation time of approximately 11 months, all of the hydrogen is consumed. The system can operate uninterrupted for 334 days. Starting from 1st of March, the system can operate continuously until 28th of January. It is also observed that it took almost one more month to completely fill the hydrogen tanks with the degraded system.

Energy flow values of the degraded system are presented in Table 17. It is observed that the overall system efficiency is decreased by 2.64% without considering the effects of the PV panels. When PV panels are taken into account, only performance drop of 0.38% is observed. When compared with the non-degraded system, it can be concluded that same amount of energy is dumped from the controller. However, there is a performance loss of 0.39% is present in the controller, since the system is simulated only for 11 months.

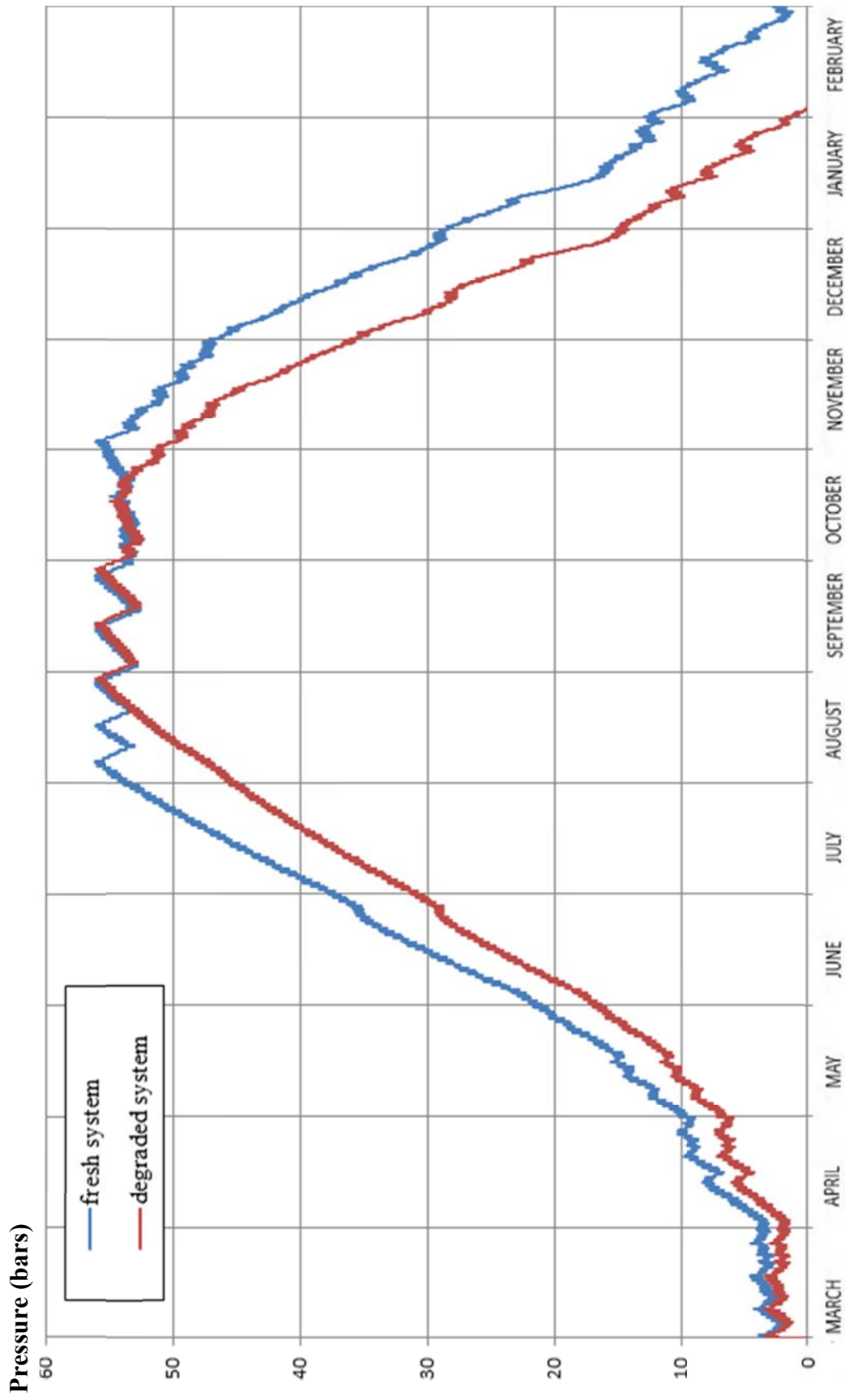


Figure 55 Comparison of pressure levels in the hydrogen tanks (after 2 years).

Table 17 Energy flow values of the degraded system (after 2 years).

Components	Input	MWh	Output	MWh	Loss MWh	Efficiency
PV Panels	E_Solar	566.66	E_PV	79.53	487.13	14.03%
Controller	E_PV	79.53	E_Inverter	18.88	E_Dump 5.03	93.68%
			E_Elz	55.62		
PEM Electrolyzer	E_Elz	55.62	E_H ₂ in	27.56	28.06	49.55%
PEM Fuel Cell	E_H ₂ out	27.56	E_FC	15.88	11.68	57.62%
Inverter	E_FC	15.88	E_User	33.02	1.74	94.99%
	E_Inverter	18.88				
Overall System	E_Solar	566.66	E_User	33.02	533.64	5.83%
Overall System	E_PV	79.53	E_User	33.02	46.51	41.52%

4.6 Economic Analysis for Degraded System

LCE analysis is repeated for the degraded system after two years operation. The straightforward way of calculating the LCE for the degraded system is comparing annual useful energy (UE_{an}) values supplied to the system. The LCE is inversely proportional with UE_{an} (Details are presented in Appendix A). In Table 17, for the degraded system UE_{an} is tabulated as 33.02 MWh and in Table 6, for the fresh system UE_{an} is tabulated as 37.23 MWh. By using this approach, LCE is calculated as 0.706 \$/kWh for the degraded system.

4.7 Discussions

In this chapter degradation of PEM fuel cells is investigated by using CFD. The CFD study is conducted to improve basic understanding of the degradation phenomenon in PEM fuel cells. Additionally, impacts of various parameters on degradation are investigated by performing a parametric analysis. It is concluded that bipolar plates are the most effective components on the fuel cell performance according to parametric analysis. Likewise, it is found that the membrane degradation is the least effective component of fuel cell degradation.

It is observed that the degradation phenomenon has substantial impacts on the overall system performance. System down time of approximately one month is possible. Thus, the system is not capable of operating continuously for a complete year, when the PEM based components are degraded.

It can be said that the degradation phenomenon significantly affects the financial aspects of the renewable energy system. The LCE value of the degraded system is found 0.08 \$/kWh higher than the fresh system. Moreover, it is also observed that the LCE value of the degraded system is also approximately 0.019 \$/kWh higher than the PV/battery system.

CHAPTER 5

CONCLUSIONS

A solar-hydrogen based stand-alone hybrid renewable energy system is modeled and system parameters are analyzed using TRNSYS. PV panels are used in the system to generate energy for the system. The dumped out energy is minimized by using hydrogen storage. Hydrogen is generated by using PEM electrolyzers. PEM fuel cells are used for generating electricity when the solar power is not available. PEM fuel cells are computationally modeled by using ANSYS Fluent. Afterwards, PEM fuel cell degradation issue is studied in detail.

Hydrogen is the only energy storage for the simulated hybrid renewable energy system. The overall efficiency of the system is improved by using variable angle of incidence for the PV panels. System was established to the hospital with a hydrogen storage capacity of 30 m³. In the system simulations, it is concluded to increase the capacity of hydrogen storage to 45 m³. Increasing the capacity of the hydrogen storage adds additional cost to the system. However, the system is capable of continuously working throughout a whole period of year when the storage capacity is increased to 45 m³. Pressure level in the hydrogen tanks is monitored to evaluate the performance of the system. It is concluded that the pressure level in the hydrogen tanks is a remarkable system performance demonstrator, as long as no system constraints are violated.

The energy-exergy analysis is performed for a complete year and average energy and exergy efficiency values are compared. The results of the energy-exergy analysis show that the PEM fuel cell and the PEM electrolyzer both have acceptable

energy and exergy efficiency values, but the PV panels have considerably low energy and exergy efficiency values. This result is expected and acceptable because unlike many other thermodynamical power cycle alternatives there is no cost associated with the incident solar radiation (or high temperature reservoir).

After examining the outcomes of the energy-exergy analysis, it is concluded that by equipping the PV panels with tiltable platforms, it is possible to obtain higher energy and exergy efficiencies than the ones for fixed angle PV panels. The exergy efficiency of the PV panels is calculated as 15.19%. This value is considerably higher than that of the fixed PV panel systems available in literature; for instance, Hepbaşlı [129] reported an exergy efficiency value of 11.2% for a fixed angle PV panel system.

It can be concluded that the degradation of PEM based components is an important phenomenon, which has considerable effects on the overall system performance. The system is not capable of operating continuously for a complete year, when the PEM based components are degraded. Hydrogen storage capacity can be increased to solve this problem. However, this also adds additional cost to the system.

According to the LCE analysis, the PV/hydrogen based energy system is slightly advantageous than the PV/battery based system, in which only batteries are used as secondary power supply for the user. In the near future, rapidly developing PEM based hydrogen technology could improve this trend even further. Considering that the component costs that are associated with the fuel cell and the electrolyzer are very high (because they are not mass produced components), a PV/hydrogen based system may become even more advantageous in the future with the predicted widespread adoption of PEM based technologies.

LCE analysis is repeated for the degraded system, and the results of the analysis are compared with the results of the PV/battery system. The LCE value of the degraded system is found higher than the PV/battery system. PV/battery system seems not

economical at the establishment stage, but after two years of operation, the PV/battery system becomes more economical than the PV/hydrogen system. On the other hand, the main drawback of the PV/battery system is the replacement time. The replacement time is too short for the PV/battery system; after four years of operation, batteries must be renewed.

LCE analysis is performed for a pure diesel generator system (most common back-up power option) for the sake of completeness. The results of the analysis show that the replacement of fossil fuel based energy systems with solar-hydrogen based energy systems is not economically feasible, unless important improvement in the cost of PV/hydrogen technologies are made in the future. On the other hand, the replacement of fossil fuel based energy systems with renewable energy systems is found technologically viable. Furthermore, replacement of fossil fuel based energy systems reduces emissions and dependency to the fossil fuels. Additionally, it is concluded that solar-hydrogen based renewable energy systems can be a possible alternative to fossil fuel based energy systems especially in long-term emergency blackout conditions.

In conclusion, degradation phenomenon in PEM fuel cells is found quite complicated. Only the final results of chemical and thermodynamical reactions are noticeable. The impacts of temperature, pressure or other operating conditions on the final degradation commonly observed as conflicting in the literature [183]. An operating condition that may speed up one stage may slow down the other. Thus, even with the help of a computational study, a complete quantitative realization of degradation phenomena is found quite difficult.

REFERENCES

- [1] Çeliktaş M.S., Koçar G., “Hydrogen is not an utopia for Turkey,” *International Journal of Hydrogen Energy*, 35, 9-18, 2010.
- [2] Yolcular S., “Hydrogen Production for Energy Use in European Union Countries and Turkey,” *Energy Sources, Part A*, 31, 1329-1337, 2009.
- [3] Yazıcı M.S., “UNIDO-ICHET support to hydrogen and fuel cell technologies in Turkey,” *International Journal of Hydrogen Energy*, 36, 11239-11245, 2011.
- [4] Chauhan A., Saini R.P., “A review on Integrated Renewable Energy System based power generation for stand-alone applications: Configurations, storage options, sizing methodologies and control,” *Renewable and Sustainable Energy Reviews*, 38, 99–120, 2014.
- [5] Barton J.P., Infield D.G., “Energy storage and its use with intermittent renewable energy,” *IEEE Transactions on Energy Conversion*, 19(2), 441-448, 2004.
- [6] Abbey C., Robinson J., Joos G., “Integrating renewable energy sources and storage into isolated diesel generator supplied electric power systems,” *IEEE 13th International Power Electronics and Motion Control Conference*, 2178-2183, 2008.
- [7] Marshall A., “Electrocatalysts for the Oxygen Evolution Electrode in Water Electrolysers using Proton Exchange Membranes: Synthesis and Characterisation,” PhD. Thesis, Norwegian University, June 2005.
- [8] Bezmalinovic D., Barbir F., Tolj I., “Techno-economic analysis of PEM fuel cells role in photovoltaic-based systems for the remote base stations,” *International Journal of Hydrogen Energy*, 38, 417-425, 2013.
- [9] Selamet Ö.F., Becerikli F., Mat M.D., Kaplan Y., “Development and testing of a highly efficient proton exchange membrane (PEM) electrolyzer stack,” *International Journal of Hydrogen Energy*, 36, 11480-11487, 2011.
- [10] Sinha S, Chandel S.S., “Review of software tools for hybrid renewable energy systems,” *Renewable and Sustainable Energy Reviews*, 32, 192-205, 2014.

- [11] Turcotte D., Ross M., Sheriff F., “Photovoltaic hybrid system sizing and simulation tools: Status and needs,” In: PV Horizon: Workshop on Photovoltaic Hybrid Systems, 1–10, Montreal, 2001.
- [12] Shahrestani M., Yao R., Cook G.K., “Developing new components for variable flow distribution system modelling in TRNSYS,” *Building Simulation*, 6, 309-322, 2013.
- [13] Duffy M.J., Hiller M., Bradley D.E., Keilholz W., Thornton J.W., “TRNSYS – Features and functionality,” *Proceedings of 11th International IBPSA Conference, Building Simulation, 1950-1954*, 2009.
- [14] Klein S.A., Beckman W.A., Mitchell J.W., Duffie J.A., Duffie N.A., Freeman T.L., Mitchell J.C., Braun J.E., Evans B.L., Kummer J.P., Urban R.E., Fiksel A., Thornton J.W., Blair N.J., Williams P.M., Bradley D.E., McDowell T.P., Kummert M., Arias D.A., “TRNSYS—a transient system simulation program. Manual v16,” Solar Energy Laboratory, University of Wisconsin, Madison, 2007.
- [15] Ulleberg O., Morner S.O., “TRNSYS simulation models for solar-hydrogen systems,” *Solar Energy*, 59 (4-6), 271-279, 1997.
- [16] Rockendorf G., Sillmann R., Podlowski L., Litzenburger B., “PV-hybrid and thermoelectric collectors,” *Solar Energy*, 67, 4-6, 1999.
- [17] Schucan T., “Case Studies of Integrated Hydrogen Systems,” International Energy Agency Hydrogen Implementing Agreement Final Report for Subtask A of Task 11 – Integrated Systems, Paul Scherrer Institute, Switzerland, 1999.
- [18] Samaniego J., Alija F., Sanz S., Valmaseda C., Frechoso F., “Economic and technical analysis of a hybrid wind fuel cell energy system,” *Renewable Energy*, 33, 839-845, 2008.
- [19] Almeida P., Carvalho M.J., Amorim R., Mendes J.F., Lopes V., “Dynamic testing of systems – Use of TRNSYS as an approach for parameter identification,” *Solar Energy* 104, 60–70, 2014.
- [20] Chargui R., Sammouda H., “Modeling of a residential house coupled with a dual source heat pump using TRNSYS software,” *Energy Conversion and Management*, 81, 384-399, 2014.
- [21] Kalogirou S.A., “Use of TRNSYS for modelling and simulation of a hybrid PV–thermal solar system for Cyprus,” *Renewable Energy*, 23, 247-260, 2001.

- [22] Ulleberg O., "Modeling of advanced alkaline electrolyzers: a system simulation approach," *International Journal of Hydrogen Energy*, 28, 21-33, 2003.
- [23] Ulleberg O., "The importance of control strategies in PV–hydrogen systems," *Solar Energy*, 76, 323-329, 2004.
- [24] Ghosh P.C., Emonts B., Janßen, H., Mergel J., Stolten D., "Ten years of operational experience with a hydrogen-based renewable energy supply system," *Solar Energy*, 75, 469-478, 2003.
- [25] Rohani G., Nour M., "Techno-economical analysis of stand-alone hybrid renewable power system for Ras Musherib in United Arab Emirates," *Energy*, 64, 828-841, 2014.
- [26] Zoulias E.I., Lymberopoulos N., "Techno-economic analysis of the integration of hydrogen energy technologies in renewable energy-based stand-alone power systems," *Renewable Energy* 32, 680–696, 2007.
- [27] Khan M.J., Iqbal M.T., "Pre-feasibility study of stand-alone hybrid energy systems for applications in Newfoundland," *Renewable Energy*, 30, 835-834, 2005.
- [28] El-Shatter T.F., Eskandar M.N., El-Hagry M.T., "Hybrid PV/fuel cell system design and simulation," *Renewable Energy* 27, 479–485, 2002.
- [29] Jiang Z., "Power management of hybrid photovoltaic - fuel cell power systems," *IEEE Power Engineering Society General Meeting*, 1-6, 2006.
- [30] Barbir F., "Fuel cells for clean power generation: status and perspectives," *Assessment of Hydrogen Energy for Sustainable Development*, 8, 113-121, 2007.
- [31] Gottesfeld S. Zawodzinski T.A., "Polymer electrolyte fuel cells," in "Advances in Electrochemical Science and Engineering," Alkire R.C., Gerischer H., Kolb D.M., Tobias C.W. (Eds)," vol. 5, Wiley-VCH, 195-302, 1997.
- [32] Barbir F., "PEM Fuel Cells: Theory and Practice," Elsevier Inc, 2005.
- [33] Larminie J., Dicks A., "Fuel Cell Systems Explained," 2nd edition, John Wiley & Sons, Chichester, 2003.
- [34] Li X., Sabir I., "Review of bipolar plates in PEM fuel cells: Flow-field designs," *International Journal of Hydrogen Energy*, 30, 359-371, 2005.

[35] Hermann A., Chaudhuri T., Spagnol P., "Bipolar plates for PEM fuel cells: A review," *International Journal of Hydrogen Energy*, 30, 1297-1302, 2005.

[36] ANSYS Fluent PEM Fuel Cell Module User Guide.

[37] Siegel C., "Review of computational heat and mass transfer modeling in polymer-electrolyte-membrane (PEM) fuel cells," *Energy*, 33, 1331-1352, 2008.

[38] Bıyıkoğlu A., "Review of proton exchange membrane fuel cell models," *International Journal of Hydrogen Energy*, 30, 1181-1212, 2005.

[39] Deshmukh S.S., Boehm R.F., "Review of modeling details related to renewably powered hydrogen systems," *Renewable and Sustainable Energy Reviews*, 12, 2301–2330, 2008.

[40] Djilali N., "Computational modeling of polymer electrolyte membrane (PEM) fuel cells: Challenges and opportunities," *Energy*, 32, 269-280, 2007.

[41] Gurau V., Liu H., Kakaç S., "Two-dimensional model for proton exchange membrane fuel cells," *AIChE Journal*, 44 (11), 2410-2422, 1998.

[42] Um S., Wang C.Y., Chen K.S., "Computational fluid dynamics modeling of proton exchange membrane fuel cells," *Journal of The Electrochemical Society*, 147, 4485-4493, 2000.

[43] Wang Z.H., Wang C.Y., Chen K.S., "Two-phase flow and transport in the air cathode of proton exchange membrane fuel cells," *Journal of Power Sources*, 94, 40-50, 2001.

[44] Berning T., Lu D.M., Djilali N., "Three-dimensional computational analysis of transport phenomena in a PEM fuel cell," *Journal of Power Sources*, 106, 284-294, 2002.

[45] Sivertsen B.R., Djilali N., "CFD-based modeling of proton exchange membrane fuel cells," *Journal of Power Sources*, 141, 65-78, 2005.

[46] Berning T., Djilali N., "A 3D, multiphase, multicomponent model of the cathode and anode of a PEM fuel cell," *Journal of The Electrochemical Society*, 150, A1589-A1598, 2003.

- [47] Berning T., Djilali N., "Three-dimensional computational analysis of transport phenomena in a PEM fuel cell—a parametric study," *Journal of Power Sources*, 124, 440–452, 2003.
- [48] Al-Baghdadi M.A.R.S., Al-Janabi H.A.K.S., "Modeling optimizes PEM fuel cell performance using three-dimensional multi-phase computational fluid dynamics model," *Energy Conversion and Management*, 48, 3102-3109, 2007.
- [49] Al-Baghdadi M.A.R.S., Al-Janabi H.A.K.S., "Parametric and optimization study of a PEM fuel cell performance using three-dimensional computational fluid dynamics model," *Renewable Energy*, 32, 1077-1101, 2007.
- [50] Dutta S., Shimpalee S., Van Zee J.W., "Numerical prediction of mass-exchange between cathode and anode channels in a PEM fuel cell," *International Journal of Heat and Mass Transfer*, 44, 2029-2042, 2001.
- [51] Nguyen P.T., "A Three-dimensional computational model of PEM fuel cell with serpentine gas channels," M.S. Thesis, University of Victoria, 2001.
- [52] Nguyen P.T., Berning T., Djilali N., "Computational model of a PEM fuel cell with serpentine gas flow channels," *Journal of Power Sources*, 130, 149-157, 2004.
- [53] Nguyen P.T., Berning T., Bang M., Djilali N., "A Three-dimensional model of PEM fuel cells with serpentine flow channels," *Hydrogen and fuel cells conference*, Vancouver, Canada, 2003.
- [54] Shimpalee S., Dutta S., Van Zee J.W., "Numerical prediction of local temperature and current density in a PEM fuel cell," *Proceedings of IMECE 2000*.
- [55] Dutta S., Shimpalee S., Van Zee J.W., "Three-dimensional numerical simulation of straight channel PEM fuel cells," *Journal of Applied Electrochemistry*, 30, 135-146, 2000.
- [56] Kumar A., Reddy R.G., "Modeling of polymer electrolyte membrane fuel cell with metal foam in the flow-field of the bipolar/end plates," *Journal of Power Sources*, 114, 54-62, 2003.
- [57] Kumar A., Reddy R.G., "Effect of channel dimensions and shape in the flow-field distributor on the performance of polymer electrolyte membrane fuel cells," *Journal of Power Sources*, 113, 11-18, 2003.

[58] Kumar A., Reddy R.G., "Polymer electrolyte membrane fuel cell with metal foam in the gas flow-field of bipolar/end plates," *Journal of New Materials for Electrochemical Systems*, 6, 213-236, 2003.

[59] Reddy E.H., Jayanti S., "Thermal management strategies for a 1 kWe stack of a high temperature proton exchange membrane fuel cell," *Applied Thermal Engineering*, 48, 465-475, 2012.

[60] Iranzo A., Munoz M., Rosa F., Pino J., "Numerical model for the performance prediction of a PEM fuel cell. Model results and experimental validation," *International Journal of Hydrogen Energy*, 35, 11533-11550, 2010.

[61] Iranzo A., Munoz M., Pino J., Rosa F., "Update on numerical model for the performance prediction of a PEM fuel cell," *International Journal of Hydrogen Energy*, 36, 9123-9127, 2011.

[62] Iranzo A., Boillat P., Rosa F., "Validation of a three dimensional PEM fuel cell CFD model using local liquid water distributions measured with neutron imaging," *International Journal of Hydrogen Energy*, 39, 7089-7099, 2014.

[63] Quan P., Zhou B., Sobiesiak A., Liu Z., "Water behavior in serpentine micro-channel for proton exchange membrane fuel cell cathode," *Journal of Power Sources*, 152, 131-145, 2005.

[64] Hontanon E., Escudero M.J., Bautista C., Garcia-Ybarra P.L., Daza L., "Optimisation of flow-field in polymer electrolyte membrane fuel cells using computational fluid dynamics techniques," *Journal of Power Sources*, 86, 363-368, 2000.

[65] Zhang Y., Pitchumani R., "Numerical studies on an air-breathing proton exchange membrane (PEM) fuel cell," *International Journal of Heat and Mass Transfer*, 50, 4698-4712, 2007.

[66] Rajani B.P.M., Kolar A.K., "A model for a vertical planar air breathing PEM fuel cell," *Journal of Power Sources*, 164, 210-221, 2007.

[67] Meng H., "Numerical investigation of transient responses of a PEM fuel cell using a two-phase non-isothermal mixed-domain model," *Journal of Power Sources*, 171, 738-746, 2007.

- [68] Pasaogullari U., Wang C.Y., "Two-phase modeling and flooding prediction of polymer electrolyte fuel cells," *Journal of The Electrochemical Society*, 152(2), A380-A390, 2005.
- [69] Wang Y., Wang C.Y., "Modeling polymer electrolyte fuel cells with large density and velocity changes," *Journal of The Electrochemical Society*, 152(2), A445-A453, 2005.
- [70] De Giorgi M.G., Ficarella A., "CFD modeling of PEM fuel cell's flow channels," *Proceedings of Energy Sustainability, Florida, USA*, 2008.
- [71] Mazumder S., Cole J.V., "Rigorous 3-D mathematical modeling of PEM fuel cells I. Model predictions without liquid water transport," *Journal of The Electrochemical Society*, 150 (11), A1503-A1509, 2003.
- [72] Mazumder S., Cole J.V., "Rigorous 3-D mathematical modeling of PEM fuel cells II. Model predictions with liquid water transport," *Journal of The Electrochemical Society*, 150 (11), A1510-A1517, 2003.
- [73] Shimpalee S., Lee W.K., Van Zee J.W., Naseri-Neshat H., "Predicting the transient response of a serpentine flow-field PEMFC I. Excess to normal fuel and air," *Journal of Power Sources*, 156, 355-368, 2006.
- [74] Shimpalee S., Lee W.K., Van Zee J.W., Naseri-Neshat H., "Predicting the transient response of a serpentine flow-field PEMFC II: Normal to minimal fuel and air," *Journal of Power Sources*, 156, 369-374, 2006.
- [75] Shimpalee S., Spuckler D., Van Zee J.W., "Prediction of transient response for a 25-cm² PEM fuel cell," *Journal of Power Sources*, 167, 130-138, 2007.
- [76] Ju H., Wang C.Y., "Experimental validation of a PEM fuel cell model by current distribution data," *Journal of The Electrochemical Society*, 151 (11), A1954-A1960, 2004.
- [77] Karvonen S., Hottinen T., Saarinen J., Himanen O., "Modeling of flow field in polymer electrolyte membrane fuel cell," *Journal of Power Sources*, 161, 876-884, 2006.
- [78] Yalcinoz T., Alam M.S., "Dynamic modeling and simulation of air-breathing proton exchange membrane fuel cell," *Journal of Power Sources*, 182, 168-174, 2008.

- [79] Mench M.M., "Fuel Cell Engines," John Wiley & Sons Ltd, 2008.
- [80] Wargo E.A., Dennison C.R., Kumbur E.C., "Durability of polymer electrolyte fuel cells: Status and targets," in: "Polymer Electrolyte Fuel Cell Degradation," Mench M.M., Kumbur E.C., Veziroğlu T.N., (Eds.)," Elsevier Inc., 1-14, 2012.
- [81] Wu J., Yuan X.Z., Martin J.J., Wang H., Zhang J., Shen J., Wu S., Merda W., "A review of PEM fuel cell durability: Degradation mechanisms and mitigation strategies," *Journal of Power Sources*, 184, 104-119, 2008.
- [82] Borup R., Meyers J., Pivovar B., Kim Y.S., Mukundan R., Garland N., Myers D., Wilson M., Garzon F., Wood D., Zelenay P., More K., Stroh K., Zawodzinski T., Boncella J., McGrath J.E., Inaba M., Miyatake K., Hori M., Ota K., Ogumi Z., Miyata S., Nishikata A., Siroma Z., Uchimoto Y., Yasuda K., Kimijima K., Iwashita N., "Scientific aspects of polymer electrolyte fuel cell durability and degradation," *Chemical Reviews*, 107, 3904-3951, 2007.
- [83] Madden T., Weiss D., Cipollini N., Condit D., Gummala M., Burlatsky S., Atrazhev V., "Degradation of polymer-electrolyte membranes in fuel cells: I. Experimental," *Journal of the Electrochemical Society*, 156 (5), B657-B662, 2009.
- [84] Gummala M., Atrazhev V., Condit D., Cipollini N., Madden T., Kuzminyh D., Weiss D., Burlatsky S., "Degradation of polymer-electrolyte membranes in fuel cells: II. Theoretical model," *Journal of the Electrochemical Society*, 157 (11), B1542-B1548, 2010.
- [85] Hinds G., "Performance and Durability of PEM Fuel Cells: A Review," NAT. PHYS. LAB, Teddington, UK, 2004.
- [86] Fowler M., Mann R.F., Amphlett J.C., Peppley B.A, Roberge P.R., "Reliability issues and voltage degradation," in: "Handbook of Fuel Cells: Fundamentals, Technology and Applications, Vielstich W., Gasteiger H.A., Lamm A., (Eds.)," vol. 3, John Wiley & Sons Ltd., 663-677, 2003.
- [87] Cleghorn S.J.C., Mayfield D.K., Moore D.A., Moore J.C., Rusch G., Sherman T.W., Sisofo N.T., Beuscher U., "A polymer electrolyte fuel cell life test: 3 years of continuous operation," *Journal of Power Sources*, 158, 446-454, 2006.
- [88] Anghel V., "Prediction failure for PEM fuel cells," *International Journal of Advances in Engineering & Technology*, 4 (2), 1-14, 2012.

- [89] Zhan Y., Guo Y., Zhu J., Li L., “Natural degradation and stimulated recovery of a proton exchange membrane fuel cell,” *International Journal of Hydrogen Energy*, 39, 12849-12858, 2014.
- [90] Wang F., Yang D., Li B., Zhang H., Hao C., Chang F., Ma., “Investigation of the recoverable degradation of PEM fuel cell operated under drive cycle and different humidities,” *International Journal of Hydrogen Energy*, 39, 14441-14447, 2014.
- [91] Zhang Y., Chen S., Wang Y., Ding W., Wu R., Li L., Qi X., Wei Z., “Study of the degradation mechanisms of carbon-supported platinum fuel cells catalyst via different accelerated stress test,” *Journal of Power Sources*, 273, 62-69, 2015.
- [92] Liu H., Coms F.D., Zhang J., Gasteiger H.A., LaConti A.B., “Chemical Degradation: Correlations between Electrolyzer and Fuel Cell Findings,” in: “Polymer Electrolyte Fuel Cell Durability,” Büchi F.N., Inaba M., Schmidt T.J., (Eds.), Springer Inc., 71-118, 2009.
- [93] Zhang S., Yuan X., Wang H., Merida W., Zhu H., Shen J., Wu S., Zhang J., “A review of accelerated stress tests of MEA durability in PEM fuel cells,” *International Journal of Hydrogen Energy*, 34, 388-404, 2009.
- [94] Knights S.D., Colbow K.M., St-Pierre J., Wilkinson D.P., “Aging mechanisms and lifetime of PEFC and DMFC,” *Journal of Power Sources*, 127, 127-134, 2004.
- [95] Collier A., Wang H., Yuan X.Z., Zhang J., Wilkinson D.P., “Degradation of polymer electrolyte membranes,” *International Journal of Hydrogen Energy*, 31, 1838-1854, 2006.
- [96] Endoh E., Terazono S., Widjaja H., Takimoto Y., “degradation study of MEA for PEMFCs under low humidity conditions,” *Electrochemical and Solid-State Letters*, A209-A211, 2004.
- [97] Tang H., Peikang S., Jiang S.P., Wang F., Pan M., “A degradation study of Nafion proton exchange membrane of PEM fuel cells,” *Journal of Power Sources*, 170, 85-92, 2007.
- [98] Cheng X., Zhang J., Tang Y., Song C., Shen J., Song D., Zhang J., “Hydrogen crossover in high-temperature PEM fuel cells,” *Journal of Power Sources*, 167, 25-31, 2007.

[99] Taniguchi A., Akita T., Yasuda K., Miyazaki Y., “Analysis of electrocatalyst degradation in PEMFC caused by cell reversal during fuel starvation,” *Journal of Power Sources*, 130, 42-49, 2007.

[100] Schmittinger W., Vahidi A., “A review of the main parameters influencing long-term performance and durability of PEM fuel cells,” *Journal of Power Sources*, 180, 1–14, 2008.

[101] Wood D.L., Borup R.L., “Durability Aspects of Gas-Diffusion and Microporous Layers,” in: “Polymer Electrolyte Fuel Cell Durability,” Büchi F.N., Inaba M., Schmidt T.J., (Eds.), Springer Inc., 159-195, 2009.

[102] Schulze M., Wagner N., Kaz T., Friedrich K.A., “Combined electrochemical and surface analysis investigation of degradation processes in polymer electrolyte membrane fuel cells,” *Electrochimica Acta*, 52, 2328-2336, 2007.

[103] Ihonen J., Mikkola M., and Lindbergh G., “Flooding of gas diffusion backing in PEFCs; physical and electrochemical characterization,” *Journal of The Electrochemical Society*, 151 (8), A1152-A1161, 2004.

[104] Mitani T., Mitsuda K., “Durability of Graphite Composite Bipolar Plates,” in: “Polymer Electrolyte Fuel Cell Durability,” Büchi F.N., Inaba M., Schmidt T.J., (Eds.), Springer Inc., 257-268, 2009.

[105] Wind J., LaCroix A., Braeuninger S., Hedrich P., Heller C., Schudy M., “Metal Bipolar Plates and Coatings,” in: “Handbook of Fuel Cells: Fundamentals, Technology and Applications, Vielstich W., Gasteiger H.A., Lamm A., (Eds.),” vol. 3, John Wiley & Sons Ltd., 294-307, 2003.

[106] Çelik A.N., “Analysis of Ankara’s exposure to solar radiation: evaluation of distributional parameters using long-term hourly measured global solar radiation data,” *Turkish Journal of Engineering and Environmental Sciences*, 30, 115–126, 2006.

[107] Product Portfolio Service Organization, Viewed on March 2015, available from: http://www.bosch-solarenergy.de/en/bosch_se_serviceorganisation/product/portfolio_2.html.

[108] TÜBİTAK Project no: 106G130 Progress Report, January 2010.

- [109] Laurencelle F., Chahine R., Hamelin J., Agbossou K., Fournier M, Bose T.K., Laperriere A., "Characterization of a Ballard MK5-E proton exchange membrane fuel cell stack," *Fuel Cells*, 1 (1), 66-71, 2001.
- [110] TRNSYS 16 Users Guide, Volume 5, Mathematical Reference.
- [111] Amphlett J.C., Baumert R.M., Mann R.F., Peppley B.A., Roberge P.R., Harris T.J., "Performance modeling of the Ballard Mark IV solid polymer electrolyte fuel cell. Part I - mechanistic model development," *Journal of Electrochemical Society*, 142 (1), 1-8, 1995.
- [112] Amphlett J.C., Baumert R.M., Mann R.F., Peppley B.A., Roberge P.R., Harris T.J., "Performance modeling of the Ballard Mark IV solid polymer electrolyte fuel cell. Part II - empirical model development," *Journal of Electrochemical Society*, 142 (1), 9-15, 1995.
- [113] Marion W., Urban, K., "User's Manual for TMY2 Data Sets," National Renewable Energy Laboratory, 1995.
- [114] Uluoğlu A., "Solar-Hydrogen Stand-Alone Power System Design and Simulations," MS Thesis, METU, May 2010.
- [115] Reviewed – Bosch PV Solar Panels, Viewed on October 2014, available from: <http://www.pvpanelguide.co.uk/guides/reviewed-bosch-pv-solar-panels>.
- [116] Yilanci A., Dinçer İ., Öztürk H.K., "Performance analysis of a PEM fuel cell unit in a solar–hydrogen system," *International Journal of Hydrogen Energy*, 33, 7538-7552, 2008.
- [117] Dinçer İ., "Technical, environmental and exergetic aspects of hydrogen energy systems," *International Journal of Hydrogen Energy*, 27, 265-285, 2002.
- [118] Kazim A., "Exergoeconomic analysis of a PEM fuel cell at various operating conditions," *Energy Conversion and Management*, 46, 1073-1081, 2005.
- [119] Ni M., Leung M.K.H., Leung D.Y.C., "Energy and exergy analysis of hydrogen production by a proton exchange membrane (PEM) electrolyzer plant," *Energy Conversion and Management*, 49, 2748-2756, 2008.
- [120] Dinçer İ., Rosen M.A., "Exergy: Energy, Environment, and Sustainable Development," Elsevier Inc, 2007.

[121] Yilanci A., Dinçer İ., Öztürk H.K., "A review on solar-hydrogen/fuel cell hybrid energy systems for stationary applications," *Progress in Energy and Combustion Science*, 35, 231-244, 2009.

[122] Calderon M., Calderon A.J, Ramiro A., Gonzalez J.F., Gonzalez I., "Evaluation of a hybrid photovoltaic-wind system with hydrogen storage performance using exergy analysis," *International Journal of Hydrogen Energy*, 33, 5751-5762, 2011.

[123] Çalışkan H., Dinçer İ., Hepbaşlı A., "Energy, exergy and sustainability analyses of hybrid renewable energy based hydrogen and electricity production and storage systems: Modeling and case study," *Applied Thermal Engineering*, 61, 784-798, 2013.

[124] Sudhakar K., Srivastava T., "Energy and exergy analysis of 36W solar photovoltaic module," *International Journal of Ambient Energy*, 35 (1), 51-57, 2014.

[125] Luque A., Hegedus S., "Handbook of Photovoltaic Science and Engineering," Wiley-Sons, 2003.

[126] Hacatoğlu K., Dinçer İ., Rosen M.A., "Exergy analysis of a hybrid solar hydrogen system with activated carbon storage," *International Journal of Hydrogen Energy*, 36, 3273-3282, 2011.

[127] Sarhaddi F., Sarahat S., Ajam H., Behzadmehr A., "Exergy efficiency of a solar photovoltaic array based on exergy destructions," *Proceedings of the IMechE Vol. 224 Part A: Journal of Power and Energy*, 813-825, 2010.

[128] Boyle G., "Renewable Energy Power for a Sustainable Future," Oxford University Press, 2004.

[129] Hepbaşlı A., "A key review on exergetic analysis and assessment of renewable energy resources for a sustainable future," *Renewable and Sustainable Energy Reviews*, 12, 593-661, 2008.

[130] Çalışkan H., Dinçer İ., Hepbaşlı A., "Exergoeconomic and environmental impact analyses of a renewable energy based hydrogen production system," *International Journal of Hydrogen Energy*, 38, 6104-6111, 2013.

- [131] Luna-Rubio R., Trejo-Perea M., Vargas-Vazquez D., Rios-Moreno G.J., "Optimal sizing of renewable hybrids energy systems: A review of methodologies," *Solar Energy*, 86, 1077-1088, 2012.
- [132] Branker K., Pathak M.J.M., Pearce J.M., "A review of solar photovoltaic levelized cost of electricity," *Renewable and Sustainable Energy Reviews*, 15, 4470-4482, 2011.
- [133] Diaf S., Notton G., Belhamel M., Haddadi M., Louche A., "Design and techno-economical optimization for hybrid PV/wind system under various meteorological conditions," *Applied Energy*, 85, 968-987, 2008.
- [134] Yang H., Lu L., Zhou W., "A novel optimization sizing model for hybrid solar-wind power generation system," *Solar energy*, 81, 76-84, 2007.
- [135] Taleb A., Maine E., Kjeang E., "Technical-economic cost modeling as a technology management tool: A case study of membranes for PEM fuel cells," *Journal of Manufacturing Technology Management*, 25(2), 279-298, 2014.
- [136] Lacko R., Drobic B., Mori M., Sekavcnik M., Vidmar M., "Stand-alone renewable combined heat and power system with hydrogen technologies for household application," *Energy*, 77, 164-170, 2014.
- [137] Vasallo M.J., Bravo J.M., Andujar J.M., "Optimal sizing for UPS systems based on batteries and/or fuel cell," *Applied Energy*, 105, 170-181, 2013.
- [138] Jeon D.H., Greenway S., Shimpalee S., Van Zee J.W., "The effect of serpentine flow-field designs on PEM fuel cell performance," *International Journal of Hydrogen Energy*, 33, 1052-1066, 2008.
- [139] Shimpalee S., Greenway S., Spuckler D., Van Zee J.W., "Predicting water and current distributions in a commercial-size PEMFC," *Journal of Power Sources*, vol. 135, 79-87, 2004.
- [140] Lee W.Kl, Shimpalee S., Van Zee J.W., "Verifying predictions of water and current distributions in a serpentine flow field polymer electrolyte membrane fuel cell," *Journal of The Electrochemical Society*, 150, A341-A348, 2003.
- [141] Shimpalee S., Dutta S., "Numerical prediction of temperature distribution in PEM fuel cells," *Numerical Heat Transfer, Part A*, 38, 111-128, 2000.

- [142] Shimpalee S., Greenway S., Van Zee J.W., "The impact of channel path length on PEMFC flow-field design," *Journal of Power Sources*, 160, 398-406, 2006.
- [143] Shimpalee S., Van Zee J.W., "Numerical studies on rib and channel dimension of flow-field on PEMFC performance," *International Journal of Hydrogen Energy*, vol. 32, 842-856, 2007.
- [144] Lee W.K., Van Zee J.W., Shimpalee S., Dutta S., "Effect of humidity on PEM fuel cell performance. Part I: Experiments," In: ASME IMECE, Nashville, TN; 1999.
- [145] Dutta S., Van Zee J.W., "Effect of humidity on PEM fuel cell performance. Part II: Numerical simulation," In: ASME IMECE, Nashville, TN; 1999.
- [146] Glandt J., Shimpalee S., Lee W.K., Van Zee J.W., "Modeling the effect of flow field configuration on PEMFC performance," In: AIChE's 2002 spring national meeting, New Orleans, LA; 2002.
- [147] Shimpalee S., Beuscher U., Van Zee J.W., "Investigation of gas diffusion media inside PEMFC using CFD modeling," *Journal of Power Sources*, 163, 480-489, 2006.
- [148] Shimpalee S., Beuscher U., Van Zee J.W., "Analysis of GDL flooding effects on PEMFC performance," *Electrochimica Acta*, 52, 6748-6754, 2007.
- [149] Martinez M.J., Shimpalee S., Van Zee J.W., Sakars A.V., "Assessing methods and data for pore-size distribution of PEMFC gas-diffusion media," *Journal of The Electrochemical Society*, 156, B558-B564, 2009.
- [150] ANSYS Fluent 14.5 User Guide.
- [151] Al-Baghdadi M.A.R.S., "PEM fuel cell modeling," in: "Fuel Cell Research Trends," Vasquez L.O., (Eds.), Nova Science Publishers Inc., 273-379, 2007.
- [152] Al-Baghdadi M.A.R.S., "A CFD study of hygro-thermal stresses distribution in PEM fuel cell during regular cell operation," *Renewable Energy*, 34, 674-682, 2009.
- [153] O'Hayre R., Cha S.W., Colella W., Prinz F.B., "Fuel Cell Fundamentals," John Wiley & Sons Inc, 2006.

- [154] De Bruijn F.A., Dam V.A.T., Janssen G.J.M., "Review: durability and degradation issues of PEM fuel cell components," *Fuel Cells*, 8(1), 3-22, 2008.
- [155] Liso V., Nielsen M.P., Kær S.K., Mortensen H.M., "Thermal modeling and temperature control of a PEM fuel cell system for forklift applications," *International Journal of Hydrogen Energy*, 39, 16694-16705, 2014.
- [156] Spiegel C., "PEM Fuel Cell Modeling and Simulation Using MATLAB," Elsevier Inc, 2008.
- [157] PEM Fuel Cell Stack, Viewed on December 2012, available from: <http://electrochem.cwru.edu/encycl/art-c01-carbon.htm>.
- [158] Shimpalee S., Ohashi M., Van Zee J.W., Ziegler C., Stoeckmann C., Sadeler C., Hebling C., "Experimental and numerical studies of portable PEMFC stack," *Electrochimica Acta*, 54, 2899-2911, 2009.
- [159] Riascos L.A.M., Pereira D.D., "Optimal temperature control in PEM fuel cells," *IEEE 35th Annual Conference, Industrial Electronics*, 2778-2783, 2009.
- [160] Hamelin J., Agbossou K., Laperriere A., Laurencelle F., Bose T.K., "Dynamic behavior of a PEM fuel cell stack for stationary applications," *International Journal of Hydrogen Energy*, 26, 625-629, 2001.
- [161] Özden E., Tolj I., Barbir F., "Designing heat exchanger with spatially variable surface area for passive cooling of PEM fuel cell," *Applied Thermal Engineering*, 51, 1339-1344, 2013.
- [162] Wu J., Martin J.J., Orfino F.P., Wang H., Legzdins C., Yuan X.Z., Sun C., "In situ accelerated degradation of gas diffusion layer in proton exchange membrane fuel cell, Part I: Effect of elevated temperature and flow rate," *Journal of Power Sources*, 195, 1888-1894, 2010.
- [163] Gittleman C.S., Coms F.D., Lai Y.H., "Membrane durability: Physical and chemical degradation," in: "Polymer Electrolyte Fuel Cell Degradation," Mench M.M., Kumbur E.C., Veziroğlu T.N., (Eds.), Elsevier Inc., 15-88, 2012.
- [164] Springer T.E., Zawodzinski T.A., Gottesfeld S., "Polymer electrolyte fuel cell model," *Journal of Electrochemical Society*, 138 (8), 2334-2342, 1991.

[165] Eaton B.M., "One Dimensional, Transient Model of Heat, Mass, and Charge Transfer in a Proton Exchange Membrane," MS Thesis, Virginia Polytechnic and State University, May 2001.

[166] Ghassemzadeh L., Kreuer K.D., Maier J., Müller K., "Chemical degradation of Nafion membranes under mimic fuel cell conditions as investigated by solid-state NMR spectroscopy," *Journal of Physical Chemistry*, 114, 14635-14645, 2010.

[167] Zhou C., Zawodzinski T.A., Schiraldi D.A., "Chemical degradation of Nafion membranes," Fourth International Symposium on Proton Conducting Membrane Fuel Cells, Honolulu, Hawaii, October 3-8, 2004.

[168] Franco A.A., "Modelling and analysis of degradation phenomena in polymer electrolyte membrane fuel cells," in: "Polymer Electrolyte Membrane and Direct Methanol Fuel Cell Technology, Hartning C., Roth C., (Eds.)," vol. 1, Woodhead Publishing Ltd., 291-367, 2012.

[169] Kamarajugadda S., Mazumder S., "Cathode catalyst layer model for polymer electrolyte membrane fuel cell," Proceedings of the ASME 2012 International Mechanical Engineering Congress & Exposition, IMECE2012-85952, Houston, Texas, November 9-15 2012.

[170] Paimushin V.N., Ivanov V.A., Lukankin S.A., Bushkov A.A., "Research in the flexural buckling modes of a cylindrical sandwich shell under the action of a temperature field inhomogeneous across its thickness," *Mechanics of Composite Materials*, 40 (6), 461-472, 2004.

[171] Williams M.V., Kunz H.R., Fenton J.M., "Influence of convection through gas-diffusion layers on limiting current in PEM FCs using a serpentine flow field," *Journal of The Electrochemical Society*, 151 (10), A1617-A1627, 2004.

[172] Lee C., Merida W., "Gas diffusion layer durability under steady-state and freezing conditions," *Journal of Power Sources*, 164, 141-153, 2007.

[173] Sierra J.M., Figueroa- Ramirez S.J., Diaz S.A, Vargas J., Sebastian P.J., "Numerical evaluation of a PEM fuel cell with conventional flow fields adapted to tubular plates," *International Journal of Hydrogen Energy*, 39, 16694-16705, 2014.

[174] Nishith P., "Local degradation of structural, mechanical, electrical and chemical properties of membrane electrode assembly in polymer electrolyte fuel cell," Master's report, Michigan Technological University, 2011.

- [175] Kraytsberg A., Auinat M., Ein-Eli Y., "Reduced contact resistance of PEM fuel cell's bipolar plates via surface texturing," *Journal of Power Sources*, 164, 697-703, 2007.
- [176] Timsit R.S., "Electrical contact resistance: properties of stationary interfaces," *IEEE Transactions on Components and Packaging Technology*, 22 (1), 85-98, 1999.
- [177] Barbir F., Braun J., Neutzler J., "Properties of molded graphite bi-polar plates for PEM fuel cell stacks," *Journal of New Materials for Electrochemical Systems*, 2, 197-200, 1999.
- [178] Dandekar N., Mendonca A., "Electrochemical Characterization and Aging in PEM Fuel Cells," Qualifying Project Report, Worcester Polytechnic Institute, February 2012.
- [179] He W., Yi J.S., Nguyen T.V., "Two-phase flow model of the cathode of PEM fuel cells using interdigitated flow fields," *AIChE Journal*, 46 (10), 2053-2064, 2000.
- [180] Iranzo A., Rosa F., López E., Pino F.J., Valverde L., Bermejo P., "Experimental and numerical investigation of a PEM fuel cell. Single cell and stack analysis," *Proceedings of I Simposium Ibérico de Hidrógeno, Pilas de Combustible y Baterías Avanzadas, HYCELTEC, Bilbao*, 2008.
- [181] Zhang X., Rui Y., Tong, Sichuan X., Yong S., Huaisheng N., "The characteristics of voltage degradation of a proton exchange membrane fuel cell under a road operating environment," *International Journal of Hydrogen Energy*, 39, 9420-9429, 2014.
- [182] Payne T., "DOE fuel cell R&D activities: transportation, stationary, and portable power applications," in: "Fuel cells durability & performance," Knowledge Press Inc., 2009.
- [183] Morimoto Y., Yamakawa S., "Computational modeling aspects of PEFC durability," in: "Polymer Electrolyte Fuel Cell Degradation," Mench M.M., Kumbur E.C., Veziroğlu T.N., (Eds.), Elsevier Inc., 423-441, 2012.
- [184] Wilcox, S., Marion W., "User's Manual for TMY3 Data Sets," National Renewable Energy Laboratory, 2008.

- [185] Nelson D.B., Nehrir M.H., Wang C., “Unit sizing and cost analysis of stand-alone hybrid wind/PV/fuel cell power generation systems,” *Renewable Energy*, 31, 1641-1656, 2006.
- [186] Mahlia T.M.I., Chan P.L., “Life cycle cost analysis of fuel cell based cogeneration system for residential application in Malaysia,” *Renewable and Sustainable Energy Reviews*, 15, 416-426, 2011.
- [187] “Solar Photovoltaics,” *Renewable Energy Technologies: Cost Analysis Series*, vol. 1: Power Sector, International Renewable Energy Agency, IRENA, 2012.
- [188] Andrews J., Shabani B., “Dimensionless analysis of the global techno-economic feasibility of solar-hydrogen systems for constant year-round power supply,” *International Journal of Hydrogen Energy*, 37, 6-18, 2012.
- [189] Lakhani R., Doluweera G., Bergerson J., “Internalizing land use impacts for life cycle cost analysis of energy systems: A case of California’s photovoltaic implementation,” *Applied Energy*, 116, 253-259, 2014.
- [190] Dufo-Lopez R., Bernal-Agustin J.L., “Design and economical analysis of hybrid PV–wind systems connected to the grid for the intermittent production of hydrogen,” *Energy Policy*, 37, 3082-3095, 2009.
- [191] Saur G., “Wind-To-Hydrogen Project: Electrolyzer Capital Cost Study,” Technical Report, National Renewable Energy Laboratory, NREL/TP-550-44103, 2008.
- [192] Bechrakis D.A., McKeogh E.J., Gallagher P.D., “Simulation and operational assessment for a small autonomous wind–hydrogen energy system,” *Energy Conversion and Management*, 47, 46-59, 2012.
- [193] Rahimi S., Meratizaman M., Monadizadeh S., Amidrpour M., “Techno-economic analysis of wind turbine-PEM (polymer electrolyte membrane) fuel cell hybrid system in standalone area,” *Energy*, 67, 381-396, 2014.
- [194] Bernal-Agustin J.L., Dufo-Lopez R., “Techno-economical optimization of the production of hydrogen from PV-Wind systems connected to the electrical grid,” *Renewable Energy*, 35, 747-758, 2010.

- [195] Beccali M., Brunone S., Cellura M., Franzitta V., “Energy, economic and environmental analysis on RET-hydrogen systems in residential buildings,” *Renewable Energy*, 33, 366-382, 2008.
- [196] Zoulias E.I., Glockner R., Lymberopoulos N., Tsoutsos T., Vosseler I., Gavalda O., Mydske H.J., Taylor P., “Integration of hydrogen energy technologies in stand-alone power systems analysis of the current potential for applications,” *Renewable and Sustainable Energy Reviews*, 10, 432-462, 2006.
- [197] Li C.H., Zhu X.J., Cao G.Y., Sui S., Hu M.R., “Dynamic modeling and sizing optimization of stand-alone photovoltaic power systems using hybrid energy storage technology,” *Renewable Energy*, 34, 815-826, 2009.
- [198] Castaneda M., Cano A., Jurado F., Sanchez H., Fernandez L.M., “Sizing optimization, dynamic modeling and energy management strategies of a stand-alone PV/hydrogen/ battery-based hybrid system,” *International Journal of Hydrogen Energy*, 38, 3830-3845, 2013.
- [199] Ismail M.S., Moghavvemi M., Mahlia T.M.I., “Techno-economic analysis of an optimized photovoltaic and diesel generator hybrid power system for remote houses in a tropical climate,” *Energy Conversion and Management*, 69, 163-173, 2013.
- [200] Chippar P., Ju H., “Numerical modeling and investigation of gas crossover effects in high temperature proton exchange membrane (PEM) fuel cells,” *International Journal of Hydrogen Energy*, 38, 7704-7714, 2013.
- [201] Houreh N.B., Afshari E., “Three-dimensional CFD modeling of a planar membrane humidifier for PEM fuel cell systems,” *International Journal of Hydrogen Energy*, 39, 14969-14979, 2014.
- [202] Barbir F., Yazıcı S., “Status and development of PEM fuel cell technology,” *International Journal of Energy Research*, 32, 369-378, 2008.
- [203] Baek S.M., Yu S.H., Nam J.H., Kim C.-J., “A numerical study on uniform cooling of large-scale PEMFCs with different coolant flow field designs,” *Applied Thermal Engineering*, 31, 1427-1434, 2011.
- [204] Tolj I., Barbir F., Bezmalinovic D., “Maintaining desired level of relative humidity throughout a fuel cell with spatially variable heat removal rates,” *International Journal of Hydrogen Energy*, 36, 13105-13113, 2011.

[205] Kandlikar S.G., Lu Z., "Thermal management issues in a PEMFC stack - a brief review of current status," *Applied Thermal Engineering*, 29, 1276-1280, 2009.

[206] Tari İ., "Passive cooling assembly for flat panel displays with integrated high power components," *IEEE Transactions on Consumer Electronics*, 55, 1707-1713, 2009.

APPENDIX A

LEVELIZED COST OF ELECTRICITY (LCE) ANALYSIS OF THE HYBRID RENEWABLE ENERGY SYSTEM

A.1 LCE Analysis Method

The purpose of the LCE analysis is to show the economical feasibility of the studied hybrid renewable energy system. LCE can be defined as the ratio of the total annualized cost of the system (SC_{an}) to the annual useful electricity supplied to the system (UE_{an}). UE_{an} could also be defined as the electricity consumed by the user in a year.

$$LCE = \frac{SC_{an}}{UE_{an}} \quad (A.1)$$

The annualized system cost can be defined with the following equation:

$$SC_{an} = NC_p \cdot CRF + ARC \cdot CRF \quad (A.2)$$

where NC_p is the net present cost, ARC is the annualized replacement cost and CRF is the capital recovery factor. CRF is defined as [4] [8] [131] [185]:

$$CRF = \frac{d \cdot (d + 1)^{ny}}{(d + 1)^{ny} - 1} \quad (A.3)$$

where d is the annual interest rate (%) and n_y is the number of years. CRF is calculated for the fixed and replaceable equipment separately, as in [185]. For the fixed equipment n_y is equal to project lifetime, and for the replaceable equipment n_y is equal to useful lifetime of each individual equipment. In reality, real annual interest rate directly depends on the inflation rate. But, for the ease of comparison of different types of systems, the annual interest rate is assumed constant. It is also assumed that the inflation rate equally affects the prices of all equipment, as in [8].

The annualized replacement cost is the multiplication of the replacement cost (RC) of individual equipment by corresponding capital recovery factor, and ARC must be calculated for each replaceable equipment separately.

$$ARC = RC \cdot CRF \quad (A.4)$$

The net present cost is the total required amount of investment for the system throughout its lifetime, and it is defined as the difference between the present system cost (SC_p) and the present system salvage cost (SS_p).

$$NC_p = SC_p - SS_p \quad (A.5)$$

The present system cost is defined as the summation of the initial capital cost (ICC), and the present operating and maintenance cost (OMC_p).

$$SC_p = ICC + OMC_p \quad (A.6)$$

The initial capital cost is defined as a summation of all the installed equipment at the time of establishment of the system. The present operating and maintenance cost includes all of the operating and maintenance spending, and replaced equipment costs throughout the lifetime of the system.

Mahlia and Chan [186] defined the system salvage cost as the value remaining in any equipment of the system after the projected lifetime. At the end of the projected lifetime, some equipment might still have some considerable value. This value is subtracted from the total cost of the system for the projected period. The system salvage cost is defined as

$$SS_p = \sum_i \left(CP_i \cdot RT_i / PT_i \right) \quad (A.7)$$

where CP_i is the price, RT_i is the remaining lifetime and PT_i is the projected lifetime of each equipment.

A.2 LCE Analysis Assumptions

The installed cost of the PV panels directly depends on the manufacturer of the equipment. The cost of a C-Si based PV system including all of the necessary equipment, materials and accessories without battery storage can vary from 3800 to 5800 \$/kW [187]. A value near to mid-range is selected, as in [188]. The operation and maintenance cost, OMC_p of PV panels is taken as 0.12% of the installed cost per year and service life of the PV panels is taken as 25 years. The assumptions used in the LCE analysis are summarized in Table 18.

The initial cost of the PEM electrolyzer is assumed as 5000 \$/kW; and initial cost of the PEM fuel cell is assumed as 2000 \$/kW. OMC_p of the PEM electrolyzer and the PEM fuel cell is taken as 0.05 \$/h, and the service life of these equipment is assumed as 10 years. The initial cost of the PEM electrolyzer includes all of the necessary equipment and accessories including dehumidifier, deionizer etc. The replacement cost of the PEM based components is assumed as 7% of the initial cost, since only the replacement of the MEA is required. During the project lifetime, MEAs of the PEM based components should be replaced twice and the inverters of the system should be replaced after 20 years of operation. For all of the other

equipment, the replacement cost is assumed to be the 100% of the initial cost; this is because these equipment need to be replaced completely at the end of the lifetime.

The initial cost of the storage tanks is assumed as 100 \$/m³, and the service life of these equipment is assumed as 25 years. The initial cost of the inverters is assumed as 1000 \$/kW and the service life of the inverters is assumed as 20 years. OMC_P values of the storage tanks and the inverters are assumed to be the 0.5% of their initial costs per year.

Table 18 The assumptions used in the LCE analysis.

Equipment	Initial Cost	OMC_P	Replacement Cost	Service Life (y)
PV Panels	5000 \$/kW [187] [188]	0.12% of the installed cost per year [189]	100%	25 [190]
PEM Electrolyzer	5000 \$/kW [8] [191]	0.05 \$/h [192]	7% [185]	10 [8] [188] [193] [194]
PEM Fuel Cell	2000 \$/kW [186] [188] [193] [195]	0.05 \$/h [192]	7% [185]	10 [188] [193] [196]
Storage Tanks	100 \$/m ³ [192]	0.5% of the installed cost per year [197]	100%	25 [193]
Inverters	1000 \$/kW [8]	0.5% of the installed cost per year [197]	100%	20 [8]

A.3 LCE Analysis for a PV/battery System

For comparison, the LCE analysis is repeated for a PV/battery energy system, in which only batteries are used instead of the hydrogen cycle of the system. The PV/battery system is chosen for comparison because it seems simpler than the

PV/hydrogen system. However, the PV/hydrogen system is more advantageous than the PV/battery system. The higher energy density and the longer life span are the main advantages of the hydrogen system over the battery system. The required battery capacity is calculated as 240 kWh. In literature, batteries up to a capacity of 10.5 kWh are used [198]. Thus, for the current system, at least twenty-four batteries with a minimum capacity of 10 kWh are needed. Also, batteries are known with their limited number of charge-discharge cycles leading to frequent replacement of the equipment. Moreover, in batteries, useable stored energy heavily depends on discharge current. In reality, this can lead to 50% decrease in rated capacity [8].

Initial cost of the batteries are assumed as 120 \$/kW, the replacement time is taken as 4 years, and OMC_P is assumed as 1% of the installed cost per year, as in [197]. Also, the replacement cost is assumed as 60% of the initial cost of the pure battery system, as in [198]. In Table 19, comparison of the assumptions used in LCE analysis of the system with PV/battery and the PV/hydrogen based system is tabulated. LCE of the PV/battery system is calculated as 0.687 \$/kWh.

Table 19 Comparison of assumptions of the batteries with other equipment.

Equipment	Initial Cost (\$)	OMC_P (\$/y)	Replacement Cost (\$)	Service Life (y)
PV Panels	198000	237.6	0	25
PEM Electrolyzer	25000	215	1750	10
PEM Fuel Cell	10000	259	700	10
Storage Tanks	4500	22.5	0	25
Inverters	35000	175	35000	20
Battery	28800	288	17280	4

A.4 LCE Analysis for a Diesel Generator System

LCE analysis is performed for a pure diesel generator energy system, in which only diesel generators are used. Pure diesel generator energy systems have some advantages over other type of backup systems. This type of energy systems are commonly used as a backup system, since the initial capital cost of the diesel generators is very low, 550 \$/kW [199]. Likewise, pure diesel energy generator systems are not complicated, since only a fuel tank and a power conditioner are needed to have a complete backup system. On the other hand, pure diesel generator energy systems have many drawbacks. In continuous operation, they have a limited lifetime of 15,000 hours [199], which corresponds to approximately 3 years. Additionally, because of the fossil fuel prices OMC_p of diesel generators are considerably high. OMC_p of diesel generators is the summation of the yearly fuel price and maintenance cost of 0.1 \$/h [8].

In diesel generator systems, it is a general approach to avoid continuously operating at maximum rated output of the diesel generator. Thus, the diesel generator capacity is selected higher than the demand of the user to increase the lifetime of the diesel generator. Consequently, a diesel generator is selected with a capacity of 7.5 kW. LCE analysis for the pure diesel generator system is conducted for two different fuel price scenarios:

- fuel price of 1.5 \$/l according to the current situation in Turkey,
- fuel price of 2.5 \$/l according to the expected global rise of fuel prices, as in [8].

Details of the LCE analysis of the pure diesel generator system and the results of the both scenarios are tabulated in Table 20. LCE values of the pure diesel generator system are calculated as 0.221 \$/kWh and 0.359 \$/kWh for the fuel price scenarios of 1.5 \$/l and 2.5 \$/l, respectively.

Table 20 Details of the LCE analysis of the pure diesel generator system.

Scenario	Fuel Price (\$/l)	OMC_p (\$/y)	Initial Cost (\$)	Service Life (y)	Replacement Cost (\$)	LCE (\$/kWh)
1	1.5	33726	4125	3	4125	0.221
2	2.5	55626	4125	3	4125	0.359

APPENDIX B

PEM FUEL CELL GOVERNING EQUATIONS

The governing equations are based on mass, momentum, energy and species conservation including appropriate source terms. Since the problem is assumed to be steady, time dependent parameters are dropped from the equations. The resulting equations are explained in the following subsections. The half-cell cross-section of the solution domain is shown in Figure 56.

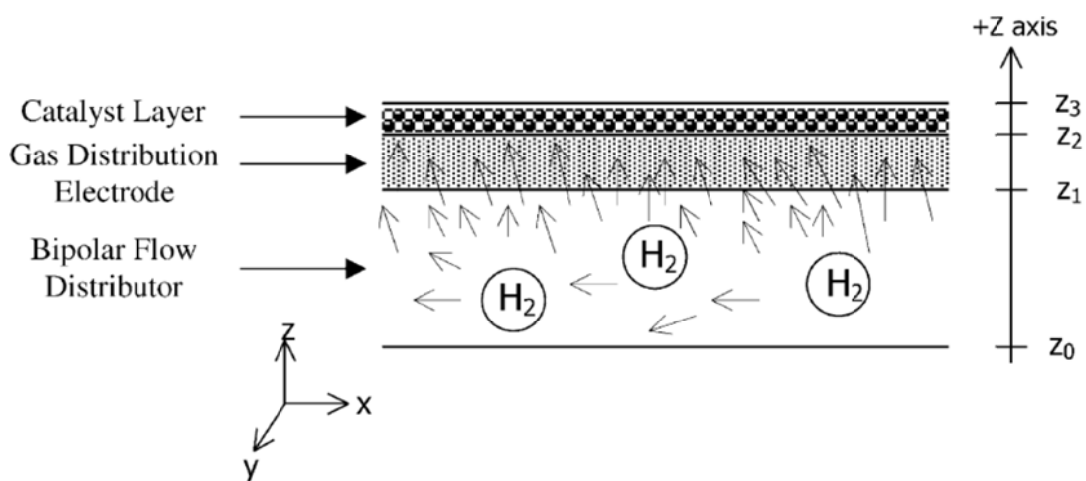


Figure 56 Half-cell cross-section of the PEM fuel cell (adapted from Kumar and Reddy [57]).

B.1 Continuity

$$\nabla \cdot (\rho \vec{V}) = S_{mass} \quad (\text{B.1})$$

where S_{mass} is the source term for the continuity equation. S_{mass} is applicable only for the catalyst region ($z_2 \leq z \leq z_3$) and defined by Equation B.2. In the flow channels, GDL and membrane, S_{mass} is set to zero.

$$S_{mass} = -\frac{\delta \xi_{H_2}}{\kappa + \xi_{H_2}}, \quad (z_2 \leq z \leq z_3) \quad (\text{B.2})$$

where ξ_{H_2} is the concentration of hydrogen in the solution domain, κ and δ are the coefficients of the mass source term equation. Details of these coefficients are explained in detail by Hontanon et al. [64].

B.2 Momentum

$$\frac{1}{\varepsilon(1-s)} \nabla \cdot (\rho \vec{V} \vec{V}) = -\nabla p + \frac{1}{\varepsilon(1-s)} \nabla \cdot (\mu_l \nabla \vec{V}) + \rho g + S_{mom} \quad (\text{B.3})$$

where S_{mom} is the source term for the momentum equation, s is the water saturation ratio (water volume fraction) and ε is the wet porosity. These terms are applicable for only porous medium ($z_1 \leq z \leq z_3$). In the flow channels and membrane, the source term S_{mom} is set to zero. S_{mom} is defined as:

$$S_{mom} = -\frac{\mu_l}{K} \vec{V}, \quad (z_1 \leq z \leq z_3) \quad (\text{B.4})$$

where K is the permeability.

B.3 Species

$$\nabla \cdot (\rho \vec{V} X_i) = -\nabla(\rho D_i \nabla X_i) + S_i \quad (\text{B.5})$$

where the index “ i ” refers to the species including oxygen, hydrogen and water. D_i is the diffusivity of species “ i ”. S_i is the source term for the species and applicable for the catalyst region only ($z_2 \leq z \leq z_3$). In the flow channels, GDL and membrane S_i is set to zero. S_i is defined for each species by the following equations:

$$S_{O_2} = -\frac{\overline{M_{O_2}}}{4F} i_c, \quad (z_2 \leq z \leq z_3) \quad (\text{B.6})$$

$$S_{H_2} = -\frac{\overline{M_{H_2}}}{4F} i_a, \quad (z_2 \leq z \leq z_3) \quad (\text{B.7})$$

$$S_{H_2O} = -\frac{\overline{M_{H_2O}}}{4F} i_c, \quad (z_2 \leq z \leq z_3) \quad (\text{B.8})$$

B.4 Energy

$$\nabla \cdot (\rho \vec{V} T) = \nabla (k^{eff} \nabla T) + S_T \quad (\text{B.9})$$

where S_T is the heat source term for the energy equation and is applicable at the cathode catalyst layer ($z_2' \leq z \leq z_3'$). For other zones S_T is set to zero. S_T is defined with the following equation [200]:

$$S_T = \eta j_c + \frac{I^2}{k^{eff}} + j_c \frac{dU_0}{dT} T - \frac{I_{H_2}^{xover}}{t_{CL}} \left(\eta + \frac{dU_0}{dT} T \right), \quad (z_2' \leq z \leq z_3') \quad (\text{B.10})$$

where U_0 is the thermodynamic equilibrium potential, $I_{H_2}^{xover}$ is the hydrogen crossover current density, t_{CL} is the catalyst layer thickness, η is the overvoltage and j_c is the transfer current density for the cathode side.

In Equation B.9 k^{eff} is the effective thermal conductivity and represents the thermal conductivity of the gas mixture in the flow channels and membrane [201]. k^{eff} is defined by the following equation:

$$k^{eff} = \frac{1}{\frac{1-\varepsilon}{3k_{MEA}} + \frac{\varepsilon}{2k_{MEA} + k_w}} - 2k_{MEA} \quad (B.11)$$

where k_{MEA} is the thermal conductivity of the MEA and k_w is the thermal conductivity of water.

B.5 Liquid Water Transport Equation

The liquid water formation and transport in the solution domain is governed by the following conservation equation:

$$\nabla \cdot (\rho_l \vec{V}s) = r_w \quad (B.12)$$

where ρ_l is the liquid density, s is the water saturation ratio (water volume fraction) and r_w is the condensation rate and calculated iteratively by using Equation B.12. Inside porous medium ($z_1 \leq z \leq z_3$) the convective term in Equation B.12 is substituted by a capillary diffusion term and governed by the following equation [61]:

$$\nabla \cdot \left(\rho_l \frac{K s^3}{\mu_l} \frac{dp_c}{ds} \nabla s \right) = r_w \quad (B.13)$$

where K is the absolute permeability, μ_l is the liquid viscosity and p_c is the capillary pressure.

B.6 Potential Equations

In the PEM fuel cell model, two potential equations are solved. One of the potential equations represents the electron transport e^- (Equation B.14) through the conductive solid materials, the other potential equation accounts for the proton transport of H^+ or O^{2-} (Equation B.15) [36]. The potential equations can be defined with the following equations:

$$\nabla \cdot (\sigma_{sol} \nabla \phi_{sol}) - S_{\phi} = 0 \quad (B.14)$$

$$\nabla \cdot (\sigma_{mem} \nabla \phi_{mem}) + S_{\phi} = 0 \quad (B.15)$$

where S_{ϕ} is the source term for the potential equations and is applicable only for the catalyst regions. S_{ϕ} can be defined by the following equations:

$$S_{\phi} = j_a \quad (z_2 \leq z \leq z_3) \quad (B.16)$$

$$S_{\phi} = j_c \quad (z_2' \leq z \leq z_3') \quad (B.17)$$

where j_a is the transfer current density for the anode side and j_c is the transfer current density for the cathode side. Details of the transfer current densities can be found in the literature [200].

APPENDIX C

DESIGNING HEAT EXCHANGER WITH VARIABLE SURFACE AREA FOR PASSIVE COOLING OF PEM FUEL CELL

The purpose of this work was to design a heat exchanger for a PEM fuel cell, which would ensure such a temperature profile along the fuel cell cathode channel resulting in close to 100% relative humidity along the channel without external humidification. To achieve this, 3D numerical simulations of a single PEM fuel cell were performed using ANSYS Fluent. Based on the simulation results a variable surface area finned heat exchanger was designed which allows for passive fuel cell cooling. The results indicate that it is possible to obtain such temperature and relative humidity conditions inside the fuel cell cathode channel, using a passive heat exchanger with variable surface area.

C.1 Introduction

One of the most important aspects of PEM fuel cells design and operation is water management. In this type of fuel cells, conductivity of protons through a polymer membrane strongly depends on membrane's water content [202]. The membrane therefore must be well hydrated throughout a fuel cell. As the state of water and its fluxes in fuel cell depend on local temperature, water management is practically inseparable from heat management and it is therefore often referred to as water and heat management. Heat is produced in the electrochemical reactions; in addition some heat is also generated due to resistive (ohmic) losses. In order to maintain the desired temperature, heat must be removed from a fuel cell. If the excess heat is not

being removed at an adequate rate, performance and durability of the fuel cell would significantly decrease [203].

Although the fuel cell produces water, and in most cases this amount of water should be sufficient to keep the reactant gases fully humidified, most fuel cells need external humidification of the reactant gases. Introduction of ambient air in a fuel cell operating at elevated temperature ($60 - 80^{\circ}\text{C}$) without additional humidification would result in temperature of the air rising quickly after entering the stack causing severe drop in relative humidity. The product water in that entrance portion of the fuel cell would not be sufficient to prevent severe dehydration. Eventually, down the cathode channel, the product water could be sufficient to humidify air, but significant portion of the cathode channel would be dry. Operation with dry gases would result in drying out of the polymer membrane, which would adversely affect the fuel cell performance and durability.

Tolj et al. [204] presented a new concept of not allowing dry conditions inside the fuel cell by controlling the local temperature, i.e., by imposing a temperature profile which would allow maintaining desired relative humidity (close to 100%) utilizing water produced in the electrochemical reaction inside the fuel cell. Figure 57 shows the temperature and relative humidity profiles along the cathode channel for a fuel cell operated with untreated ambient air. In case when the fuel cell temperature is maintained constant, the temperature of air increases sharply as soon as it enters the fuel cell. As a result, relative humidity drops to a very low level ($\sim 20\%$) and then it gradually increases to 100% at the fuel cell outlet. This means that the fuel cell polymer membrane is exposed to dry conditions throughout the fuel cell. However, it should be possible to impose a temperature profile along the cathode channel such that relative humidity quickly reaches saturated or close to saturated conditions, and then maintains such conditions throughout the fuel cell until the exit. In cases, inlet and outlet conditions are identical but the temperature and relative humidity profiles are drastically different, the later resulting in more favorable conditions and thus should result in better performance and longer life.

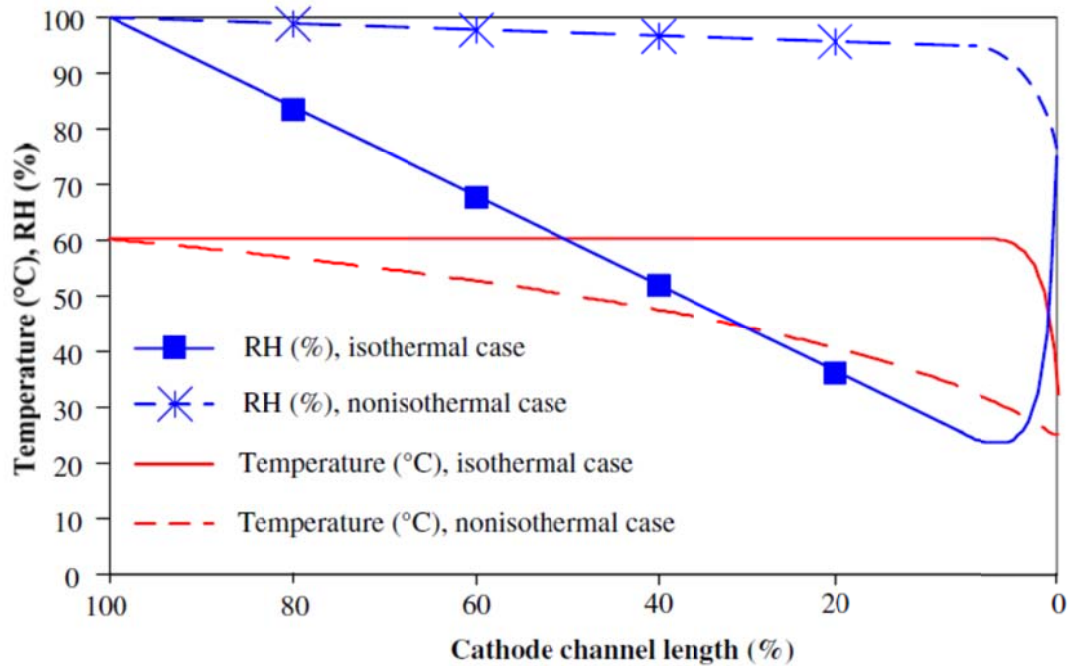


Figure 57 Temperature and relative humidity profiles along the fuel cell cathode channel for two cases a) isothermal and b) non-isothermal so that relative humidity is kept close to 100% (adapted from Tolj et al. [204]).

Such a temperature profile may be imposed by spatially variable heat transfer rates. Tolj et al. [204] accomplished such a profile by using a segmented fuel cell, where each segment was kept at the previously calculated required temperature by attached Peltier elements. However, although very effective in laboratory testing, the use of Peltier elements would not be practical in real life fuel cells. It is therefore the objective of this work to design a heat exchanger for heat removal from a fuel cell segment which would replace the Peltier element and enable required profile along the fuel cell cathode channel.

C.2 Methodology

In order to achieve the objective, following methodology has been applied: (i) development of a 3D model of a PEM fuel cell by using ANSYS Fluent; (ii) use of the 3D model to find a temperature profile along the cathode channel that will ensure close to saturation conditions throughout the channel; (iii) design of a passive cooled heat exchanger to obtain desired temperature profile; and (iv) verification of the designed heat exchanger performance using the 3D model.

In the previous study [204], five fuel cell segments were connected in series. Each segment was an individual 20 x 1 cm active area single cell with 5 straight channels for supply and distribution of hydrogen and air on both anode and cathode side, respectively. Hydrogen and air flow in counter-current mode. One of these fuel cell segments designed in previous study [204] is modeled using the ANSYS Fluent Fuel Cells Module.

Geometrical details and boundary conditions are presented in Table 21. The actual fuel cell segment and its 3D CFD model are shown in Figure 58. As seen on the figure, the collector plates are somewhat larger than the active area of the fuel cell, because of the area needed to seal the cell. From the heat transfer point of view this may be advantageous, because a larger heat transfer area is exposed to passive cooling.

Continuity, momentum, species, energy, electrochemical and water transport equations were solved simultaneously by the ANSYS Fluent program to obtain the results. Details of the implementation of the equations can be found in [36]. To ensure that the solution was grid-independent, calculations were performed with different mesh sizes. The reference parameter was the average current density at a fixed voltage for the grid independence. The number of elements which led to grid-independent solution was 3,752,000. Tetragonal hybrid type elements were used. The generated mesh was not uniform. In the membrane electrode assembly, because

of the thin layers, the mesh was generated with higher refinement. In the collector plate and flow channels a coarser mesh was generated.

The temperature profile that was required to ensure 100% relative humidity was obtained by performing CFD simulations. First, 100% relative humidity condition was achieved at the exit section of the cathode flow channel by applying proper temperature boundary condition at the outside wall of cathode collector plate. Then, the non-uniform boundary condition, which was necessary to give 100% relative humidity along the cathode flow channel, was obtained by CFD simulations.

Table 21 Values for parameters used in CFD model experimental set-up [204].

Parameters	Values
Cathode stream pressure	1.01 bar
Anode stream pressure	1.01 bar
Cathode stream inlet temperature	30 °C
Anode stream inlet temperature	25 °C
Fuel cell hardware temperature	60 °C or variable
Relative humidity of cathode stream	75%
Relative humidity of anode stream	Dry
Cathode stoichiometry	2.15
Current density	0.5 A cm ⁻²
Cathode stream (air) inlet mass flow rate	0.0077 g s ⁻¹
Channel length	200 mm
Channel width at anode and cathode	1mm
Channel height at anode and cathode	1mm
Number of channels	5
Effective area of the cell	20 cm ²
Membrane thickness	0.005 cm
Membrane dry density	2 g cm ⁻³

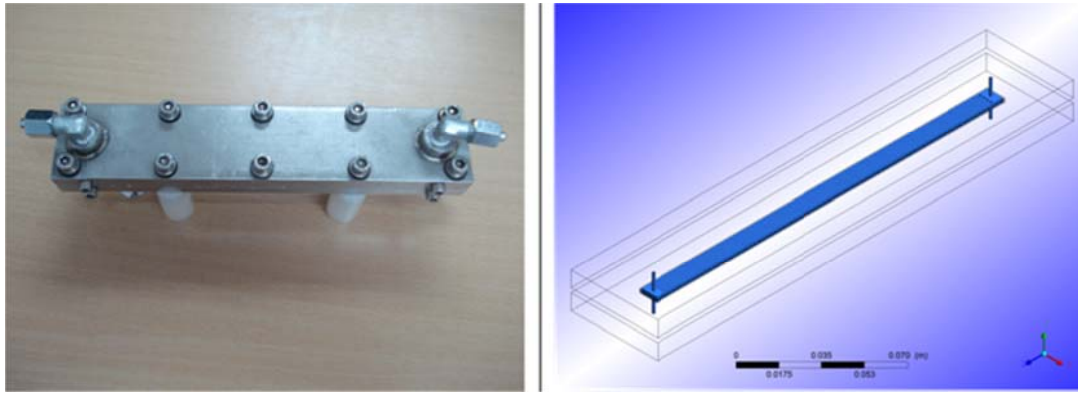


Figure 58 PEM fuel cell segment (left); 3D PEM fuel cell model (right).

The next step was to design a heat exchanger which will give the desired temperature profile along the cathode collector plate. An ancillary cooling system is needed in PEM fuel cells since the outlet streams contribute little to heat removal [205]. By using heat exchanger, the necessity of the external humidification and any other power consuming devices such as fans or Peltier elements would be eliminated. The designed heat exchanger would be capable of removing the generated excess heat through the PEM fuel cell.

Because of a specific required (non-uniform) temperature profile along the collector plate, the heat exchanger removing the heat from the fuel cell should have variable heat transfer area. This could be a simple heat exchanger, consisting of straight fins with variable fin height. Simple heat sink geometries could provide enough passive heat dissipation for a wide range of applications [206]. For the heat exchanger material aluminum was selected, as it has high thermal conductivity and low cost when compared to other materials.

The model domain and heat transfer paths included in the model are presented in Figure 59. Heat generated in the catalyst layers and the membrane is transferred mainly by conduction to the exterior walls of the fuel cell. From the exterior walls,

heat is removed to the surrounding mostly by convection. The boundary conditions applied to the model are described below.

C.3 Boundary Conditions

C.3.1 Inlet Boundary Conditions

For the anode and the cathode inlet mass flow rate boundary condition is applied. Mass flow rate, fluid temperature and mass fraction of the species are specified for the inlet boundary condition.

C.3.2 Outlet Boundary Conditions

To the anode and the cathode outlets, pressure outlet boundary condition is applied. This boundary condition is used at the continuum domain exits where pressure values are not known prior to the solution.

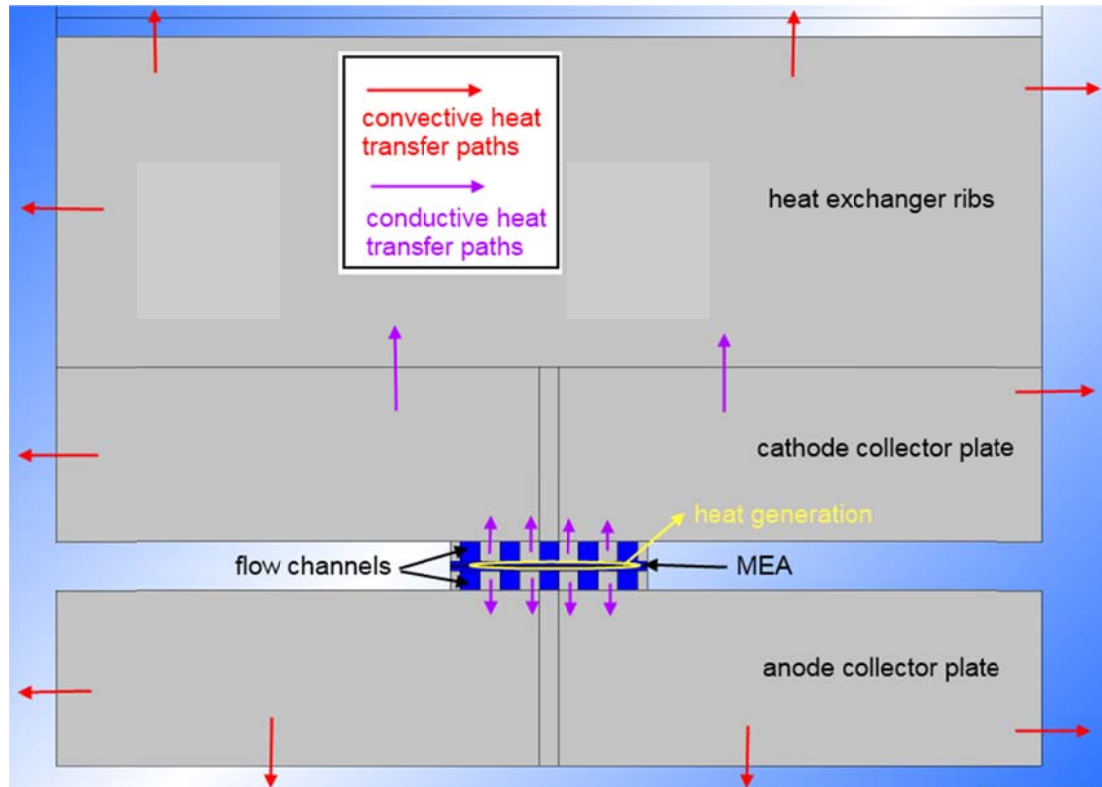


Figure 59 Heat transfer paths of the model.

C.3.3 Outer Wall Boundary Conditions

No slip boundary condition is applied at the walls of the model. For the outer walls of the model convective boundary condition is applied using following equation:

$$Q_w = h_{conv} A_w (T_w - T_{amb}) \quad (C.1)$$

For the outer walls convective heat transfer coefficient h_{conv} and ambient temperature T_{amb} are specified. Q_w (heat transfer rate) and T_w (wall temperature) calculated by ANSYS Fluent. A_w is the heat exchange area.

There is no need to define the boundary conditions at the inside cathode channel walls. The program (ANSYS Fluent) calculates the local heat transfer coefficient, local wall temperatures and local heat flux between the channel and the wall. The fluid (cathode air) temperature changes along the cathode channel in accordance with the previously calculated temperature profile needed to maintain 100% (or close to 100%) relative humidity, and this profile is used as an input parameter. Inlet parameters (fluid, mass flow rate, temperature and pressure are listed in Table 21).

C.4 Results and Discussion

Base on the simulation results, confirmed experimentally in the previous study [204], the heat exchanger area along the cathode channel required for maintaining close to saturation conditions of air along the cathode channel was calculated. First, the temperature profile that resulted in 100% humidity in the cathode channel was calculated. Then, according to the resulting temperature profile, the required heat transfer area was calculated for different heat transfer coefficients. The results are presented in Figure 60. Calculations were made for two different values of heat transfer coefficient i.e., 5.0 W/mK for natural convection (still air in laboratory conditions) and 19.0 W/mK for forced convection. To achieve heat transfer coefficient values greater than 5.0 W/mK, a fan would be required, which would

require additional power, which in turn would adversely affect the fuel cell efficiency. The value of 19.0 W/mK was found to be a limiting heat transfer coefficient value. Above this value the PEM fuel cell outer area would have to be decreased in order to achieve saturation conditions, which would be physically impossible.

After examining the CFD simulations obtained for the 100% humidity condition, it was observed that there was no localized high flux heat source present. Therefore, by increasing the surface area of the cathode collector plate, it would be possible to have the desired temperature profile. Also it was observed that radiative heat transfer through the heat exchanger was very low when it was compared with the convective heat transfer, because of the low emissivity and low temperature differences. Therefore, radiative heat transfer could be neglected.

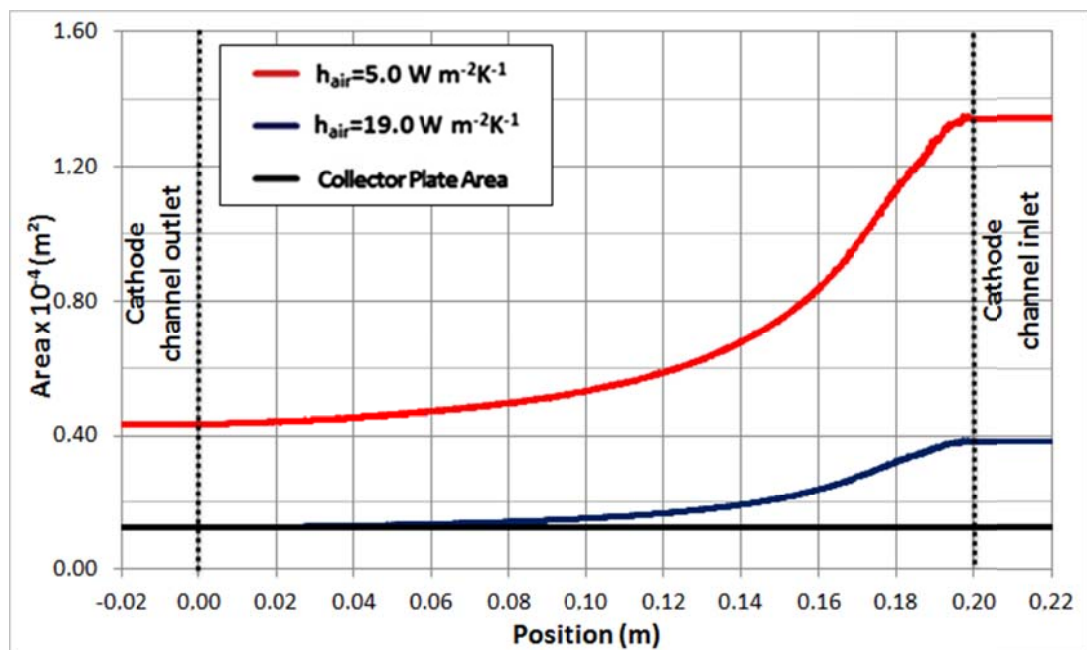


Figure 60 Required heat exchanger area along the cathode channel.

After necessary heat transfer area for ensuring saturated condition of air was calculated, a finned heat exchanger was designed. The required heat dissipation rate of the entire heat exchanger is 8.5W. It consists of 24 ribs, with decreasing rib height in the fluid stream direction from 62 mm to 16 mm, as shown in Figure 61. The ribs' thickness is 2 mm and the spacing between the ribs is 8 mm.

The next step was to couple the designed heat exchanger with cathode side of the fuel cell and to perform final simulation, Figure 62. The heat exchanger was mounted to the cathode side of the fuel cell. By performing CFD simulations it was expected to obtain relative humidity along the cathode channel and to compare with the previous CFD simulations without the heat exchanger. Also, heat dissipation rate of the heat exchanger could be calculated.

The resulting temperature distribution of the heat exchanger is shown in Figure 63. The temperature distribution was as expected, keeping the cathode inlet side of the fuel cell cooler than the outlet side. This model was developed to support that the heat exchanger was capable of removing excess heat from the fuel cell. From the CFD simulations, it was observed that the heat removal rate of the heat exchanger was sufficient to cool the fuel cell. Total resulting heat transfer rate of the heat exchanger is 8.78 W, which is 3.3% higher than the calculated or required value of 8.5 W.

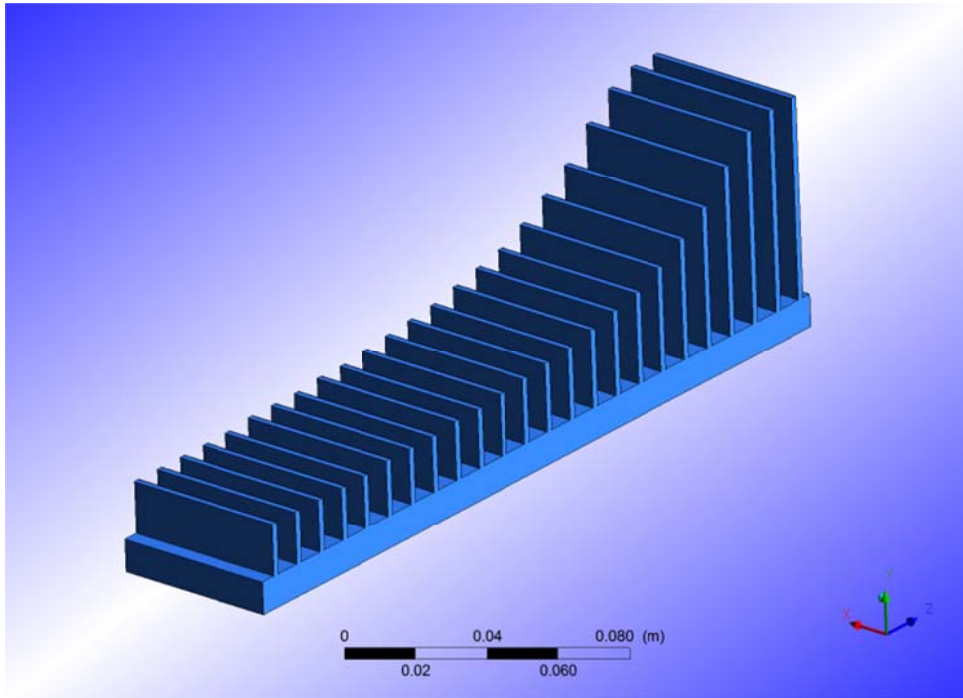


Figure 61 Resulting heat exchanger with variable length fins.

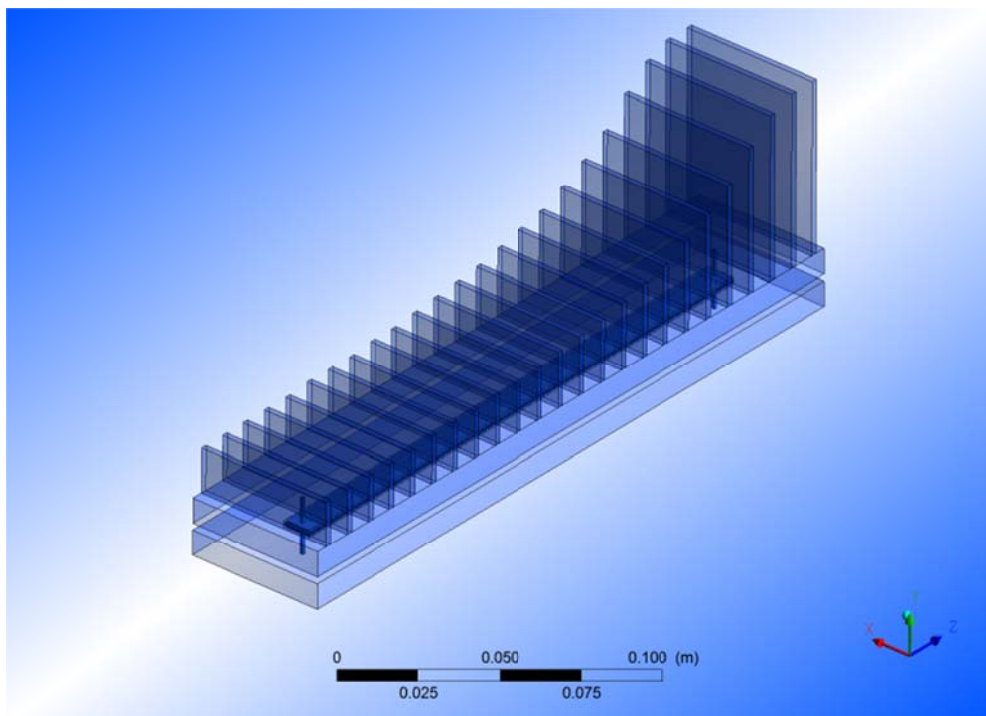


Figure 62 Heat exchanger coupled with cathode side of the PEM fuel cell segment.

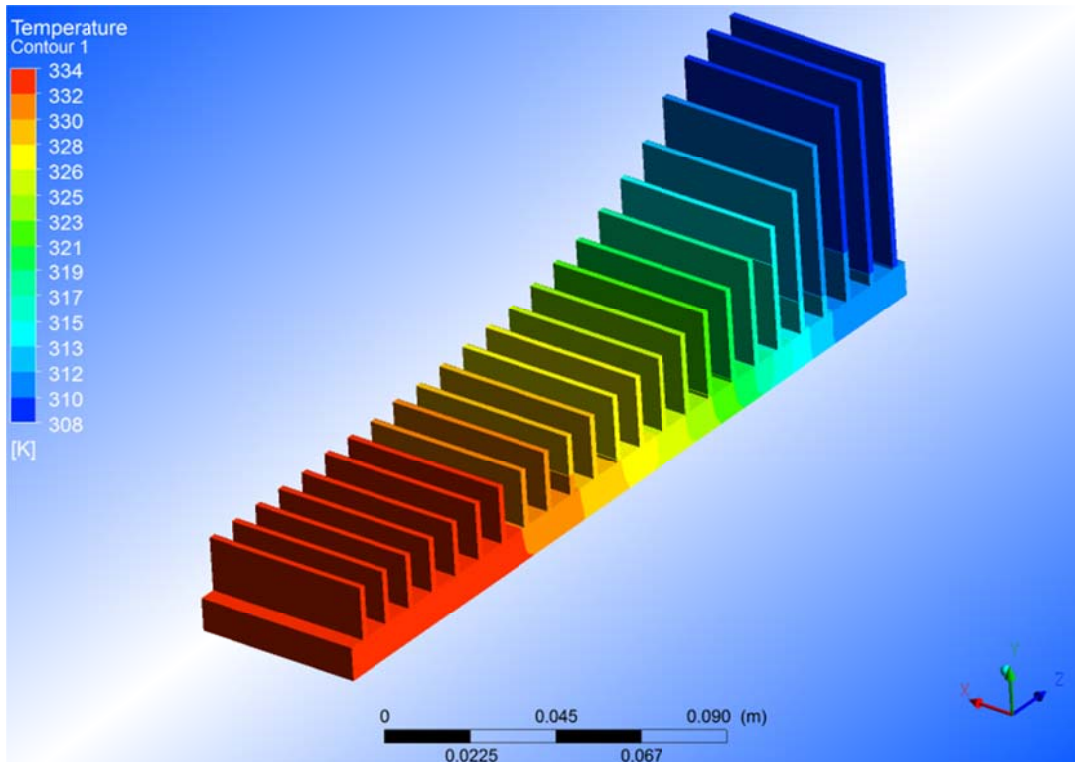


Figure 63 Temperature distribution of the heat exchanger.

Resulting relative humidity of air along the cathode channel is shown in Figure 64. In this figure, PEM fuel cell with and without heat exchanger is compared. For the case without the heat exchanger, the air stream heats up quickly after entering the cell, which causes drop in relative humidity. By the end of the channel the air stream gets fully saturated, but throughout the cathode channel the air is practically dry. For the case with the heat exchanger, relative humidity only slightly drops below the inlet value and then increases to near fully saturated condition and remains at that level throughout the channel. Therefore, more favorable conditions are achieved and resulted in better fuel cell performance. In addition, one may expect that operation at close to 100% relative humidity should result in longer cell durability as compared to operation with dry conditions throughout the channel.

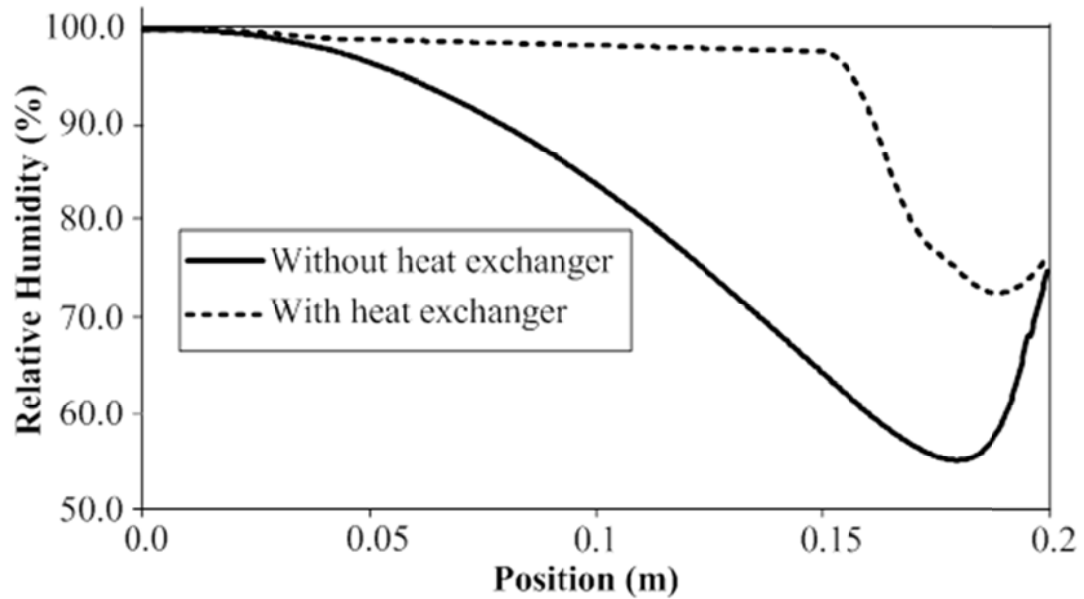


Figure 64 Relative humidity of air along the cathode channel (air entrance is on the right side).

C.5 Conclusions

In this appendix a 3D CFD model of a PEM fuel cell was applied in order to find a temperature profile that ensures close to 100% relative humidity along the cathode flow channel. Base on the simulation results, necessary heat exchanger area was calculated and the heat exchanger was designed. In order to confirm that designed heat exchanger was capable to ensure desired temperature profile, and in such way achieve close to saturation conditions along the cathode channel, the heat exchanger was coupled with a PEM fuel cell. The results show that relative humidity of air was close to 100% along the cathode channel.

This method of operating a PEM fuel cell with dry air by maintain the required temperature profile along the fuel cell cathode, and the resulting simple passive heat exchanger may have application for relatively low fuel cell power (up to a few hundred watts). In laboratory fuel cell testing, it will replace the Peltier elements and eliminate additional power consumed by fans and Peltier elements. Further

work will be aimed at investigations and design of variable heat exchange area within the fuel cell stacks.

VITA

PERSONAL INFORMATION

Surname, Name: Özden, Ender

Nationality: Turkish (T.C.)

Date and Place of Birth: 20 November 1981

Marital Status: Married

Phone: +90 536 587 4828

e-mail: enderozden@gmail.com

EDUCATION

Degree	Institution	Year of Graduation
MS	METU Mechanical Engineering	2007
BS	METU Mechanical Engineering	2004
High School	Milli Piyango Anadolu Lisesi, Ankara	1999

WORK EXPERIENCE

Year	Place	Enrollment
2013-Present	TAI	Design Engineer
2012-2013	EKO Mühendislik	System Design Engineer
2011	University of Split, Croatia	Guest Research Assistant
2007-2011	METU Mechanical Engineering	Project Assistant
2005-2007	EKO Mühendislik	Project Engineer

FOREIGN LANGUAGES

English, Advanced

German, Beginner

PUBLICATIONS

- "System modeling of a solar-hydrogen hybrid renewable energy system in Ankara", Proceedings of the SOLARTR Conference and Exhibition, İzmir - Turkey, November 2014.
- "Designing heat exchanger with spatially variable surface area for passive cooling of PEM fuel cell," Applied Thermal Engineering, 51, 1339-1344, 2013.
- "Multi-physics simulation of PEM electrolyzers," Proceedings of the NAFEMS European Conference Multi-Physics Simulation, Frankfurt – Germany, November 2012.
- "Shell side CFD Analysis of a Small Shell-and-tube Heat Exchanger," Energy Conversion and Management, 51, 1004-1014, 2010.
- "CFD modeling and analysis of a small shell-and-tube heat exchanger", Proceedings of the ASME Heat Transfer Conference, Florida - USA, August 2008.
- "Detailed design of shell-and-tube heat exchangers using CFD". MS Thesis, METU, September 2007.

HOBBIES

Table tennis, Theatre, Model making